Spatio-temporal modelling

– with a view to biological growth patterns

Kristjana Ýr Jónsdóttir

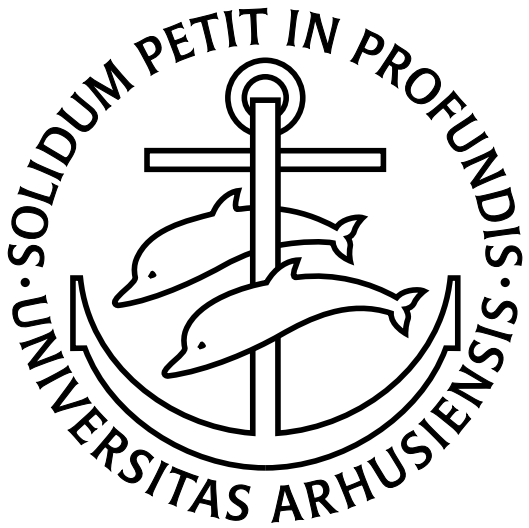

PhD Thesis

Department of Mathematical Sciences
University of Aarhus

February 2006

Preface

Spatio-temporal modelling of biological systems is a field of mathematical biology which has received a great deal of attention in recent years. This PhD thesis is a contribution to this field with focus on modelling of biological growth patterns.

The thesis consists of a review together with five independent papers and is submitted to the Faculty of Science, University of Aarhus. The review provides an introduction to spatio-temporal modelling of growing objects and a presentation of the main results of the accompanying papers. Finally, it contains a short introduction to non-stationary spatial survival analysis, which was the topic of my studies during a stay at School of Mathematics and Statistics, University of Western Australia.

First of all, I would like to express my sincere gratitude to my supervisor Professor Eva B. Vedel Jensen for the excellent supervision and constant support during the three years of my PhD studies. She has been a very valuable support for me, both academically as well as personally. I am also grateful to my friend and fellow PhD student, Þórdís Linda Þórarinsdóttir, for many stimulating discussions, great support and making my daily life easier through the studies. I also want to thank Professor Adrian J. Baddeley, University of Western Australia, for hospitality during my stay abroad and for sharing his knowledge with me. Finally, I would like to thank my friends and family for being there for me, believing in me, and encouraging me.

Århus, February 3rd, 2006 Kristjana Ýr Jónsdóttir

Summary

Growth is a fundamental property of biological systems, occurring at the level of populations, individual animals and plants, as well as within organisms. An overview of spatio-temporal modelling of biological growth can be found in Chaplain et al. (1999), a monograph from the conference *On Growth and Form* held in 1998 in honour of D'Arcy Thompson (1960-1948) and his famous book on the subject, cf. Thompson (1917). Examples of biological growth phenomena include tumour growth, bacterial growth, spread of diseases, growth of year rings of a tree, growth of plant populations, just to name a few. The main aim of the modelling is to capture various spatio-temporal interactions in an observed growth pattern and try to relate the suggested model to specific biological entities. Models do of course not tell the truth about the biological phenomena, but they may provide a deeper understanding of it.

Tumour growth patterns have been intensively studied in recent years. The majority of the models considered are deterministic. Problems concerning the pattern formation and progression of the tumour are important, as well as shape. Different tumour types have specific characteristics and it is of importance to find a realistic modelling framework to try to understand the underlying dynamics. Models can also serve as a support for grading the malignancy of the tumour. The roughness of the tumour boundary can for example serve as in indicator of the malignancy of the tumour. Being able to describe the morphology of the boundary of the tumour, a useful tool is obtained, to help classifying and determining the malignancy. A part of this thesis concerns stochastic spatio-temporal models which describe how the boundary of a star-shaped object expands in time. These models are characterised as supracellular models. Two different approaches are used to describe the morphology of the boundary. The first approach is based on ideas from shape theory. The boundary of an expanding object is modelled in discrete time, by representing the object at present time as a transformation of the object at the immediate past. The main aim of this approach is to capture the important features of the transformation such as global and local shape deviations, using few model parameters. The parametric model suggested is inspired by the p-order model which has been used to model the shape of featureless objects. The second approach is based on recent advances in Lévy theory which has recently been used with success in the development of spatio-temporal models for turbulence. The ideas of Lévy based modelling originate from modelling of turbulence. The models are based on Lévy bases and integration with respect to those. A great advantage of these models is the possibility to control the spatio-temporal correlation structure of the expanding object and therefore to characterise the morphology of the boundary of the expanding object. Accordingly, the models can be a valuable tool for monitoring the dynamics of growth patterns.

The main characteristic of the supracellular models is that only the macroscopic level of the observed patterns is modelled. It is, however, of importance to construct models with known relation between the microscopic and the macroscopic level of the biological growth pattern. A step forward in this direction are the socalled cellular models, discussed in this thesis. The cellular models are based on spatio-temporal point processes. Growth of plant populations, earthquake occurrences, and spread of diseases are among the phenomena that can be modelled using spatio-temporal point processes. Tumour growth has also been modelled using cellular models.

The thesis contains further studies of shape and point processes, relating to stereological variance estimation and non-stationary spatial survival analysis.

The thesis consists of a review and five independently written papers. One of the papers has already been published. Three of the papers are submitted or will be submitted in the nearest future. The co-authors of the papers are my supervisor Eva B. Vedel Jensen, Ole E. Barndorff-Nielsen, and Jürgen Schmiegel, all from University of Aarhus, Asger Hobolth, North Carolina State University, and Lars M. Hoffman, University of Karlsruhe.

Contents

Accompanying papers

A Jónsdóttir, K.Ý. and Jensen, E.B.V. (2005).
Gaussian radial growth.
Image Analysis & Stereology, 24:117–26.

B Jensen, E.B.V., Jónsdóttir, K.Ý., Schmiegel, J. and Barndorff-Nielsen, O. (2006).
Spatio-temporal modelling - with a view to biological growth.
To appear in *Statistics of Spatio-Temporal Systems*, Monographs on Statistics and Applied Probability, Chapman & Hall/CRC.

C Jónsdóttir, K.Ý., Schmiegel, J. and Jensen, E.B.V. (2006).
Lévy based growth models.
To appear as Thiele Research Report. To be submitted.

D Jónsdóttir, K.Ý., Hoffman, L., Hobolth, A. and Jensen E.B.V. (2006).
On error prediction in circular systematic sampling.
To appear in *Journal of Microscopy*.

E Jónsdóttir, K.Ý. (2006).
Non-stationary spatial survival analysis.
To appear as Thiele Research Report.

1 Introduction

The first main group of models to be described is the supracellular models. Here, the entity modelled is the boundary of a full-dimensional star-shaped object expanding in time. The boundary of a star-shaped object is completely determined by its radius vector function. Therefore the model can be expressed in terms of the radius vector function. The supracellular models do not give any information about the interior of the object. The second group of models, the cellular models, can provide such information. They are based on spatio-temporal point processes. We focus on models for inhomogeneous spatial point patterns and their extension to a spatio-temporal framework. Dynamic random compact sets are also discussed.

The review is organised as follows. In Section 2, supracellular models are presented using shape theory and Lévy theory. In Section 3, two applications of the supracellular models are presented, dealing with tumour growth and growth of year rings of a tree, respectively. Section 3 concludes with an application to model-based stereology. Section 4 gives a short review on spatio-temporal point processes. Spatio-temporal extensions of recent models for inhomogeneous spatial point patterns are discussed, as well as models for dynamic random compact sets. The review concludes with a discussion of non-stationary spatial survival analysis, a topic that can be read independently of other material in this review.

2 Supracellular models

Consider a compact object $Y_t \subset \mathbb{R}^2$ which is star-shaped with respect to a specific point $z \in \mathbb{R}^2$ for all $t \geq 0$. Then the boundary of Y_t can be determined by its radius vector function $R_t = \{R_t(\phi) : \phi \in [-\pi, \pi)\}$ with respect to z, where

$$R_t(\phi) = \max\{r : z + r(\cos\phi, \sin\phi) \in Y_t\}, \quad \phi \in [-\pi, \pi).$$

In the following we will describe two different approaches to model the object Y_t using the radius vector function R_t. First a dynamic version of the deformable template model is discussed, cf. Hobolth et al. (2001) and Hobolth et al. (2003). The model is formulated in discrete time, using Gaussian stochastic processes. The second and more general model type is the Lévy based growth models introduced in Jónsdóttir et al. (2006b). The Lévy based growth models describe how the boundary of the object Y_t expands in continuous time. The strength of the Lévy based growth models is that they allow analytical control of the covariance structure of the radius vector function in time and space in accordance with experimental results.

The two approaches discussed in this section only describe how the boundary of the object moves in time and does not give any information about the interior of the object. The models are, however, expected to be a useful empirical tool for monitoring growth patterns.

It should be noted that both model types can easily be extended to three dimensions. This issue will not be discussed further here.

2.1 The template approach and the p-order growth model

Several different representations of the shape of featureless objects have been suggested in recent years. The deformable template representation has played an important role. Here, an observed object is represented as a deformation of an underlying template. For a more detailed description of the method, see Grenander et al. (1991) and Grenander and Miller (1994). In Hobolth et al. (2001), the authors use non-circular templates for such models, while circular templates are discussed in Hobolth et al. (2003). They only consider star-shaped objects.

A star-shaped object Y with radius vector function R is said to be a deformation of a known template object Y^0 with radius vector function R^0, if

$$R(\phi) = R^0(\phi) + U^0(\phi), \quad \phi \in [-\pi, \pi), \tag{2.1}$$

where $U^0 = \{U^0(\phi) : \phi \in [-\pi, \pi)\}$ is a zero mean cyclic stochastic process.

This representation can be used to describe an object with size and shape changing over time, by letting the object at time $t+1$ be represented as a stochastic transformation of the object at time t, such that

$$R_{t+1}(\phi) = R_t(\phi) + V_t(\phi), \quad \phi \in [-\pi, \pi), \tag{2.2}$$

where $V_t = \{V_t(\phi) : \phi \in [-\pi, \pi)\}$ is a cyclic stochastic process. The focus is on modelling the transformation, i.e. the increments $V_t = R_{t+1} - R_t$.

The initial object Y_0 is assumed to be known with radius vector function r_0. The stochastic process V_t is assumed to be of the form

$$V_t(\phi) = \mu_t + U_t(\phi), \quad \phi \in [-\pi, \pi),$$

where $\mu_t \in \mathbb{R}$ represents a constant radial addition and U_t is a cyclic stochastic process with mean zero. In this way one can say that the object Y_{t+1} is a stochastic deformation of the expanded object $Y_t \oplus b(0, \mu_t)$ with radius vector function $R_t + \mu_t$, where $b(0, r)$ denotes the circular disc in $\mathbb{R}^2$ with radius r centred at the origin and $\oplus$ denotes the Minkowski sum

$$A \oplus B = \{a + b : a \in A, b \in B\},$$

cf. Figure 2.1. Note that if the series of increment processes $\{V_t\}$ is assumed to be independent, the conditional distribution of R_{t+1} given $R_t, \ldots, R_0$ depends only on R_t. The model in (2.2) is thus Markovian in discrete time. The model described in Cressie and Hulting (1992) possesses a similar Markov property. See also Section 4.3.

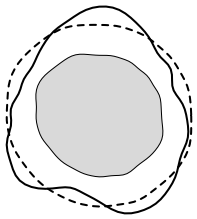

Figure 2.1: The object Y_{t+1} is a stochastic deformation of the object $Y_t \oplus b(0, \mu_t)$ (dashed). The object Y_t is shown grey.

The p-order growth model, introduced in Jónsdóttir and Jensen (2005), is a parametric model for the increment processes $\{V_t\}$. It is inspired by the p-order model for a non-dynamic object Y described by (2.1), cf. Hobolth et al. (2003), where the stochastic fluctuation U^0 around the template is a zero-mean cyclic stationary Gaussian process with an attractive covariance structure.

Cyclic stationary Gaussian processes on $[-\pi, \pi)$ have an interesting geometric interpretation in connection with shape, as we shall see now.

A stochastic process U^0 is a cyclic stationary Gaussian process on $[-\pi, \pi)$ with mean μ and covariance function $\sigma(\phi)$ if and only if there exists $\lambda_k \geq 0$, $k = 0, 1, \ldots$, such that

$$U^0(\phi) = A_0 + \sum_{k=1}^{\infty} (A_k \cos(k\phi) + B_k \sin(k\phi)), \phi \in [-\pi, \pi),$$

where $A_0, A_k, B_k,\ k = 1, 2, \ldots$ are all independent, $A_0 \sim N(\mu, \lambda_0)$, $A_k \sim B_k \sim N(0, \lambda_k)$, $k = 1, 2, \ldots$. Furthermore, the covariance function of U^0 is

$$\sigma(\phi) = \sum_{k=0}^{\infty} \lambda_k \cos(k\phi), \quad \phi \in [-\pi, \pi),$$

and the Fourier coefficients of U^0 are given by

$$\begin{aligned} A_0 &= \frac{1}{2\pi} \int_{-\pi}^{\pi} U^0(\phi) d\phi, \\ A_k &= \frac{1}{\pi} \int_{-\pi}^{\pi} U^0(\phi) \cos(k\phi) d\phi, \\ B_k &= \frac{1}{\pi} \int_{-\pi}^{\pi} U^0(\phi) \sin(k\phi) d\phi. \end{aligned}$$

The Fourier coefficient A_0 determines the average of U^0. The lower order Fourier coefficients determine the global fluctuation of U^0, whereas the higher order Fourier coefficients determine the local fluctuations of U^0. These observations are important in shape theory, as the global and local fluctuations determine the global and local deformation of Y^0. In Hobolth et al. (2001) and Hobolth et al. (2003), the stochastic process U^0 is modelled by the p-order model which is defined by letting $A_0 = A_1 = B_1 = 0$ and

$$A_k \sim B_k \sim N(0, \lambda_k), \quad \lambda_k = (\alpha + \beta(k^{2p} - 2^{2p}))^{-1},$$

for $k = 2, 3, \ldots$. The parameters α and β determine the local and global shape of Y, respectively. The parameter p determines the smoothness of the deformation U^0 and it can be shown that U^0 is $k - 1$ times differentiable where k is the integer satisfying $p \in (k - \frac{1}{2}, k + \frac{1}{2}]$. The coefficients A_1 and B_1 are set to zero, since large values of these coefficients will imply asymmetry of Y with respect to Y^0.

The covariance structure of the p-order model is used to model the increment processes $\{V_t\} = \{\mu_t + U_t\}$. We let $\{U_t\}$ be a series of independent stochastic processes, where U_t follows a p-order model with time dependent parameters, $t = 0, 1, \ldots$. Then

$$V_t(\phi) = \mu_t + \sum_{k=2}^{\infty} (A_{k,t} \cos(k\phi) + B_{k,t} \sin(k\phi)), \quad \phi \in [-\pi, \pi), \tag{2.3}$$

where the Fourier coefficients are all independent, $A_{k,t} \sim B_{k,t} \sim N(0, \lambda_{k,t})$, for $k = 2, 3, \ldots$, $t = 0, 1, \ldots$, and

$$\lambda_{k,t} = (\alpha_t + \beta_t(k^{2p} - 2^{2p}))^{-1}.$$

The parameters satisfy $\mu_t \in \mathbb{R}$, $\alpha_t, \beta_t > 0$ and $p > \frac{1}{2}$. We write $V_t \sim G_p(\mu_t, \alpha_t, \beta_t)$ if V_t is on the form (2.3) and say that $\{V_t\}$ follows a p-order growth model. This approach can be generalised to three dimensions, cf. Jónsdóttir and Jensen (2005).

The overall growth from Y_t to Y_{t+1} is determined by the radial addition parameter μ_t. The parameter p determines the smoothness of the deformation of the expanded object $Y_t \oplus b(0, \mu_t)$ to Y_{t+1}. The parameters α_t and β_t, which are also called the shape parameters, determine the global and local deformation of the expanded object, respectively. Therefore they determine the appearance of the growth at time t.

An interesting subclass of the p-order growth model is obtained by letting the shape parameters be proportional, i.e. $\alpha_t = \gamma\beta_t$. Under this model we can write

$$V_t = \mu_t + \tau_t X_t,$$

where $X = \{X_t\}$ is a series of independent and identically distributed stochastic processes with distribution $G_p(0, \alpha, \beta)$. Note that $\gamma = \frac{\alpha}{\beta}$, $\tau_t = \sqrt{\frac{\beta_t}{\beta}}$ and $Z_t(\phi) \sim N(0, \tau_t^2\sigma^2)$, where

$$\sigma^2 = \sum_{k=2}^{\infty}(\alpha + \beta(k^{2p} - 2^{2p}))^{-1}.$$

The parameters μ_t and τ_t can be chosen arbitrarily, resulting in a variety of different growth patterns for different choices of these parameters. The limiting shape of the object Y_t when $t \to \infty$ may be circular, but there are many other possibilities. In Figure 2.2 and 2.3 two simulated growth patterns are shown as well as the normalised objects of the pattern, which represent the shape of the object. In Figure 2.2 we have $\mu_t = \mu$ and $\tau_t = 1$ for all t and the object becomes more circular as $t \to \infty$, whereas in Figure 2.3 we have $\tau_t = \sum_{i=0}^{t} \mu_i$ and the object becomes more irregular as $t \to \infty$.

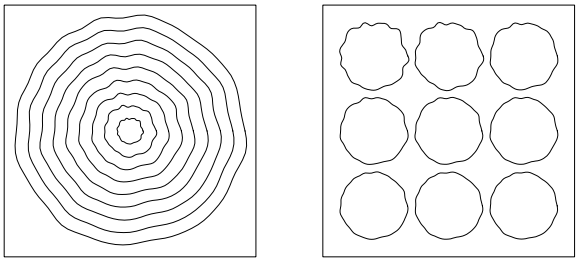

Figure 2.2: Left: Simulated growth pattern under a second-order growth model with proportional shape parameters, $\mu_t = \mu$ and $\tau_t = 1$ for all t. Right: The corresponding normalised profiles, representing the shape of the object.

Other stochastic processes than Gaussian can also be used to model the increment processes $V = \{V_t\}$. The Fourier coefficients of V_t can for example be modelled by Gamma distributed random variables or V_t could by modelled by a log-Gaussian process. It might also be more natural to define the model in terms of the logarithm of the radius vector function, i.e.

$$\log R_{t+1}(\phi) = \log R_t(\phi) + V_t(\phi), \quad \phi \in [-\pi, \pi),$$

where V_t is a cyclic Gaussian stochastic process, resulting in a multiplicative model for the radius-vector function

$$R_{t+1}(\phi) = R_t(\phi)\tilde{V}_t(\phi), \quad \phi \in [-\pi, \pi),$$

where $\tilde{V}_t(\phi)$ is a log-Gaussian stochastic process.

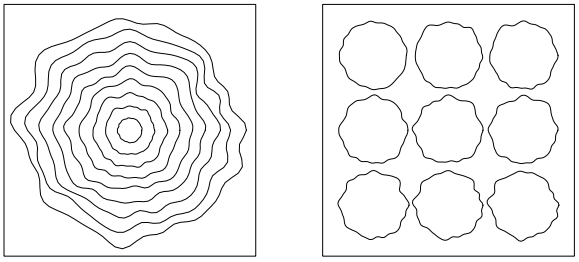

Figure 2.3: Left: Simulated growth pattern under the second-order growth model with proportional shape parameters, $\tau_t = \sum_{i=0}^{t} \mu_t$. Right: The corresponding normalised profiles, representing the shape of the object.

The estimation of parameters in the p-order growth model is not difficult, since the series $V = \{V_t\}$ is assumed to be independent. Let us assume that the data consists of the increments

$$v_t(\frac{2\pi i}{n_t}), i = 0, 1, \ldots, n_t - 1,$$

in n_t direction, equidistant in angle, $t = 0, 1, \ldots, T$. The increments are measured from a reference point z which usually will be taken to be the centre of mass of Y_0.

Since the stochastic process V_t is stationary under the p-order growth model, the size parameter μ_t can be estimated by the average observed increment at time t,

$$\mu_t = \frac{1}{n_t} \sum_{i=0}^{n_t-1} v_t(\frac{2\pi i}{n_t}).$$

The shape parameters $\{(\alpha_t, \beta_t)\}_{t=0}^{T}$ can be estimated by maximising the likelihood function

$$\mathcal{L}(\{(\alpha_t, \beta_t)\}_{t=0}^{T}) = \prod_{t=0}^{T} \mathcal{L}_t(\alpha_t, \beta_t),$$

where $\mathcal{L}_t(\alpha_t, \beta_t)$ is the likelihood function based on the Fourier coefficients $A_{t,k}$ and $B_{t,k}$ of V_t of order $k = 2, \ldots, K_t$. The likelihood $\mathcal{L}_t(\alpha_t, \beta_t)$ is of the same type as the likelihood used for estimation under the p-order model, cf. Hobolth et al. (2001) and Hobolth et al. (2003), i.e.

$$\mathcal{L}_t(\alpha_t, \beta_t) = \prod_{k=2}^{K_t} (\alpha_t + \beta_t(k^{2p} - 2^{2p})) \exp\left(-\frac{a_{t,k}^2 + b_{t,k}^2}{2} (\alpha_t + \beta_t(k^{2p} - 2^{2p})) \right),$$

where $a_{t,k}$ and $b_{t,k}$ are the discrete versions of the integrals

$$A_{t,k} = \frac{1}{\pi} \int_{-\pi}^{\pi} V_t(\phi) \cos k\phi d\phi, \quad B_{t,k} = \frac{1}{\pi} \int_{-\pi}^{\pi} V_t(\phi) \sin k\phi d\phi,$$

$k = 2, 3, \ldots$. Note that the choice of the cut-off value K_t is important. It must not be too large in order to avoid that the estimates are influenced by digitisation effects. If K_t is too small, however, information about the growth pattern may be lost. In practise, we may choose the value of K_t for which our estimates are stable and judge whether the specific choice of K_t is appropriate from visual inspection of simulated growth patterns under the estimated model.

2.1.1 Extensions

The series $\{V_t\}$ of the stochastic deformation processes is assumed to be independent under the p-order growth model. For many applications this is a severe restriction. In Section 3.1 below, an example of the growth of year rings of a tree is given. It can be seen that the increment processes $\{V_t\}$ are strongly correlated. This is usually assumed in dendrochronology, cf. Kronborg (1981). If the number of increments observed is not too small it is possible to model the dependency in the series $\{V_t\}$. A model for the dependency, based on time series, is proposed in Jónsdóttir and Jensen (2005).

The time series extension concerns the subclass of p-order growth models with proportional parameters

$$V_t = \mu_t + \tau_t X_t.$$

Instead of assuming that the series $X = \{X_t\}$ is independent and identically distributed, we assume that $X = \{X_t\}$ is a stationary time series of cyclic Gaussian processes satisfying an ARMA model. Let $W = \{W_t\}$ be a sequence of independent and identically distributed stationary Gaussian processes on $[-\pi, \pi)$, such that $W_t \sim G_p(0, \alpha, \beta)$. Then we assume that the series $X = \{X_t\}$ satisfies the ARMA(r, s) model

$$X_t - \phi_1 X_{t-1} - \cdots - \phi_r X_{t-r} = W_t - \psi_1 W_{t-1} - \cdots \psi_s W_{t-s}.$$

The Fourier coefficients of X of a given order k will follow an ordinary ARMA(r, s) model under this extended p-order growth model, with white noise parameter equal to $(\alpha + \beta(k^{2p} - 2^{2p}))^{-1}$.

A special case of the ARMA(r, s) model is the MA(s) model. Under this model we have that $\phi_1 = \cdots = \phi_r = 0$ and the marginal distribution of V_t is of $G_p(\mu_t, \alpha_t, \beta_t)$ distribution, where

$$\alpha_t = \frac{\alpha}{\tau_t^2(1 + \psi_1^2 + \cdots \psi_s^2)}, \quad \beta_t = \frac{\beta}{\tau_t^2(1 + \psi_1^2 + \cdots \psi_s^2)}.$$

Accordingly, shape parameters are proportional. Note that V_t and $V_{t'}$ are independent here if $|t - t'| > s$.

2.2 Lévy based models

The Lévy based growth models proposed in Jensen et al. (2006) and Jónsdóttir et al. (2006b) describe how the boundary of the object Y_t expands in continuous time. The models are based on Lévy theory, in particular Lévy bases and integration with respect to those. The disadvantage of the p-order growth model, discussed in the last section, is that the temporal correlation structure of the transformation processes $\{V_t\}$ is quite restrictive. The Lévy based growth models, on the contrary, have the advantage that

the temporal correlation structure can be controlled in an elegant way by using the cumulant function of the radius vector function. In the following we let $C(\lambda \ddagger X) = \log \mathbb{E}(e^{i\lambda X})$ denote the cumulant function of a random variable X.

Let $\mathcal{R} = \mathcal{S} \times \mathbb{R}$, where $\mathcal{S} = [-\pi, \pi)$ and let $\mathfrak{A}$ be the Borel σ-algebra of $\mathcal{R}$. Further, let L be an independently scattered random measure on $\mathcal{R}$ with cumulant function represented in Lévy-Khintchine form

$$C(\lambda \ddagger L(A)) = i\lambda a(A) - \frac{1}{2}b(A) + \int_{\mathbb{R}} (e^{i\lambda u} - 1 - i\lambda u \mathbf{1}_{[-1,1]}(u))U(du, A),$$

where a is a signed measure on $\mathcal{R}$, b is a positive measure on $\mathcal{R}$ and $U(du, A)$ is a Lévy measure on $\mathbb{R}$ for fixed $A \in \mathfrak{A}$ and a measure on $\mathfrak{A}$ for fixed du. Then L is said to be a Lévy basis with characteristics (a, b, U). Assume that $U(du, d\xi) = V(du, \xi)\mu(d\xi)$ and that the measures a and b are absolutely continuous with respect to μ with densities $\tilde{a}$ and $\tilde{b}$, respectively. It can be shown that the cumulant function of

$$f \bullet L = \int_{\mathcal{R}} f(\xi) L(d\xi),$$

is given by

$$C(\lambda \ddagger f \bullet L) = \int_{\mathcal{R}} C(\lambda f(\xi) \ddagger L'(\xi))\mu(d\xi). \tag{2.4}$$

Here, $L'(\xi)$ is a random variable with cumulant function

$$C(\lambda \ddagger L'(\xi)) = i\lambda\tilde{a}(\xi) - \frac{1}{2}\lambda^2\tilde{b}(\xi) + \int_{\mathbb{R}} (e^{i\lambda u} - 1 - i\lambda u \mathbf{1}_{[-1,1]}(u))V(du, \xi).$$

Note that if $L'(\xi)$ does not depend on ξ, the densities $\tilde{a}$ and $\tilde{b}$ are constants.

The most common types of Lévy bases are the Gaussian, Poisson, Gamma and Inverse Gaussian Lévy bases. In the case where the random variable $L'(\xi)$ does not depend on ξ, we get that

$$\begin{aligned}
&L(A) \sim N(\nu\mu(A), \sigma^2\mu(A)), && \text{if } L \text{ is Gaussian,}\\
&L(A) \sim \text{Pois}(\mu(A)), && \text{if } L \text{ is Poisson,}\\
&L(A) \sim \Gamma(\beta\mu(A), \alpha), && \text{if } L \text{ is Gamma,}\\
&L(A) \sim \text{IG}(\eta\mu(A), \gamma), && \text{if } L \text{ is Inverse Gaussian,}
\end{aligned}$$

where $\nu \in \mathbb{R}$ and σ, β, α, η, γ are positive parameters.

Two types of Lévy based models are introduced in Jensen et al. (2006) and Jónsdóttir et al. (2006b), the linear Lévy growth model and the exponential Lévy growth model. The linear Lévy growth model is defined by the equation

$$R_t(\phi) = \mu_t(\phi) + \int_{A_t(\phi)} f_t(\xi; \phi) L(d\xi), \quad \phi \in [-\pi, \pi),$$

where $A_t(\phi) \subset \mathcal{S} \times [0, t]$ and $f_t(\xi; \phi)$ and $\mu_t(\phi)$ are deterministic functions, all defined cyclically such that the radius vector function is cyclic. In the following all angular operations will be regarded as cyclic. The set $A_t(\phi)$, called the ambit set associated with the point (t, ϕ), describes the dependency of the past. Its form is usually taken to be

$$A_t(\phi) = \{(\theta, s) \in \mathcal{R} : \theta \in \Delta_s(\phi), s \leq t\},$$

where $\Delta_s(\phi) \subset \mathcal{S}$ is a neighbourhood of ϕ, consisting of those angles at time s influencing the radius vector function at time t and angle ϕ. The deterministic weight function $f_t(\xi;\phi)$ is assumed to be suitable for the integral to exist. Moreover, the four ingredients of the model must be chosen such that $R_t(\phi) > 0$ almost surely.

Using equation (2.4), the cumulant function of the radius vector function $R_t(\phi)$ can be obtained for all $(\phi, t) \in \mathcal{R}$. The cumulant function can then be used to calculate the mean value and covariances of the radius vector function

$$\mathbb{E}(R_t(\phi)) = \mu_t(\phi) + \int_{A_t(\phi)} f_t(\xi;\phi)\mathbb{E}(L'(\xi))\mu(d\xi), \tag{2.5}$$

$$\mathrm{Cov}(R_t(\phi), R_{t'}(\phi')) = \int_{A_t(\phi)\cap A_{t'}(\phi')} f_t(\xi;\phi) f_{t'}(\xi;\phi')\mathbb{V}(L'(\xi))\mu(d\xi), \tag{2.6}$$

$(\phi, t), (\phi', t') \in \mathcal{R}$. If the random variable $L'(\xi) = L$ does not depend on ξ and the weight functions are constants, $f_t(\xi;\phi) \equiv f$, the covariance only depends on the μ-measure of the intersection of the two ambit sets up to a constant, i.e.

$$\mathrm{Cov}(R_t(\phi), R_{t'}(\phi')) \propto \mu(A_t(\phi) \cap A_{t'}(\phi')).$$

The exponential Lévy growth model is defined by the equation

$$R_t(\phi) = \exp\left(\mu_t(\phi) + \int_{A_t(\phi)} f_t(\xi;\phi)L(d\xi)\right), \quad \phi \in [-\pi, \pi),$$

where the four ingredients are as in the linear Lévy growth model above. This definition ensures that the radius vector function is always positive.

If $R_t(\phi)$ follows an exponential Lévy growth model, it is possible to get an explicit expression for n-point correlations

$$\mathbb{E}(R_{t_1}(\phi_1)\cdots R_{t_n}(\phi_n)),$$

using equation (2.4). Usually, 2-point correlators are used to model a specific correlation structure if $R_t(\phi)$ follows an exponential Lévy growth model. The 2-point correlators are defined by

$$\mathrm{Corr}\big(R_t(\phi), R_{t'}(\phi')\big) = \frac{\mathbb{E}\big(R_t(\phi)R_{t'}(\phi')\big)}{\mathbb{E}\big(R_t(\phi)\big)\mathbb{E}\big(R_{t'}(\phi')\big)}.$$

It can be shown that

$$\mathrm{Corr}\big(R_t(\phi), R_{t'}(\phi')\big) = \exp\left(\int_{A_t(\phi)\cap A_{t'}(\phi')} \log\left(\mathrm{Corr}\big(e^{f_t(\xi;\phi)L'(\xi)}, e^{f_{t'}(\xi;\phi')L'(\xi)}\big)\right)\mu(d\xi)\right),$$

where the integrand can be calculated using the the cumulant function of $L'(\xi)$. As in the linear case, the correlators become much more simple in the case where the random variable $L'(\xi) = L$ does not depend on ξ and the weight functions are constant $f_t(\xi;\phi) = f$. Then,

$$\mathrm{Corr}\big(R_t(\phi), R_{t'}(\phi')\big) = \exp\big(\tilde{C}\mu(A_t(\phi) \cap A_{t'}(\phi'))\big),$$

where $\tilde{C} = C(-2if \ddagger L') - 2C(-if \ddagger L')$. Higher order correlations can also be expressed through different overlaps of ambit sets under these assumptions.

Other formulations of the Lévy growth models can be considered, e.g. models for the time derivative of $R_t(\phi)$ or $\ln(R_t(\phi))$. In these cases the induced model for the radius vector function is again a Lévy growth model. A model for the time derivative can also be extended by using a more complicated stochastic representation of the ambit set. If the stochastic time transformation $t \to R_t(\phi)$ is non-decreasing almost surely for all $\phi \in \mathcal{S}$, the stochastic ambit set can be represented by

$$\tilde{A}_t(\phi) = \{(s\cos\theta, s\sin\theta) : (\theta, u) \in A_t(\phi), R_u(\theta) = s\}.$$

This random set is a subset of Y_t. Ambit sets of this type depend on the radius vector function itself and therefore the model equation

$$R'_t(\phi) = \int_{\tilde{A}_t(\phi)} f_t(\xi;\phi) Z(d\xi), \tag{2.7}$$

becomes a stochastic differentiable equation. This stochastic differential equation has a geometric intuitive meaning in some applications and a connection to cellular models, described in Section 4. In the simple case where Z is a Poisson measure, the model equation (2.7) can be written on the form

$$R'_t(\phi) = \sum_{(x,y)\in N\cap\tilde{A}_t(\phi)} f_t((x,y);\phi),$$

where N is a Poisson point process on $\mathbb{R}^2$. The points of N lying within Y_t can be thought of as cells, all contributing to the growth at time t. Under this model, the cells in $\tilde{A}_t(\phi) \subset Y_t$ determine the growth rate at time t and angle ϕ. In relation to tumour growth, the intensity function of the Poisson point process N could, for example, determine the concentration of cells.

Various growth dynamics for the stochastic object Y_t can be obtained under this model setup. The four ingredients, the Lévy basis L, the ambit sets $A_t(\phi)$, the weight functions $f_t(\xi;\phi)$ and the function $\mu_t(\phi)$ determine the growth dynamics. For example, the local and global fluctuations of the boundary of Y_t can be controlled by the size of the ambit sets. The weight function $f_t(\xi;\phi)$ may also control the direction of growth by letting the weight function $f_t(\xi;\phi)$ depend on the angle ϕ. In the next section, some examples of the induced covariance structure for the radius vector function are given.

Different choices of Lévy bases can result in different appearance of growth. Given means and variances of the radius vector function, different growth patterns can be produced without changing the ambit sets and weight functions, simply by changing the underlying Lévy basis.

As a more concrete example, consider a Gaussian Lévy model given by

$$R_t(\phi) = \mu_t + \int_{A_t(\phi)} f_t(\xi;\phi) Z(d\xi),$$

where $Z(A) \sim N(0, \sigma^2\mu(A))$, $A \in \mathfrak{A}$ and an Inverse Gaussian Lévy model given by

$$\tilde{R}_t(\phi) = \tilde{\mu}_t + \int_{A_t(\phi)} f_t(\xi;\phi) \tilde{Z}(d\xi),$$

where $\tilde{Z}(A) \sim \mathrm{IG}(\eta\mu(A), \gamma)$, $A \in \mathfrak{A}$. Furthermore assume that

$$\int_{A_t(\phi)} f_t(\xi; \phi)\mu(d\xi)$$

does not depend on ϕ. If the mean and the variance of $R_t(\phi)$ and $\tilde{R}_t(\phi)$ are the same for all $(\phi, t) \in \mathcal{R}$, then

$$\tilde{\mu}_t = \mu_t - \frac{\eta}{\gamma} \int_{A_t(0)} f_t(\xi; 0)\mu(d\xi),$$
$$\sigma^2 = \frac{\eta}{\gamma^3}.$$

For a fixed value of σ^2, different choices of the parameters of the Inverse Gaussian basis can be chosen and therefore different appearances of the growth pattern can be obtained. Figure 2.4 shows a density plot for two different Inverse Gaussian variables $\mathrm{IG}(\eta, \gamma)$ where the parameters η and γ fulfil $\frac{\eta}{\gamma^3} = 1$. One of the distributions has a heavy right tail while the other is approximately symmetric.

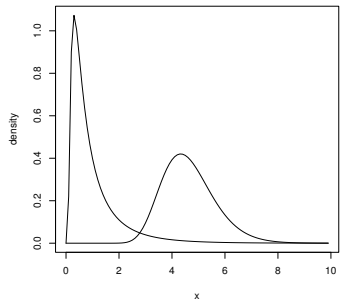

Figure 2.4: The density of two Inverse Gaussian variables $\mathrm{IG}(\eta, \gamma)$, where η and γ fulfil $\frac{\eta}{\gamma^3} = 1$.

2.2.1 The induced covariance structure

We will now give some examples of the different covariance structures that can be obtained by choosing special forms of the ambit sets and weight functions. We will concentrate on the linear Lévy growth model in this section but remind that the results will hold for the logarithm of the radius vector function if it follows an exponential Lévy model.

We will now assume that the random object Y_t is statistically isotropic in the sense that

$$\{R_t(\phi) : \phi \in [-\pi, \pi)\} \sim \{R_t(\phi + \phi_0) : \phi \in [-\pi, \pi)\},$$

for all $\phi_0 \in [-\pi, \pi)$. Under this assumption estimates can be obtained using spatial averaging, even when we observe only one growth pattern.

Let us consider a linear Lévy growth model where

$$\mathbb{V}(L'(\xi))\mu(d\xi) = g(s)dsd\theta,$$

the ambit sets have full angular range

$$A_t(\phi) = [-\pi, \pi) \times [t - T(t), t]$$

for all $(\phi, t) \in \mathcal{R}$ and weight functions are on the form

$$f_t(\xi; \phi) = a_0^t(s) + \sum_{k=1}^{\infty} a_k^t(s) \cos(k(\phi - \theta)).$$

Here, $\xi = (\theta, s)$. Under these assumptions it can be shown that the spatial covariances of the radius vector function R_t are given by

$$\mathrm{Cov}(R_t(\phi), R_t(\phi')) = 2\lambda_0^t + \sum_{k=1}^{\infty} \lambda_k^t \cos(k(\phi - \phi')),$$

where

$$\lambda_k^t = \pi \int_{t-T(t)}^{t} (a_k^t(s))^2 g(s) ds, \quad k = 0, 1, \ldots,$$

and the temporal covariances of $R(\phi)$ are given by

$$\mathrm{Cov}(R_t(\phi), R_{t'}(\phi)) = 2\tau_0(t, t') + \sum_{k=1}^{\infty} \tau_k(t, t'),$$

where

$$\tau_k(t, t') = \pi \int_{t \cap t'} a_k^t(s) a_k^{t'}(s) g(s) ds,$$

and

$$t \cap t' = \begin{cases} [\max(t - T(t), t' - T(t')), \min(t, t')] & \text{if } \max(t - T(t), t' - T(t')) \leq \min(t, t') \\ \emptyset & \text{otherwise.} \end{cases}$$

Note that the spatial covariance only depends on the distance between the angles ϕ and ϕ', whereas the temporal covariances do not depend on the angle ϕ.

If the Fourier coefficients of the weight function are of the form $a_k^t(s) = a_k^t$, then the correlation function ρ_t of the stochastic process R_t is completely determined by the weight function

$$\rho_t(\phi) = \frac{\mathrm{Cov}(R_t(0), R_t(\phi))}{\sqrt{\mathbb{V}(R_t(0))\mathbb{V}(R_t(\phi))}} = \frac{2(a_0^t)^2 + \sum_{k=1}^{\infty} (a_k^t)^2 \cos(k\phi)}{2(a_0^t)^2 + \sum_{k=1}^{\infty} (a_k^t)^2}.$$

Moreover, if $a_k^t = b_t c_k$, then $\rho_t(\phi)$ does not depend on t and the correlation function of $R(\phi) = \{R_t(\phi) : t \geq 0\}$ is determined by the temporal extension $T(t)$ of the ambit set at time t and the function g,

$$\rho(t, t') = \frac{\mathrm{Cov}(R_t(\phi), R_{t'}(\phi))}{\sqrt{\mathbb{V}(R_t(\phi))\mathbb{V}(R_{t'}(\phi))}} = \frac{\int_{t \cap t'} g(s) ds}{\sqrt{\int_{t-T(t)}^{t} g(s) ds \int_{t'-T(t')}^{t'} g(s) ds}}.$$

A dynamic version of the p-order model described in Hobolth et al. (2003) can be obtained under the above assumptions, by letting $a_0^t(s) = a_1^t(s) = 0$ and $a_k^t(s) =$

$(\alpha_t + \beta_t(k^{2p} - 2^{2p}))^{-\frac{1}{2}}$, for all $k = 2, 3, \ldots$. This will induce a specific temporal covariance structure. A dynamic model of this type was discussed in Section 2.1. There, the increment process $\{V_t\}$ was modelled by a dynamic p-order model where it was assumed that $\{V_t\}$ was independent.

As mentioned earlier, the shape of the object at any specific time point is important in many applications. For a Lévy growth model of the type considered above the Fourier coefficients will also follow a linear Lévy growth model. Moreover, if L is a Gaussian Lévy basis, we get that

$$R_t(\phi) = A_0^t + \sum_{k=1}^{\infty}(A_k^t \cos(k\phi) + B_k^t \sin(k\phi)), \quad \phi \in [-\pi, \pi), \tag{2.8}$$

where $A_0 = \{A_0^t\}_{t\geq 0}$, $A_k = \{A_k^t\}_{t\geq 0}$ and $B_k = \{B_k^t\}_{t\geq 0}$, $k = 1, 2, \ldots$ are independent Gaussian stochastic processes. The process A_0 has covariance function $2\tau_0(t, t')$ and the processes $A_k \sim B_k$ have covariance functions $\tau_k(t, t')$, $k = 1, 2, \ldots$. Likelihood based inference is quite simple in this case. Assume that the stochastic processes A_0, A_k and B_k, $k = 1, 2, \ldots, K$ are observed at n time points, $t_1, \ldots, t_n$. These $n(2K + 1)$ variables can by separated into $2K+1$ mutually independent classes, where in each class we have n dependent random variables. By suitable reorganisation of the variables we can write down the covariance matrix for the collection of Gaussian random variables. The covariance matrix will be on the form

$$\Sigma = \text{diag}(2\Sigma_0, I_2 \otimes \Sigma_1, I_2 \otimes \Sigma_2, \ldots, I_2 \otimes \Sigma_K),$$

where $\Sigma_k = \{\tau_k(t_i, t_j)\}$ is a $n \times n$ covariance matrix, I_2 is the 2×2 identity matrix and $A \otimes B$ denotes the Kronecker product of the matrices A and B.

A different approach to study the covariance structure is to consider constant weight functions and more complicated ambit sets. In the case where the random variable $L'(\xi)$ does not depend on ξ, it can for example be shown that a special type of an extended p-order model can be obtained under this set-up, cf. Jónsdóttir et al. (2006b).

Unless the underlying Lévy basis is Gaussian, likelihood based inference does not seem to be feasible. Usually, inference based on mean and either covariances or two-point correlators is used, depending on which type of Lévy growth model is being studied.

3 Applications

In this section we will give examples of applications of the models considered in Section 2. We study three different biological growth patterns, cf. Figure 3.1. In Figure 3.1 (a) a growth pattern of human breast cancer cell islands is represented. This data set was studied originally by Cressie (1991a). Figure 3.1 (b) shows a growth pattern of year rings of a tree and Figure 3.1 (c) shows a growth pattern of brain tumour cell islands, cf. Brú et al. (1998).

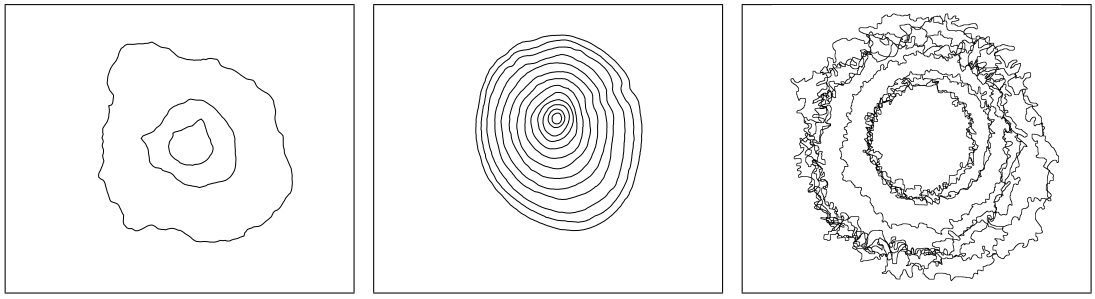

(a) (b) (c)

Figure 3.1: Growth patterns. (a) Contours of human breast cancer cell islands, cf. Cressie and Hulting (1992). (b) Year rings from a Danish pine tree. (c) Contours of brain tumour cell islands, cf. Brú et al. (1998).

We will also give an example of how the p-order model discussed in Section 2.1 can be used for improving statistical methods for analysing data based on circular systematic sampling in stereology.

3.1 The p-order growth model

The data sets in Figure 3.1 (a) and 3.1 (b) have been studied using the second-order growth model. The analysis of the human breast cancer cell islands was presented in Jónsdóttir and Jensen (2005). The parameters of the second-order growth model μ_t, α_t and β_t were estimated and the model fitted the data well, according to the model control procedures developed in Jónsdóttir and Jensen (2005). Simulation based methods were used to evaluate the hypothesis of independent increments, i.e. whether the V_t's are independent. The results are shown in Figure 3.2 for the tumour growth data shown in Figure 3.1 (a). The second row shows conditional simulations under

the second-order growth model with μ_t, α_t and β_t replaced by its estimates $\hat{\mu}_t$, $\hat{\alpha}_t$ and $\hat{\beta}_t$. The simulations are conditional in the sense that when simulating R_{t+1} we use the observed r_t and then simulate V_t according to the distribution $G_2(\hat{\mu}_t, \hat{\alpha}_t, \hat{\beta}_t)$. The third row shows simulations under the second-order growth model with independent increments. The data set and the simulations in the second and third row in Figure 3.2 look very similar, indicating that the hypothesis of independent increments is likely to be accepted. In the case where the number of observed increments is large, a more sophisticated test of the hypothesis can be constructed, e.g. using a runs test.

Figure 3.3 shows simulations for the year rings data of the same kind as shown in Figure 3.2 for the tumour growth data. The difference between the simulations under the second-order growth model with independent increments and the data indicates that the assumption of independent increments may not hold. If the number of observed increments had been larger, the dependency in the series $\{V_t\}$ could have been studied by e.g. using the extensions of the p-order model suggested in Section 2.1.1.

It does not seem feasible to describe the growth pattern in Figure 3.1 (c) by the p-order growth model since the profiles are very irregular on a local scale. Also, sudden outburst of the profiles are present which is impossible to model using Gaussian processes with covariance structures based on a p-order model.

3.2 Lévy based growth models

The data set in Figure 3.1 (c) has been analysed in Schmiegel (2005) and Jónsdóttir et al. (2006b), using an exponential Lévy based growth model. The model was defined by

$$R_t(\phi) = \exp\left(\mu_t + \alpha(t)\int_{t-T(t)}^{t-t_0(t)}\int_{-\pi}^{\pi}\cos(\theta-\phi)L(ds\times d\theta) + \beta(t)\int_{t-t_0(t)}^{t}\int_{\phi-h_t(s-t+t_0(t))}^{\phi+h_t(s-t+t_0(t))}L(ds\times d\theta)\right), \quad (3.1)$$

where $h_t : [0, t_0(t)] \to \mathbb{R}$ is a deterministic and decreasing function with $h_t(t_0(t)) = 0$ and L is a Gaussian Lévy basis. Accordingly, the ambit set is on the following form

$$A_t(\phi) = C_t \cup B_t(\phi),$$

where C_t and $B_t(\phi)$ are the following disjoint sets

$$C_t = [-\pi, \pi) \times [t - T(t), t - t_0(t)),$$
$$B_t(\phi) = \{(\theta, s) : |\theta - \phi| \leq h_t(s - t + t_0(t)), s \in [t - t_0(t), t]\},$$

and

$$f_t((s,\theta);\phi) = \begin{cases} \alpha(t)\cos(\theta-\phi), & \text{if } (s,\theta) \in C_t, \\ \beta(t), & \text{if } (s,\theta) \in B_t(\phi). \end{cases}$$

Note that $B_t(\phi)$ concerns the immediate past while C_t concerns the more distant past. The concrete analysis was done by using a linear function h_t on the form

$$h_t(s) = \frac{\phi_0(t)}{2} - \frac{\phi_0(t)}{2t_0(t)}s, \quad s \in [0, t_0(t)],$$

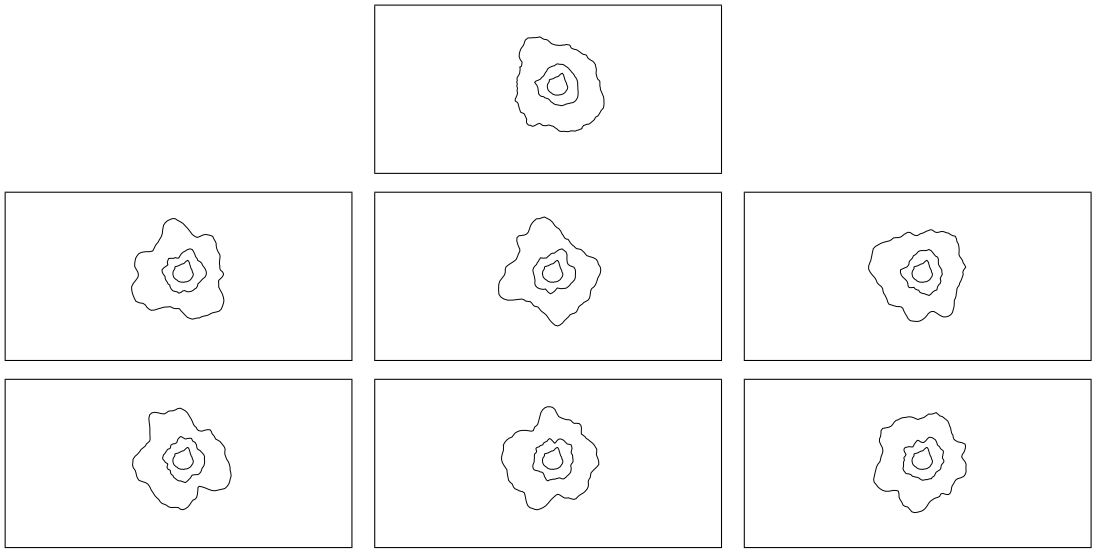

Figure 3.2: The human breast cancer cell islands. The data set (top), conditional simulations under the second-order growth model with μ_t, α_t and β_t replaced by the maximum likelihood estimates (second row) and simulations under the second-order growth model with independent increments and μ_t, α_t and β_t replaced by the maximum likelihood estimates (third row).

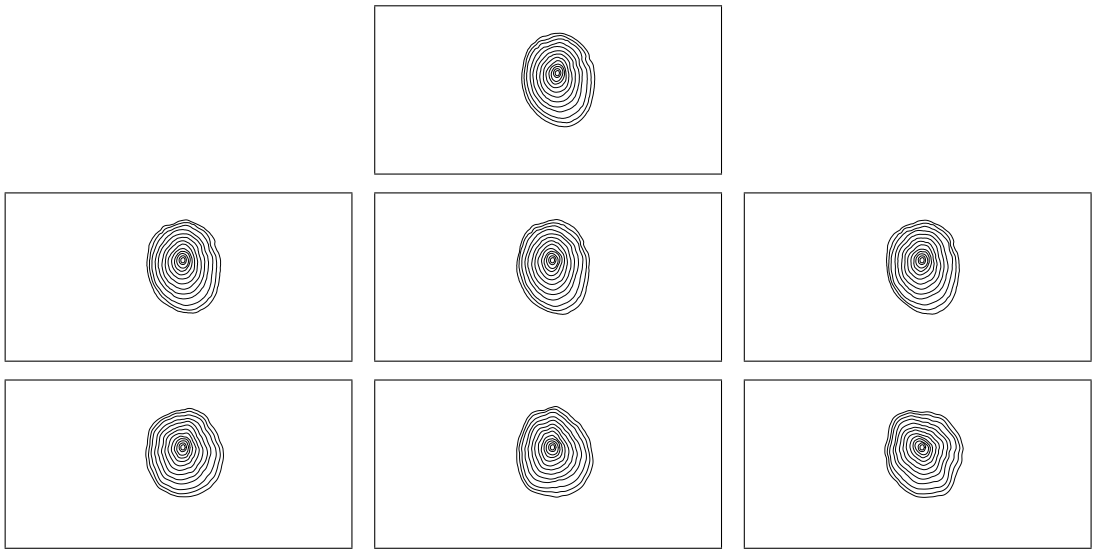

Figure 3.3: The year rings of a tree. The data set (top), conditional simulations under the second-order growth model with μ_t, α_t and β_t replaced by the maximum likelihood estimates (second row) and simulations under the second-order growth model with independent increments and μ_t, α_t and β_t replaced by the maximum likelihood estimates (third row).

and the parameters of the model were estimated using mean and covariance estimation for three time points, $t = 21, 25, 55$. The data and the simulation under the model using the estimated parameters are shown in Figure 3.4. Notice that even though the overall appearance is similar for the data and the simulation, sudden outbursts are present in the data set which are not seen for the simulated profiles.

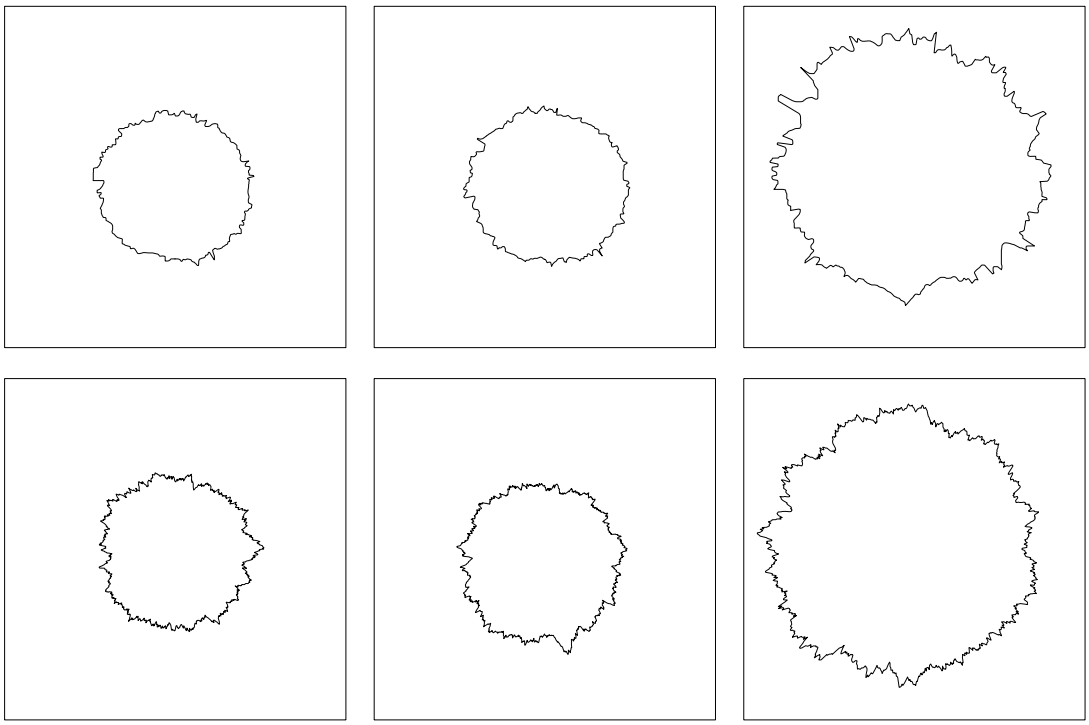

Figure 3.4: Top: The data from Brú et al. (1998) at time points $t = 21, 25, 51$. Bottom: Simulations of the model (3.1) for time points $t = 21, 25, 51$, using a Gaussian Lévy basis.

For this reason we tried in Jónsdóttir et al. (2006b) to use Gamma and Inverse Gaussian bases instead of the Gaussian, since these distributions are known to have heavier tails than the Gaussian. The parameters of the underlying basis are chosen such that the mean and variance of $R_t(\phi)$ are the same as when the Gaussian basis was used. As mentioned in Section 2.2, there are a lot of possibilities. Two simulations using different Inverse Gaussian bases are shown in Figure 3.5. The first row shows a simulation very similar to the Gaussian simulation, but more outbursts are observed in the second row. The difference is due to the fact that the two Inverse Gaussian bases chosen have very different right tails.

3.3 Circular systematic sampling using the p-order model

It turns out that shape modelling, using the p-order model, has an important application in a quit different area, error prediction in circular systematic sampling, cf. Hobolth and Jensen (2002) and Jónsdóttir et al. (2006a). Hobolth and Jensen (2002) also discusses recent design-based approaches, cf. Gual-Arnau and Cruz-Orive (2000)

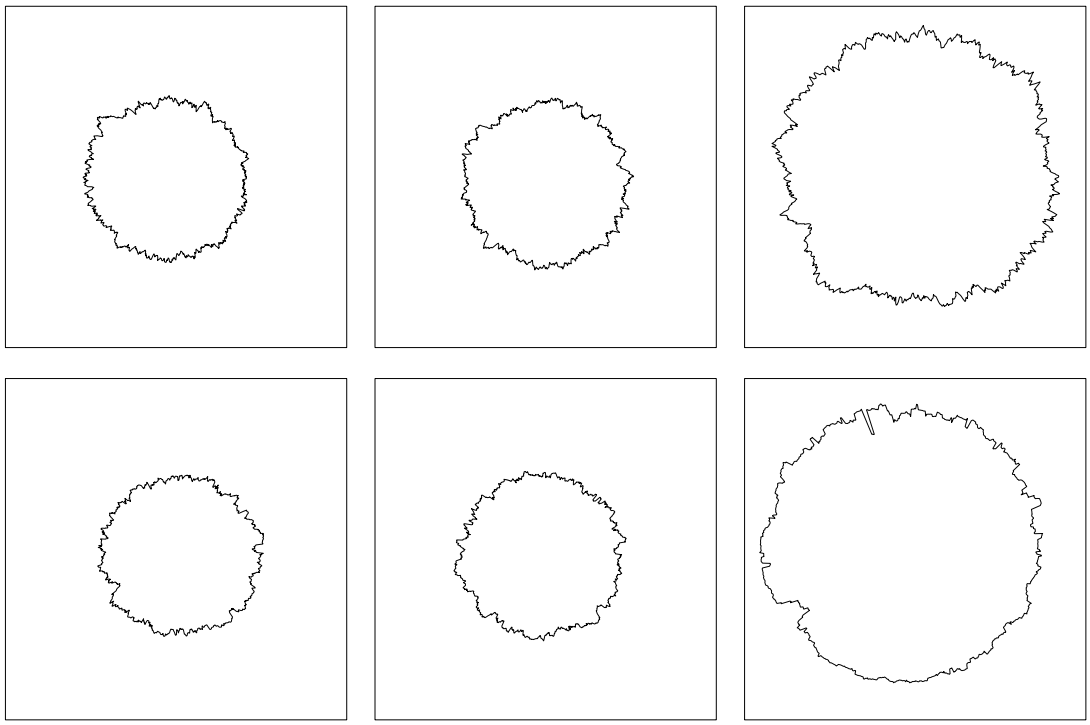

Figure 3.5: Simulations of the model (3.1) for time points $t = 21, 25, 51$, using two different types of Inverse Gaussian Lévy basis.

and Cruz-Orive and Gual-Arnau (2002), where a global polynomial model for the covariogram is used for variance estimation.

The model-based setting discussed here concerns the estimation of an integral

$$Q = \frac{1}{2\pi} \int_{-\pi}^{\pi} F(\phi) d\phi,$$

where $F = \{F(\phi) : \phi \in [-\pi, \pi)\}$ is a cyclic stationary stochastic process with mean μ and covariance function

$$\sigma(\phi) = \lambda_0 + 2 \sum_{k=1}^{\infty} \lambda_k \cos(k\phi).$$

It is assumed that the process F is square integrable and piecewise continuous. The integral Q could for example be a geometric property of an object, such as boundary length or area. The estimator of Q to be studied, based on n observations of F, is of the form

$$\hat{Q}(F, \phi, n) = \frac{1}{n} \sum_{j=0}^{n-1} F\Big(2\pi\big(\phi + \frac{j}{n}\big)\Big),$$

where $\phi \in [0, 1)$ and the aim is to estimate the prediction error

$$\mathbb{E}(\hat{Q}(F, \phi, n) - Q)^2 = 2 \sum_{k=1}^{\infty} \lambda_{kn},$$

using likelihood-based methods, given that F follows a specific parametric model.

Assume that F is a cyclic stationary Gaussian process. As mentioned in Section 2.1 the coefficients λ_k determine the global fluctuations of F for small k, whereas for large k they determine the local fluctuations of F. Hobolth and Jensen (2002) discuss a parametric model where the Fourier coefficients of σ are given by

$$\begin{aligned} \lambda_k &= \frac{(2p)!}{k^{2p}}\beta, \quad k = 1, 2, \ldots, \\ \lambda_0 &= \beta_0 - 2\sum_{k=1}^{\infty}\lambda_k, \end{aligned} \tag{3.2}$$

where p is a positive integer and the remaining parameters are chosen such that $\lambda_k \geq 0$ for $k = 0, 1, \ldots$. The prediction error under this model will only depend on the parameter β and as shown in Hobolth and Jensen (2002) the maximum likelihood estimator of β is unbiased with minimum variance, given the n observations of F. The prediction error can then be estimated by

$$(-1)^{p-1}(2\pi)^{2p}B_{2p}\frac{1}{n^{2p}}\hat{\beta},$$

where B_{2p} is a Bernoulli number and $\hat{\beta}$ is the maximum likelihood estimator of β.

This parametric model is inspired by the design-based approach of Gual-Arnau and Cruz-Orive (2000), where the above parametrisation of the covariance function is used to model the Fourier coefficients of the covariogram of a realisation of F. The model defined by (3.2) is a special case of the more general model of p-order type, where the Fourier coefficients of σ are given by

$$\lambda_0 \geq 0, \quad \lambda_k = (\tilde{\alpha} + \tilde{\beta}k^{2p})^{-1}, \quad k = 1, 2, \ldots, \tag{3.3}$$

where $\tilde{\beta} > 0$, $\tilde{\alpha} + \tilde{\beta} > 0$ and $p > \frac{1}{2}$. As mentioned in Section 2.1, p determines the smoothness of F, whereas the parameters $\tilde{\alpha}$ and $\tilde{\beta}$ determine the global and local fluctuations of F, respectively.

If the variable Q determines the area of a star-shaped object Y with radius vector function R with respect to a point $z \in \mathbb{R}^2$, we can take $F = R^2$. Note that small values of $\tilde{\alpha}$ imply large global fluctuations of F, implying that the object Y is expected to have some deviations from circular shape on a global scale. Also it should be noted that large values of λ_1 will produce an object Y which is asymmetric with respect to z. The model given by (3.2) can be obtained by letting $\tilde{\alpha} = 0$ and $\tilde{\beta} = ((2p)!\beta)^{-1}$ and using the intuitive interpretation of the parameters $\tilde{\alpha}$ and $\tilde{\beta}$ in the case where $F = R^2$, it seems natural to include the extra parameter $\tilde{\alpha}$ in the model.

We suggest using a p-order model as described in Section 2.1, with the following reparametrisation

$$\begin{aligned} &\lambda_0 \geq 0, \quad \lambda_1 = 0 \\ &\lambda_k = (\tilde{\alpha} + \tilde{\beta}(k^{2p} - 2^{2p}))^{-1}, \quad k = 2, 3, \ldots, \end{aligned} \tag{3.4}$$

where $\tilde{\alpha}, \tilde{\beta} > 0$. For a fixed p and given n observations of F, μ can be estimated by the empirical mean of the observations and the parameters $\tilde{\alpha}$ and $\tilde{\beta}$ can be estimated using maximum likelihood estimation of the same type as discussed in Section 2.1. See

also Hobolth et al. (2003). If the estimates are denoted by $\hat{\alpha}$ and $\hat{\beta}$, the prediction error can be estimated by

$$2\sum_{k=1}^{\infty}(\hat{\alpha}+\hat{\beta}((kn)^{2p}-2^{2p}))^{-1}. \tag{3.5}$$

The parameter p can also be estimated using maximum likelihood estimation.

In Jónsdóttir et al. (2006a) a simulation study is presented to assess the statistical properties of the estimator (3.5) of the prediction error compared to earlier design based predictions of Gual-Arnau and Cruz-Orive (2000) and Cruz-Orive and Gual-Arnau (2002). The preliminary conclusions are that (3.5) is superior.

4 Cellular models

This section contains a discussion of models based on spatio-temporal point processes. A short review of recent models for inhomogeneous point patterns will be given and it will be shown how these models can be extended to a spatio-temporal framework. A short discussion of dynamic random compact sets will follow.

A number of applications fit into the spatio-temporal cellular models discussed in this section. This includes e.g. modelling of plant populations, occurrences of earthquakes, fires and diseases. It should be noted that many spatial point patterns analysed, using purely spatial models, are indeed cumulative point patterns. It is therefore of interest to identify spatio-temporal point process model for which the cumulative spatial point process has specified properties like a given intensity function.

The potential of formulating tumour growth models via spatio-temporal processes has been shown as early as in Cressie and Hulting (1992).

4.1 Spatio-temporal point processes

Let χ be a bounded subset of $\mathbb{R}^d$, with positive volume $|\chi|$. Consider a spatio-temporal point process $Z = \{(\xi_j, t_j)\}$ on $S = \chi \times \mathbb{R}_+$ and let Z_t be the restriction of Z to $S_t = \chi \times (0, t]$, i.e.

$$Z_t = \{(\xi_j, t_j) \in Z : t_i \leq t\}.$$

Assume that the projections of Z on χ and $\mathbb{R}_+$ are both simple processes. Since the projection on $\mathbb{R}_+$ is simple, there exists a natural ordering of the time points of $\{t_j\}$,

$$t_1 < t_2 < \cdots < t_n < \cdots .$$

We use this ordering later on. Furthermore, we use the short notation $\xi_{(n)}, t_{(n)}$ for the first n points, $(\xi_1, t_1), \ldots, (\xi_n, t_n)$, of the process Z.

The projections of Z and Z_t on χ, are given by

$$X = \{\xi_j : (\xi_j, t_j) \in Z\}, \quad X_t = \{\xi_j : (\xi_j, t_j) \in Z_t\},$$

respectively, and are also called the cumulative spatial point processes. Note that the random set X_t is growing in time since $X_t \subseteq X_{t'}$ for $t \leq t'$.

The distribution of Z_t can be specified by simply writing down the density of Z_t with respect to the unit rate Poisson process on S_t. An alternative and a more natural way is to specify the distribution by two families of conditional probability densities. The first family

$$\{p_n(t|\xi_{(n-1)}, t_{(n-1)}) : n \in \mathbb{N}\}$$

describes the arrival times of Z, while the second family

$$\{f_n(\xi|\xi_{(n-1)}, t_{(n-1)}, t_n) : n \in \mathbb{N}\},$$

describes the spatial positions of Z. More precisely, the density $p_n(\cdot|\xi_{(n-1)}, t_{(n-1)})$ describes the distribution of the n-th time point given the first $n-1$ points of the process Z and has support (t_{n-1}, ∞). The density $f_n(\cdot|\xi_{(n-1)}, t_{(n-1)}, t_n)$, on the other hand, describes the distribution of the spatial point at the arrival time t_n given the first $n-1$ points of the process Z and the n-th time point t_n. This density has support χ. Daley and Vere-Jones (2002) treat in detail spatio-temporal point processes defined using this mechanism.

Let $S_n(\cdot|\xi_{(n-1)}, t_{(n-1)})$ be the survival function and $h_n(\cdot|\xi_{(n-1)}, t_{(n-1)})$ be the hazard rate of $p_n(\cdot|\xi_{(n-1)}, t_{(n-1)})$. For convenience we define

$$\lambda_g(t) = h_n(t|\xi_{(n-1)}, t_{(n-1)}), \qquad \text{if } t_{n-1} < t \leq t_n, \tag{4.1}$$

$$f^\star(\xi|t) = f_n(\xi|\xi_{(n-1)}, t_{(n-1)}, t_n), \quad \text{if } t_{n-1} < t \leq t_n. \tag{4.2}$$

It can be shown that the density of Z_t can be written as

$$g_{Z_t}(z) = \exp(t|\chi|)g_n(z)S_{n+1}(t|\xi_{(n)}, t_{(n)}),$$

where

$$g_n(z) = \prod_{j=1}^{n} p_j(t_j|\xi_{(j-1)}, t_{(j-1)})f_j(\xi_j|\xi_{(j-1)}, t_{(j-1)}, t_j).$$

By using the functions $\lambda_g(t)$ and $f^\star(\xi|t)$, we obtain an alternative expression for the density,

$$g_{Z_t}(z) = \exp\left(-\int_{S_t}(\lambda_g(s)f^\star(\eta|s) - 1)d\eta ds\right)\prod_{j=1}^{n}\lambda_g(t_j)f^\star(\xi_j|t_j). \tag{4.3}$$

Note that $\lambda_g(t)f^\star(\xi|t)d\xi dt$ can be interpreted as the conditional probability of observing a point at (ξ, t) given the previous history of the process and a waiting time for the n-th point at least up till t.

The simplest example of a spatio-temporal point process is the Poisson process with intensity function λ. This process has density function

$$g_{Z_t}(z) = \exp\left(-\int_{S_t}(\lambda(\eta, s) - 1)d\eta ds\right)\prod_{i=1}^{n}\lambda(\xi_i, t_i).$$

Assume that

$$\int_t^\infty \int_\chi \lambda(\eta, s)d\eta ds = \infty \text{ for all } t \geq 0.$$

Then

$$\lambda_g(t) = \int_\chi \lambda(\eta, t)d\eta,$$

$$f^\star(\xi|t) = \frac{\lambda(\xi, t_n)}{\lambda_g(t_n)}$$

and the conditional distribution of the n-th time point is given by

$$p_n(t|\xi_{(n-1)}, t_{(n-1)}) = \lambda_g(t) \exp\left(-\int_{t_{n-1}}^{t} \lambda_g(s)ds\right), \quad t > t_{n-1}.$$

If the intensity function is on the form $\lambda(\xi, t) = \lambda(\xi)$, we get that given the history $(\xi_{(n-1)}, t_{(n-1)})$, the waiting time to the n-th time point T_n, $T_n - t_{n-1}$, is exponentially distributed with parameter $\int_\chi \lambda(\eta)d\eta$. More generally, given $(\xi_{(n-1)}, t_{(n-1)})$,

$$\int_{t_{n-1}}^{T_n} \lambda_g(s)ds$$

is exponential distributed with parameter 1. Note that the density of the n-th spatial position is proportional to $\lambda(\xi, t_n)$. The distribution of the cumulative process X_t is also Poisson with intensity function

$$\lambda^t(\xi) = \int_0^t \lambda(\xi, s)ds.$$

Furthermore, for all $t' < t$, $X_{t'}$ can be obtained via thinning of X_t, using the retaining probability

$$p_{t',t}(\xi) = \frac{\lambda^{t'}(\xi)}{\lambda^t(\xi)}. \tag{4.4}$$

Cox processes are an important tool describing clustered point patterns. A spatio-temporal Cox process on S is simply a spatio-temporal Poisson point process with random intensity function Λ, i.e. its intensity function is $\lambda(\xi, t) = \mathbb{E}(\Lambda(\xi, t))$. The cumulative process X_t is also a Cox process driven by the random intensity function

$$\Lambda^t(\xi) = \int_0^t \Lambda(\xi, s)ds,$$

i.e. its intensity is given by $\lambda^t(\xi) = \mathbb{E}(\Lambda^t(\xi))$. As for the spatio-temporal Poisson processes, $X_{t'}$ can be obtained from X_t if $t' < t$. This is done in the same manner as before, via independent thinning with retaining probability given by (4.4).

A large class of spatio-temporal Cox processes can be obtained by modelling the random intensity function by a Lévy based spatio-temporal model, cf. Jónsdóttir et al. (2006b). Assume that L is a positive Lévy basis on $(S, \mathcal{B}(S))$ with characteristics $(a, 0, U)$, where $\mathcal{B}(S)$ is the Borel σ-algebra of S. Let Z be a spatio-temporal Cox process with random intensity function

$$\Lambda(\xi, t) = m(\xi, t) + \int_S f_t((\eta, s); \xi)L(ds \times d\eta), \quad (\xi, t) \in S,$$

where $m(\xi, t)$ and $f_t((\eta, s); \xi)$ are deterministic functions, chosen such that $\Lambda(\xi, t) \geq 0$ and $(\xi, t) \to \Lambda(\xi, t)$ is locally integrable, almost surely. Using the Lévy-Ito representation for positive Lévy basis, we can write

$$\Lambda(\xi, t) = m(\xi, t) + a_0(S) + \sum_{(u,\eta)\in N} u f_t(\eta; \xi),$$

where N is a Poisson process on $\mathbb{R}_+ \times S$ with intensity measure U and

$$a_0(S) = \int_S f_t((\eta, s); \xi) a(d\eta \times ds) - \int_S \int_0^1 u f_t((\eta, s); \xi) U(du, d\eta \times ds).$$

There are enormous possibilities of defining different Cox processes using this representation. As an example, let $m(\xi, t) = -a_0(S)$ and $f_t((\eta, s), \xi) = k((\eta, s), (t, \xi))$, where $k((\eta, s), \cdot)$ is a probability density on S. Then Z is a spatio-temporal shot noise Cox process. As mentioned above, the cumulative spatial processes will also be Cox processes, but not necessarily shot-noise Cox processes. For more details on spatial shot noise Cox processes, cf. Møller (2003). Brix (1998), Brix (1999) and Brix and Chadoeuf (2002) study an important type of shot-noise Cox processes, the shot-noise G Cox processes, to model weed data.

Another example, using Lévy based spatio-temporal models, is a Cox process Z with random intensity

$$\Lambda(\xi, t) = \exp\Big(m(\xi, t) + \int_S f_t((\eta, s); \xi) L(ds \times d\eta)\Big),$$

where L is a Gaussian Lévy basis on S, i.e. $L(A) \sim N(a(A), b(A))$ for all $A \in \mathcal{B}(S)$. Here, the functions $m(\xi, t)$ and $f_t((\eta, s); \xi)$ are chosen such that the random field $(\xi, t) \to \Lambda(\xi, t)$ is locally integrable almost surely. This type of process is called a log-Gaussian spatio-temporal Cox process. Møller et al. (1998) and Brix and Møller (2001) use a special type of log-Gaussian Cox processes to study weed data.

Note that the intensity function and the pair correlation function of a spatio-temporal Cox process can easily be calculated using the cumulant function of $\Lambda(\xi, t)$, i.e.

$$C(\lambda \ddagger \Lambda(\xi, t)) = \log\Big(\mathbb{E}\big(\exp(i\lambda\Lambda(\xi, t))\big)\Big),$$

if $\Lambda(\xi, t)$ follows a spatio-temporal Lévy model. For more details on spatio-temporal Lévy models, see Jónsdóttir et al. (2006b).

4.2 Extensions of inhomogeneous spatial point processes

Models for inhomogeneous point processes have been studied quite intensively in recent years. Most of these models introduce inhomogeneity into a homogeneous template point process. Ogata and Tanemura (1986) and Stoyan and Stoyan (1998) suggest to introduce inhomogeneity into Gibbs and Markov models by location dependent first order interaction. Quite different approaches are inhomogeneity by independent location dependent thinning and transformation of the template process, cf. Baddeley et al. (2000) and Jensen and Nielsen (2000). Inhomogeneity may also be constructed such that the resulting inhomogeneous process is a locally scaled version of the template process, cf. Hahn et al. (2003).

A spatial point process X is said to be a pairwise interaction point process if its density is on the form

$$f_X(x) \propto \prod_{\xi \in x} \phi(\xi) \prod_{\{\xi, \eta\} \subset x} \phi(\{\xi, \eta\}), \tag{4.5}$$

where ϕ is an interaction function, i.e. ϕ is a nonnegative function such that the right hand side of (4.5) is integrable with respect to the unit rate Poisson point process on χ. The range of interaction is defined by

$$R = \inf\{r > 0 : \text{ for all } \{\xi, \eta\} \subset S, \phi(\{\xi, \eta\} = 1 \text{ if } |\xi - \eta| > r\}.$$

A simple way of constructing a spatio-temporal extension of a pairwise interaction process is to write down its density. Let

$$z = \{(\xi_1, t_1), \ldots, (\xi_n, t_n)\} \text{ and } x = \{\xi_1, \ldots, \xi_n\}.$$

An obvious suggestion of a density for the spatio-temporal extension would be

$$f_{Z_t}(z) \propto \prod_{(\xi,t)\in z} \lambda(\xi, t) \prod_{\{\xi,\eta\}\subset x} \phi(\{\xi, \eta\}),$$

if the interactions are purely spatial. Such processes are applicable if the spatial interaction does not change in time.

If the first-order interaction function is on the form

$$\lambda(\xi, t) = \lambda_1(\xi)\lambda_2(t),$$

then it can be shown that the cumulative process X_t is a pairwise interaction point process with density

$$f_{X_t}(x) \propto \prod_{\xi\in x} a(t)\lambda_1(\xi) \prod_{\{\xi,\eta\}\subset x} \phi(\{\xi, \eta\})$$

with respect to the unit rate Poisson point process on χ, where

$$a(t) = \int_0^t \lambda_2(s)ds.$$

It can further be shown that if $t' < t$, the cumulative point process $X_{t'}$ can be obtained by independent thinning of X_t.

More generally, any given point process X on χ can be used to construct a spatio-temporal point process model using backwards temporal thinning. Assume that X has intensity function λ. We can define a spatio-temporal point process based on X by letting

$$Z = \{(\xi, T_\xi) : \xi \in X\},$$

where conditionally on X, $\{T_\xi\}_{\xi\in X}$ are independent and T_ξ has probability density p_ξ. The cumulative process X_t has intensity function

$$\lambda^t(\xi) = \lambda(\xi) \int_0^t p_\xi(s)ds,$$

and for all $t' < t$, $X_{t'}$ can be obtained from X_t using independent location dependent thinning, with retention probability

$$p_{t',t}(\xi) = \frac{\int_0^{t'} p_\xi(s)ds}{\int_0^t p_\xi(s)ds}.$$

A backwards temporal thinning of this type implies that for small t, X_t may look like a realisation of a Poisson point process. Note also that the inhomogeneous version of the K-function defined in Baddeley et al. (2000) will be the same for all X_t, $t > 0$.

An alternative procedure for extending inhomogeneous spatial point processes to a spatio-temporal framework is to extend expressions for the Papangelou conditional intensity, used in a purely spatial context, to expressions for the conditional intensity $\lambda_g(\cdot)f^\star(\cdot|\cdot)$ of the spatio-temporal point process. In Jensen et al. (2006), this approach and the approach based on backwards thinning have been tried out in the case where the purely spatial point process is a locally scaled Strauss process, cf. Hahn et al. (2003). Simulated processes can be seen in Figure 4.1 and 4.2.

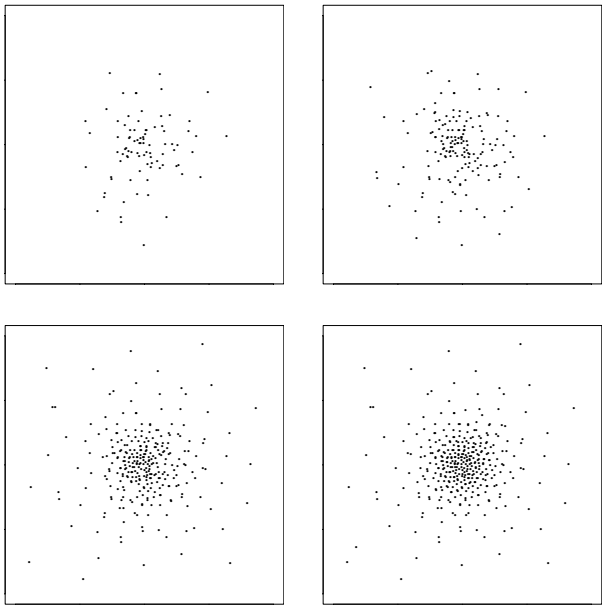

Figure 4.1: Result of a simulation of a backwards thinning of a locally scaled Strauss process on $[-1, 1]^2$. The figure shows the cumulative point patterns at time points $t = 2, 4, 8, 12$.

4.3 Dynamic random compact sets

Spatio-temporal point processes may be used to construct models for growing objects $Y_t \subset \mathbb{R}^d$. One approach is to let the object at time t consist of the union of some random compact sets centred at the points born at time t or before. More precisely, let Z be a spatio-temporal point process. The object at time t is then

$$Y_t = \bigcup_{(\xi,s)\in Z, s\leq t} (\xi \oplus \Xi_\xi), \tag{4.6}$$

where conditionally on Z, $\{\Xi_\xi\}$ is a series of independent and identically distributed random compact sets centred at the origin with distribution $\mathcal{Q}$. Here $\oplus$ denotes the Minkowski sum,

$$\xi \oplus \Xi_\xi = \{\xi + \eta : \eta \in \Xi_\xi\}.$$

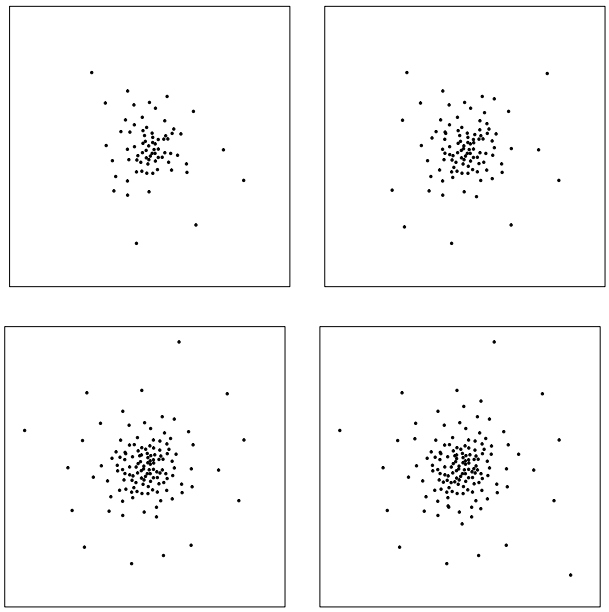

Figure 4.2: Result of a simulation on $[-1,1]^2$ of the spatio-temporal extension using conditional intensities and probabilities. The figure shows the cumulative point patterns at time point $t = 2, 4, 8, 12$.

The object Y_t is clearly increasing in time in the sense that $Y_{t'} \subset Y_t$ if $t' < t$. In the case where the point process Z is Poisson, the model (4.6) is a dynamic version of the well known Boolean model. For a detailed discussion on Boolean models and random compact sets, see Molchanov (2005).

A more general model for Y_t can be obtained by letting the series of random compact sets be independent, but with distribution depending on the spatial position ξ and/or the birth time of ξ. This means that

$$Y_t = \bigcup_{(\xi,s)\in Z, s\leq t} (\xi \oplus \Xi_{(\xi,s)}),$$

where conditionally on Z, $\{\Xi_{(\xi,s)}\}$ is a series of independent random compact sets centred at the origin, where $\Xi_{(\xi,s)}$ has distribution $\mathcal{Q}_{(\xi,s)}$.

Deijfen (2003) studies a model similar to the model in (4.6) with the random set $\Xi_\xi = b(0, R_\xi)$ for all ξ. Here, the R_ξ's are independent and identically distributed and $b(0, R_\xi)$ denotes the sphere in $\mathbb{R}^d$ with radius R_ξ centred at the origin. The asymptotic shape of the object Y_t is shown to be circular. This is also the case for many stochastic models for tumour growth, cf. Richardson (1973), Schruger (1979), Bramson and Griffeath (1980), Bramson and Griffeath (1981) and Durret and Ligget (1981).

In Cressie and Laslett (1987), Cressie (1991a), Cressie (1991b), and Cressie and Hulting (1992) a Boolean model is used to model tumour growth patterns. Their model is a discrete time model of Markov type defined by

$$Y_t = \bigcup_{\xi\in Y_{t-1}\cap\Pi} b(\xi, R_\xi),$$

where Π is a homogeneous Poisson process on χ and conditionally on Π, $\{R_\xi\}$ are independent and identically distributed variables with support $\mathbb{R}_+$. They also consider other point processes than Poisson and other random compact sets than balls and establish in that way a relation to interacting particle systems, cf. Ligget (1986).

Another type of cellular models are the cellular automaton models. A cellular automaton model is a discrete model on a regular grid of cells defined on χ. The models are discrete time models and the state of the cells at time t is a function of its neighbouring cells at the previous time, where different neighbouring relations can be used. A cell at time t is updated according to a predefined rule based on its neighbour cells. Qi et al. (1993) and Kansal et al. (2000) study cellular automaton models in relation to tumour growth.

5 Non-stationary spatial survival analysis

This section contains further results on modelling of random sets. They have consequences for the modelling and analysis of non-stationary point processes. The results have not yet been put into a spatio-temporal framework. First, we need to recall some material on spatial survival analysis.

Consider a stationary random compact set Y in $\mathbb{R}^d$ observed within a compact and regular window W. The empty space function F for the random set Y is given by the distribution function of the distance from the origin to the random set Y, i.e.

$$F(r) = \mathbb{P}(\rho(0, Y) \leq r), \quad r > 0,$$

where

$$\rho(\xi, Y) = \inf\{|\xi - \eta| : \eta \in Y\}.$$

The survival function of $\rho(0, Y)$ is defined by $S(r) = 1 - F(r)$. If the empty space function is differentiable for all $r > 0$, we let f be the derivative of F and define the hazard rate of $\rho(0, Y)$ by

$$\lambda(r) = \frac{f(r)}{S(r)}, \quad r > 0,$$

which implies that

$$S(r) = \exp\left(-\int_0^r \lambda(s)ds\right), r > 0.$$

Given the information $Y \cap W$ and W, estimates of these functions can be used to check for complete randomness of the spatial pattern. This is done by comparing the estimated function to its theoretical counterpart of a completely random spatial pattern.

One of the most simple estimators for the empty space function F is based on minus sampling. This estimator is called the reduced-sample estimator. It is unbiased, but has the disadvantage that it is not necessarily a distribution function.

The distance from a fixed point to the nearest point of the random set is censored by the distance to the observation window. Based on the analogy with censored survival data, Baddeley and Gill (1997) propose a Kaplan-Meier type estimator of F

$$\hat{F}(r) = 1 - \frac{|Y \setminus W|_k}{|W|_k} \exp\left(-\int_0^r \hat{\lambda}(s)ds\right),$$

where $\hat{\lambda}$ is the ratio-unbiased estimate of λ,

$$\hat{\lambda}(r) = \frac{|\partial(Y_{\oplus r}) \cap W_{\ominus}|_{k-1}}{|W_{\ominus r} \setminus Y_{\oplus r}|_k}.$$

Here, $\partial(Y)$ denotes the boundary of Y, $|\cdot|_k$ is the k-dimensional Lebesgue measure,

$$A_{\oplus r} = \{\xi \in \mathbb{R}^d : \rho(\xi, A) \leq r\},$$
$$A_{\ominus r} = \{\xi \in \mathbb{R}^d : \rho(\xi, A^{\mathrm{c}}) > r\},$$

and $^{\mathrm{c}}$ denotes the compliment. This estimator is known to be more efficient than the reduced-sample estimator.

Let us now consider the case where Y is not necessarily stationary. Then, we need a local version of the empty space function defined by

$$F_\xi(r) = \mathbb{P}(\rho(\xi, Y) \leq r), \quad r > 0,$$

i.e. the distribution function of the random variable $\rho(\xi, Y)$. The local version of the survival function is $S_\xi(r) = 1 - F_\xi(r)$ and if the local empty space function is differentiable for all $\xi \in \mathbb{R}^d$ and $r > 0$, we let f_ξ be the derivative of F_ξ and define the local hazard rate by

$$\lambda_\xi(r) = \frac{f_\xi(r)}{S_\xi(r)}, \quad r > 0.$$

The question is now whether we can find some non-parametric or semi-parametric methods to analyse non-stationary data sets using methods from classical survival analysis as has been done in the stationary case.

5.1 Hazard rate models

The classical Cox proportional hazard model and accelerated lifetime model for hazard rates are popular models in classical survival analysis. These models describe how the survival distributions depend on known covariates. The Cox proportional hazard model is defined by

$$\lambda_\xi(r) = g(\beta, s(\xi))\lambda(r),$$

where λ is some baseline hazard rate, $g(\beta, s(\xi))$ is a positive function independent of r which can incorporate the effect of a vector valued covariate $s : \mathbb{R}^d \to \mathbb{R}^k$ and β is a k-dimensional vector of parameters. The accelerated lifetime model is defined by

$$\lambda_\xi(r) = g(\beta, s(\xi))\lambda(g(\beta, s(\xi))),$$

where g and β are as above, but the baseline hazard is assumed to come from some class of parametric distributions. Different forms of g can be used, but we will consider the exponential form $g(\beta, s(\xi)) = \exp(\beta \cdot s(\xi))$ which is the most commonly used.

These methods can be adapted to spatial statistics, where the covariates are a known or an observed function of ξ, e.g. temperature, soil type or altitude at position ξ, or a function derived from another spatial pattern.

Hazard rate models of this type have an interesting intuitive appeal in spatial statistics. Consider a stationary random closed set with empty space function F and

hazard rate λ. A union $Y^\star$ of n independent copies of the stationary random closed set Y will have empty space function and hazard rate

$$F^\star(r) = 1 - (1 - F(r))^n, \quad \lambda^\star(r) = n\lambda(r), \quad r > 0,$$

respectively. If $Y^\star$ is a scaled version of Y, $Y^\star = cY$, $c > 0$, the empty space function and hazard rate of $Y^\star$ will be

$$F^\star(r) = F\left(\frac{r}{c}\right), \quad \lambda^\star(r) = \frac{1}{c}\lambda\left(\frac{r}{c}\right), \quad r > 0,$$

respectively. These types of transformations of the hazard rate occur in the Cox proportional hazard model and the accelerate lifetime model and the two models have therefore the intuitive appeal of describing non-stationary change of intensity and scale, respectively.

Typically, the properties of the local empty space function can not be obtained for known models for non-stationary random closed sets. As an example, it seems impossible to explicitly calculate the empty space function for the models for inhomogeneous point patterns discussed in Section 4.2. Until now, we have not been able to find any random compact set such that the local hazard rate fulfils the accelerated lifetime model. A special class of germ-grain models for non-stationary random compact sets, however, fulfils a Cox proportional hazard model for the local hazard rate with $s(\xi) = \xi$. This model is defined by letting

$$Y = \bigcup_{\xi \in X} \{\xi \oplus \Xi_\xi\},$$

where X is a non-stationary Poisson process on $\mathbb{R}^d$ with a log-linear intensity function

$$\gamma(\xi) = \alpha \exp(\beta \cdot \xi), \quad \alpha > 0, \ \ \beta \in \mathbb{R}^d$$

and $\{\Xi_\xi\}_{\xi \in X}$ is a sequence of independent and identically distributed, random compact sets that are independent of the process X and have distribution $\mathcal{Q}$. The local empty space function and the local hazard rate of Y are given by

$$F_\xi(r) = 1 - (1 - F_0(r))^{\exp(\beta \cdot \xi)}, \quad \lambda_\xi(r) = \exp(\beta \cdot \xi)\lambda_0(r),$$

respectively, where F_0 and λ_0 are the empty space function and hazard rate at 0.

A special case of this germ-grain model is the non-stationary Poisson process with intensity function γ. In this case, explicit equations can be obtained for the local empty space function and hazard rate

$$\begin{aligned} F_\xi(r) &= 1 - \exp\left(-\frac{2\pi r \alpha \exp(\beta \cdot \xi)}{|\beta|} I_1(r|\beta|)\right), \\ \lambda_\xi(r) &= 2\pi \exp(\beta \cdot \xi) \alpha r I_0(r|\beta|), \end{aligned}$$

where I_ν is the modified Bessel function of the first kind of order ν.

5.2 Estimation methods

The partial likelihood is usually used to estimate the parameters in the Cox proportional hazard model and non-parametric methods are used to estimate the baseline hazard. Like in survival analysis we define failure times and censoring indicators by

$$t(\xi) = \min\{\rho(\xi, Y), \rho(\xi, \partial W)\}, \quad d(\xi) = \mathbf{1}[\rho(\xi, Y) \leq \rho(\xi, \partial W)],$$

respectively. Observing $(t(\xi), d(\xi))$ for some points ξ in a regular lattice L on W, we use the standard methods to estimate β and λ_0. This estimation method is, however, quite fragile. The standard partial likelihood estimation holds for independent survival times. This is, on the other hand, not the case for spatial data. Note that $(t(\xi), d(\xi))$ can be observed at every point $\xi \in W$. Therefore, a continuous analogue of the partial likelihood estimation method is needed. The discrete version of the partial likelihood method will, however, probably always be used in practise. This involves a number of open questions concerning the dependence of the data and asymptotic properties of the estimators.

The Cox proportional hazard model only includes the parameter β and therefore an estimator of α is missing. If the observed random compact set is modelled by a germ-grain model and the grains do not intersect, a reasonable estimator of the parameter α can be found by solving the equation

$$\mathbb{E}(n(Y \cap W)) = \alpha \int_W \exp(\hat{\beta} \cdot \eta) d\eta$$

for α, where $n(x)$ denotes the cardinality of x and $\hat{\beta}$ is the estimate of β. This implies that the estimator of α is

$$\hat{\alpha} = n_W \left(\int_W \exp(\hat{\beta} \cdot \eta) d\eta \right)^{-1},$$

where n_W is the observed number of grains in the window W. Clearly, this will hold if Y is a point process.

5.3 Application to non-stationary point processes

Assume that Y is a non-stationary point process and consider fitting a Cox proportional hazard model to its local hazard rate. A test for complete randomness of the point process Y can be performed by comparing the estimated baseline hazard rate $\hat{\lambda}_0$ to the hazard rate λ_0 of the Poisson process with intensity function $\gamma(y) = \hat{\alpha} \exp(\hat{\beta} \cdot y)$, where $\hat{\alpha}$ and $\hat{\beta}$ are the estimated parameters under the model. The deviations between the two hazard rates can give an indication of clustering or regularity. At least for small values of r, $\hat{\lambda}_0(r) \leq \lambda_0(r)$ indicates clustering while $\hat{\lambda}_0(r) \geq \lambda_0(r)$ indicates regularity. The estimation method described in the last section was used to fit a Cox proportional hazard model to data simulated from a Poisson point process on the unit square window with intensity function $\gamma(x, y) = 300 \exp(-2x)$. Figure 5.1 shows the estimated local hazard rate $(0.5, 0.5)$ (full line) and the local hazard rate at $(0.5, 0.5)$ of a Poisson process with intensity $\hat{\alpha} \exp(\hat{\beta} \cdot \xi)$ (dotted line), where $\hat{\alpha}$ and $\hat{\beta}$ are the estimators of α and β. The figure indicates that the non-stationary Poisson process is a good fit to the simulated data, as expected.

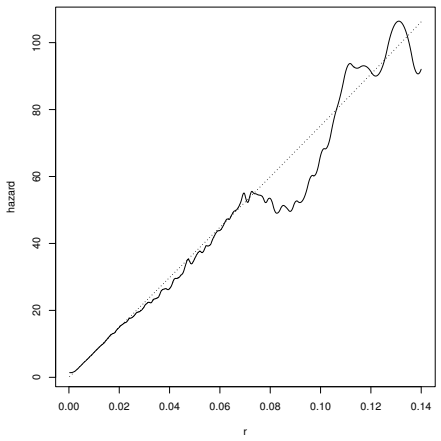

Figure 5.1: The estimated local hazard rate $\hat{\lambda}_{(0.5,0.5)}$ for the simulated data (full line) and the local hazard rate of an inhomogeneous Poisson process with intensity $\hat{\alpha}\exp(\hat{\beta}\cdot(0.5,0.5))$ (dotted line).

We also fitted the Cox proportional hazard model to real data. The data is a subset of a larger data set which has been analysed in e.g. Cressie (1991b) and consists of location of adult Longleaf Pine trees in a 200×200 metre region, see Figure 5.2 (left). Figure 5.2 (right) shows a plot of the estimated local hazard rate $\hat{\lambda}_{(100,100)}$ for the data (full line) and the local hazard rate at $(100, 100)$ of a Poisson process with intensity $\hat{\alpha}\exp(\hat{\beta}\cdot\xi)$ (dotted line), where $\hat{\alpha}$ and $\hat{\beta}$ are the estimators of α and β. Note that the estimated local hazard rate cannot be interpreted for large values of r due to the finite size of the window. By comparing the two hazard rates for smaller values of r, one can see an indication of clustering of the trees.

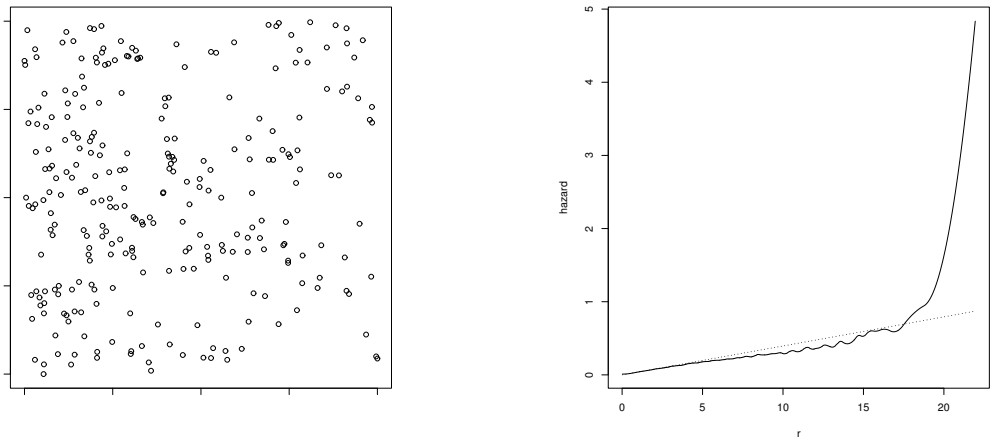

Figure 5.2: Left: The locations of adult Longleaf Pine trees. Right: A plot of the estimated local hazard rate for the adult Longleaf Pine tree data at $(100, 100)$ (full line) and the local hazard rate at $(100, 100)$ of an inhomogeneous Poisson process with intensity $\hat{\alpha}\exp(\hat{\beta}\cdot\xi)$ (dotted line).

6 Conclusions

In this thesis, we have studied two classes of spatio-temporal models that can be used in the modelling of growing patterns. The first model class is the supracellular models describing the movement of the boundary of the growing object. Important tools are here the theory of Lévy bases and the p-order models from shape theory. Growing cancer cell islands and growth patterns of tree year rings are analysed, using these models. The second model class is the cellular models, based on spatio-temporal point processes. Here, a main issue is extension of existing models for spatial point processes to a spatio-temporal framework. The thesis also contains further results on modelling of random sets, using spatial survival analysis.

Bibliography

Baddeley, A. J. and Gill, R. D. (1997). Kaplan–Meier estimators of interpoint distance distributions for spatial processes. *Ann. Statist.*, 25:263–292.

Baddeley, A. J., Møller, J., and Waagepetersen, R. P. (2000). Non- and semiparametric estimation of interaction in inhomogeneous point patterns. *Statistica Neerlandica*, 54:329–350.

Bramson, M. and Griffeath, D. (1980). The Asymptotic Behaviour of a Probabilistic Model for Tumour Growth. In Jager, W., Rost, H., and Tautu, P., editors, *Biological Growth and Spread*, number 38 in Springer Lecture Notes in Biomathematics, pages 165–172.

Bramson, M. and Griffeath, D. (1981). On the Williams-Bjerknes tumour growth model, I. *Ann. Prob.*, 9:173–185.

Brix, A. (1998). *Spatial and Spatio-temporal Models for Weed Abundance*. PhD thesis, Royal Veterinity and Agricultural University, Copenhagen.

Brix, A. (1999). Generalized gamma measures and shot-noise Cox processes. *Adv. Appl. Prob.*, 31:929–953.

Brix, A. and Chadoeuf, J. (2002). Spatio-temporal modelling of weeds by shot-noise G Cox processes. *Biom. J.*, 44:83–99.

Brix, A. and Møller, J. (2001). Space-time multitype log Gaussian Cox processes with a view to modelling weeds. *Scand. J. Statist.*, 28:471–488.

Brú, A., Pastor, J. M., Fernaud, I., Brú, I., Melle, S., and Berenguer, C. (1998). Super-rough dynamics of tumour growth. *Physical Review Letters*, 81:4008–4011.

Chaplain, M. A. J., Singh, G. D., and McLachlan, J. C. (1999). *On Growth and Form: Spatio-temporal Pattern Formation in Biology*. Wiley, Chichester.

Cressie, N. (1991a). Modelling growth with random sets. In Possolo, A. and Hayward, C., editors, *Spatial Statistics and Imaging*, pages 31–45. IMS Lecture Notes. Proceedings of the 1988 AMS-IMS-SIAM Joint Summer Research Conference.

Cressie, N. (1991b). *Statistics for Spatial Data*. John Wiley & Sons, New York.

Cressie, N. and Hulting, F. L. (1992). A spatial statistical analysis of tumor growth. *J. Amer. Statist. Assoc.*, 87:272–283.

Cressie, N. and Laslett, G. M. (1987). Random set theory and problems of modelling. *SIAM Review*, 87:272–283.

Cruz-Orive, L. M. and Gual-Arnau, X. (2002). Precision of circular systematic sampling. *J. Microsc.*, 207:225–242.

Daley, D. J. and Vere-Jones, D. (2002). *An Introduction to the Theory of Point Processes. Volume I: Elementary Theory and Methods.* Springer, New York, second edition.

Deijfen, M. (2003). Asymptotic shape in a continuum growth model. *Adv. Appl. Prob. (SGSA)*, 35:303–318.

Durret, L. and Ligget, T. (1981). The shape of the limit set in Richardsons growth model. *Ann. Prob.*, 9:186–193.

Grenander, U., Chow, Y., and Keenan, D. M. (1991). Hands: A Pattern Theoretic Study of Biological Shapes. Research notes on Neural Computing. Springer, Berlin.

Grenander, U. and Miller, M. (1994). Representations of knowledge in complex systems (with discussion). *J.R. Statist. Soc. B*, 56:549–603.

Gual-Arnau, X. and Cruz-Orive, L. M. (2000). Systematic sampling on the circle and on the sphere. *Adv. Appl. Prob. (SGSA)*, 34:484–490.

Hahn, U., Jensen, E. B. V., van Lieshout, M. N. M., and Nielsen, L. S. (2003). Inhomogeneous point processes by location dependent scaling. *Adv. Appl. Prob. (SGSA)*, 35(2):319–336.

Hobolth, A. and Jensen, E. B. V. (2002). A note on design-based versus model-based variance estimation in stereology. *Adv. Appl. Prob. (SGSA)*, 34:484–490.

Hobolth, A., Pedersen, J., and Jensen, E. B. V. (2001). A deformable template model, with special reference to elliptical templates. Research report no. 17, Laboratory for Computational Stochastics, University of Aarhus.

Hobolth, A., Pedersen, J., and Jensen, E. B. V. (2003). A continuous parametric shape model. *Ann. Inst. Statist. Math.*, 55:227–242.

Jensen, E. B. V., Jónsdóttir, K. Ý., Schmiegel, J., and Barndorff-Nielsen, O. E. (2006). Spatio-temporal modelling – with a view to biological growth. To appear in *Statistics of Spatio-Temporal Systems*, Monographs on Statistics and Applied Probability, Chapman & Hall/CRC.

Jensen, E. B. V. and Nielsen, L. S. (2000). Inhomogeneous Markov point processes by transformation. *Bernoulli*, 6:761–782.

Jónsdóttir, K. Ý., Hoffmann, L. M., Hobolth, A., and Jensen, E. B. V. (2006a). On error prediction in circular systematic sampling. To appear in *J. Microsc.*

Jónsdóttir, K. Ý. and Jensen, E. B. V. (2005). Gaussian radial growth. *Image Analysis & Stereology*, 24:117–26.

Jónsdóttir, K. Ý., Schmiegel, J., and Jensen, E. B. V. (2006b). Lévy based growth models. To appear as Thiele Research Report.

Kansal, A. R., Torquato, S., Harsh, G. R., Chiocca, E. A., and Deisboeck, T. S. (2000). Simulated brain tumor growth dynamics using a three-dimensional cellular automaton. *J. Theor. Biol.*, 203:367–382.

Kronborg, D. (1981). Distribution of crosscorrelations in two-dimensional time series, with application to dendrochronology. Research report no. 72, Department of Theoretical Statistics, Institute of Mathematics, University of Aarhus.

Ligget, T. M. (1986). *Interacting Particle Systems*. Springer, New York.

Molchanov, I. S. (2005). *Theory of Random Sets.* Springer, London.

Møller, J. (2003). Shot noise Cox processes. *Adv. Appl. Prob. (SGSA)*, 35:614–640.

Møller, J., Syversveen, A. R., and Waagepetersen, R. P. (1998). Log Gaussian Cox processes. *Scand. J. Statist.*, 25:451–482.

Ogata, Y. and Tanemura, M. (1986). Likelihood estimation of interaction potentials and external fields of inhomogeneous spatial point patterns. In Francis, I. S., Manly, B. F. J., , and C., L. F., editors, *Proc. Pacific Statistical Congress*, pages 150–154. Elsevier.

Qi, A. S., Zheng, X., Du, C. Y., and An, B. S. (1993). A cellular automaton model of cancerous growth. *J. Theor. Biol.*, 161:1–12.

Richardson, D. (1973). Random growth in a tessellation. *Proc. Camb. Phil. Soc.*

Schmiegel, J. (2005). Self-scaling tumor growth. To appear in *Physica A*.

Schruger, K. (1979). On the asymptotic geometrical behaviour of a class of contact interaction processes with a monotone infection rate. *Zeitschrift für Wahrscheinlichkeitstherorie und verwandte Gebiete*, 48:35–48.

Stoyan, D. and Stoyan, H. (1998). Non homogeneous Gibbs process models for forestry – a case study. *Biometrical Journal*, 40:521–531.

Thompson, D. W. (1917). *On Growth and Form.* Cambridge University Press, Cambridge.

Paper A

Jónsdóttir, K.Ý. and Jensen, E.B.V. (2005).
Gaussian radial growth.
Image Analysis & Stereology, 24:117–26.

Gaussian radial growth

Kristjana Ýr Jónsdóttir and Eva B. Vedel Jensen
University of Aarhus

Abstract

The growth of planar and spatial objects is often modelled using one-dimensional size parameters, e.g. volume, area or average width. We take a more detailed approach and model how the boundary of a growing object expands in time. We mainly consider star-shaped planar objects. The model can be regarded as a dynamic deformable template model. The limiting shape of the object may be circular but this is only one possibility among a range of limiting shapes. An application to tumour growth is presented. A 3D version of the model is presented and an extension of the model, involving time series, is briefly touched upon.

Keywords: Fourier expansion, Gaussian process, growth pattern, periodic stationary, radius vector function, shape, star-shaped objects, transformation

1 Introduction

Modelling of biological growth patterns is a rapidly developing field of mathematical biology. Its state-of-the-art was explored at the successful conference *On Growth and Form*, held in 1998 in honour of D'Arcy Thompson (1860-1948) and his famous book, cf. Thompson (1917). Out of the conference grew a monograph which contains substantial biological material and an overview of mathematical modelling of spatio-temporal systems, cf. Chaplain et al. (1999). Examples of growth mechanisms studied are growth of capillary networks, skeletal growth and tumour growth.

Modelling of tumour growth has attracted particular interest in recent years. Tumour growth was one of the high priority topics of the recent multidisciplinary conference arranged by the European Society for Mathematical and Theoretical Biology in July 2002. More than 500 scientists from a wide range of disciplines participated. One of the subjects discussed was pattern formation problems, relating to tumour formation and progression, in particular the question of tumour shape.

The models suggested for tumour growth are either continuous or discrete. In Murray (2003), the continuous approach is explained in relation to brain tumours. The simplest models involve only total number of cells in the tumour, with growth of the tumour usually assumed to be exponential, Gompertzian or logistic (Swan (1987); Marusic et al. (1994)). More powerful deterministic models describe the change of the spatial arrangement of the cells under tumour growth. The discrete models are most often cellular automaton models, cf. Qi et al. (1993) and Kansal et al. (2000).

The growth literature contains very few examples of statistical modelling and analysis of growth patterns. An exception is the paper by Cressie and Hulting (1992). Growth of a planar star-shaped object is here modelled, using a sequence of Boolean

models. The object Y_{t+1} at time $t+1$ is the union of independent random compact sets placed at uniform random positions inside the object Y_t at time t. More formally,

$$Y_{t+1} = \cup\{Z(x_i) : x_i \in Y_t\},$$

where $\{x_i\}$ is a homogeneous Poisson point process in the plane and $Z(x_i)$ is a random compact set with position x_i. Note that this model is Markov since Y_{t+1} only depends on the previous objects via Y_t. The model is applied to describe the growth pattern of human breast cancer cell islands. Practical methods of estimating the model parameters, using the information of the complete growth pattern, are devised. A related continuous model has recently been discussed in Deijfen (2003). The object Y_t is here a connected union of randomly sized Euclidean balls, emerging at exponentially distributed times. It is shown that the asymptotic shape is spherical.

In the present paper, we propose a Gaussian radial growth model for star-shaped planar objects. The model is a dynamic version of the $p-$order shape model introduced in Hobolth et al. (2003). The object at time $t+1$ is a stochastic transformation of the object at time t such that the radius vector function of the object fulfils

$$R_{t+1}(\theta) = R_t(\theta) + Z_t(\theta), \quad \theta \in [0, 2\pi),$$

where Z_t is a cyclic Gaussian process. The coefficients of the Fourier series of Z_t

$$Z_t(\theta) = \mu_t + \sum_{k=1}^{\infty}[A_{t,k}\cos(k\theta) + B_{t,k}\sin(k\theta)], \tag{1}$$

$\theta \in [0, 2\pi)$, have important geometric interpretations relating to the growth process. The overall growth from time t to $t+1$ is determined by the parameter μ_t. The coefficients $A_{t,1}$ and $B_{t,1}$ determine the asymmetry of growth from time t to $t+1$, while $A_{t,k}$ and $B_{t,k}$ affect how the growth appears globally for small $k \geq 2$ and locally for large $k \geq 2$. Under the proposed p-order growth model

$$A_{t,k} \sim B_{t,k} \sim N(0, \lambda_{t,k}), \quad k = 2, 3, \ldots,$$

$A_{t,k}$, $B_{t,k}$, $k = 2, 3, \ldots$, independent, where the variances satisfy the following regression model

$$\lambda_{t,k}^{-1} = \alpha_t + \beta_t(k^{2p} - 2^{2p}), \quad k = 2, 3, \ldots.$$

In Section 2 we introduce the Gaussian radial growth model. In Section 3, we study the induced distributions of object size and shape under the model. An application to tumour growth is discussed in Section 4. An extension of the model, involving time series, is briefly described in Section 5 and a 3D version of the Gaussian radial growth model is presented in Section 6.

2 The Gaussian radial growth model

Consider a planar bounded and topologically closed object with size and shape changing over time. The object at time t is denoted by $Y_t \subset \mathbb{R}^2$, $t = 0, 1, 2, \ldots$. We suppose that Y_t is star-shaped with respect to a point $z \in \mathbb{R}^2$ for all t. Then, the boundary of Y_t can

be determined by its radius vector function $R_t = \{R_t(\theta) : \theta \in [0, 2\pi)\}$ with respect to z, where

$$R_t(\theta) = \max\{r : z + r(\cos\theta, \sin\theta) \in Y_t\},$$

$\theta \in [0, 2\pi)$. In Hobolth et al. (2003), a deformable template model is introduced, describing a random planar object as a stochastic deformation of a known star-shaped template, see also the closely related models described in Hobolth and Jensen (2000), Kent et al. (2000) and Hobolth et al. (2002). We use this approach here and describe the object at time $t+1$ as a stochastic transformation of the object at time t, such that

$$R_{t+1}(\theta) = R_t(\theta) + Z_t(\theta), \quad \theta \in [0, 2\pi). \tag{2}$$

Here, $\{Z_t\}$ is a series of independent stationary cyclic Gaussian processes with Z_t short for $\{Z_t(\theta) : \theta \in [0, 2\pi)\}$. The process Z_t is stationary if the distribution of $Z_t(\theta + \theta_0) - Z_t(\theta)$ does not depend on θ, while the process is said to be cyclic if $Z_t(\theta + 2\pi k) = Z_t(\theta)$, for all $k \in \mathbb{Z}$. The initial value R_0 of the radius vector function is assumed to be known.

Note that Y_t is used as a template in the stochastic transformation, resulting in Y_{t+1}. The increment process Z_t can be written as

$$Z_t(\theta) = \mu_t + U_t(\theta), \quad \theta \in [0, 2\pi),$$

where $\mu_t \in \mathbb{R}$ represents a constant radial addition at time t and U_t a stochastic deformation with mean zero of the expanded object with radius vector function $R_t + \mu_t$, cf. Figure 1. (The object with radius vector function $R_t + \mu_t$ is in geometric tomography known as the radial sum of Y_t and a circular disc of radius μ_t, cf. Gardner (1995).) Because of the independence of the Z_ts, the model is Markov in time, in the sense that

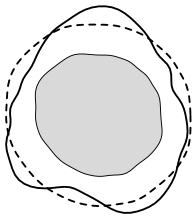

Figure 1: The object Y_{t+1} is a stochastic transformation of the object Y_t (grey), using a constant radial addition (shown stippled) followed by a deformation.

it uses information about the object at the immediate past to describe the object at the present time. More specifically, under (2) the conditional distribution of R_{t+1} given $R_t, \ldots, R_0$ depends only on R_t. The model suggested in Cressie and Hulting (1992) possesses a similar Markov property.

If Y_t is non-circular, it can be natural to extend the model (2), using an increasing time change function $\Gamma_t : [0, 2\pi] \to [0, 1]$ such that $Z_t \circ \Gamma_t^{-1}$ is a stationary stochastic process on $[0, 1]$. If the boundary length of Y_t is finite, one possibility is to choose

$$\Gamma_t(\theta) = \frac{L_t(\theta)}{L_t(2\pi)}, \tag{3}$$

where $L_t(\theta)$ is the distance travelled along the boundary of Y_t between the points indexed by 0 and θ. Note, however, that if $R_0 \equiv 0$, then the boundary of Y_t is expected to be approximately circular, since $\mathrm{E}(Z_t(\theta)) = \mu_t$ does not depend on $\theta \in [0, 2\pi)$.

The following result is important for the construction of parametric models in the framework of model (2). The result also implies a simple simulation procedure for a stationary cyclic Gaussian process on $[0, 2\pi)$.

Proposition 2.1. The process Z_t is a stationary cyclic Gaussian process on $[0, 2\pi)$ with mean $\mu_t \in \mathbb{R}$ if and only if there exist $\lambda_{t,k} \geq 0, k = 0, 1, 2, \ldots$, such that $\sum_{k=0}^{\infty} \lambda_{t,k} < \infty$ and

$$Z_t(\theta) = A_{t,0} + \sum_{k=1}^{\infty} [A_{t,k} \cos(k\theta) + B_{t,k} \sin(k\theta)],$$

$\theta \in [0, 2\pi)$, where $A_{t,0}$, $A_{t,k}$, $B_{t,k}$, $k = 1, 2, \ldots$, are all independent, $A_{t,0} \sim N(\mu_t, \lambda_{t,0})$ and $A_{t,k} \sim B_{t,k} \sim N(0, \lambda_{t,k})$.

The proof of Proposition 2.1 is not complicated. Given a stationary cyclic Gaussian process Z_t on $[0, 2\pi)$ with mean μ_t, consider the stochastic Fourier expansion of Z_t. Then, simple calculations involving the stochastic Fourier coefficients give the result. The other assertion is trivial.

Note that in Proposition 2.1, the $\lambda_{t,k}$s are allowed to be zero, meaning that $A_{t,k} \equiv 0$, almost surely.

The Fourier coefficients

$$A_{t,0} = \frac{1}{2\pi} \int_0^{2\pi} Z_t(\theta)\, d\theta,$$

$$A_{t,k} = \frac{1}{\pi} \int_0^{2\pi} Z_t(\theta) \cos(k\theta)\, d\theta, \tag{4}$$

$$B_{t,k} = \frac{1}{\pi} \int_0^{2\pi} Z_t(\theta) \sin(\theta k)\, d\theta, \tag{5}$$

$k = 1, 2, \ldots$, have interesting geometric interpretations relating to the growth process. It is clear that the coefficient $A_{t,0}$ determines the overall growth from Y_t to Y_{t+1}. The Fourier coefficients $A_{t,1}$ and $B_{t,1}$ play also a special role. Numerically large values of the coefficients will imply an asymmetric growth from Y_t to Y_{t+1}. In order to interpret geometrically the remaining Fourier coefficients $A_{t,k}$ and $B_{t,k}$, $k = 2, 3, \ldots$, let us consider an increment process for which all Fourier coefficients except those of order 0 and k are zero,

$$Z_t(\theta) = A_{t,0} + A_{t,k} \cos(k\theta) + B_{t,k} \sin(k\theta),$$

$\theta \in [0, 2\pi)$. Such a process exhibits k-fold symmetry, i.e.

$$Z_t\Big(\theta + \frac{2\pi i}{k}\Big), \quad i = 0, 1, \ldots, k-1,$$

$\theta \in [0, 2\pi)$, does not depend on i. Therefore, $A_{t,k}$ and $B_{t,k}$ affect how the growth appears globally for small k and locally for large k. The variances $\lambda_{t,k}$ control the magnitude of the spread of the Fourier coefficients.

Since the zero- and first-order Fourier coefficients play a special role in relation to the growth process and may in applications well depend on explanatory variables, we shall desist from specific modelling of these coefficients. In the following we will assume that $A_{t,0} = \mu_t$ is deterministic. Furthermore, we suppose that $A_{t,1} = B_{t,1} = 0$ or, equivalently, we concentrate on modelling

$$Z_t(\theta) - A_{t,1} \cos\theta - B_{t,1} \sin\theta, \quad \theta \in [0, 2\pi).$$

A special case of the Gaussian radial growth model is the p-order growth model. This model is inspired by the p-order model described in Hobolth et al. (2003), where the stochastic deformation process is a stationary Gaussian process with an attractive covariance structure, described below. The model is called p-order because it can be derived as a limit of discrete p-order Markov models defined on a finite, systematic set of angles θ, cf. Hobolth et al. (2002).

Definition 2.2. A stochastic process $Y = \{Y(\theta) : \theta \in [0, 2\pi)\}$ follows a *p-order model* with $p > \frac{1}{2}$, if there exist $\mu \in \mathbb{R}$, $\alpha, \beta > 0$, such that

$$Y(\theta) = \mu + \sum_{k=2}^{\infty} [A_k \cos(k\theta) + B_k \sin(k\theta)],$$

$\theta \in [0, 2\pi)$, where $A_k \sim B_k \sim N(0, \lambda_k)$ are all independent and

$$\lambda_k^{-1} = \alpha + \beta(k^{2p} - 2^{2p}), \quad k = 2, 3, \ldots.$$

If Y follows a $p-$order model, we will write $Y \sim G_p(\mu, \alpha, \beta)$. Clearly, μ is the mean of Y. Furthermore, the covariance function of Y is of the form

$$\begin{aligned}\sigma(\theta) = \mathrm{Cov}(Y(0), Y(\theta)) &= \sum_{k=2}^{\infty} \lambda_k \cos(k\theta) \\ &= \sum_{k=2}^{\infty} \frac{\cos(k\theta)}{\alpha + \beta(k^{2p} - 2^{2p})},\end{aligned}$$

$\theta \in [0, 2\pi)$. The parameters α and β determine the variance of lower order and higher order Fourier coefficients, respectively. Furthermore, p determines the smoothness of the curve Y. In fact, the curve Y is $k-1$ times continuously differentiable where k is the unique integer satisfying $p \in (k - \frac{1}{2}, k + \frac{1}{2}]$ (Hobolth et al. (2003)). Note that the first Fourier coefficients of Y are set to zero.

We can now give the definition of the $p-$order growth model.

Definition 2.3. The series $Z = \{Z_t\}$ follows a $p-$order growth model if the Z_ts are independent and $Z_t \sim G_p(\mu_t, \alpha_t, \beta_t)$ for all t.

The parameters α_t and β_t determine, respectively, the global and local appearance of growth from Y_t to Y_{t+1}. As before, p determines the smoothness of the curves Z_t. The overall growth pattern is specified by the μ_ts. Their actual form depends on the specific application. Tumour growth has often been described by a Gompertz growth pattern

$$\kappa_t = \kappa_0 \exp\Big[\frac{\eta}{\gamma}(1 - \exp(-\gamma t))\Big],$$

where κ_t is the average radius at time t and η and γ are positive parameters determining the growth, implying that

$$\mu_t = \kappa_t\Big(\exp\Big[\frac{\eta}{\gamma}\exp(-\gamma t)(1 - \exp(-\gamma))\Big] - 1\Big).$$

For more details, see e.g. Steel (1977).

Note that the p-order growth model allows for negative values of $R_t(\theta)$. However, the parameters μ_t, α_t and β_t will be chosen such that this will practically never occur.

Figure 2 shows simulations of the increment process Z_t from time t to $t+1$ for different values of α_t and β_t under the second-order growth model, i.e. $p = 2$. A large value of α_t gives increments that are fairly constant while a small value of α_t provides a more irregular growth on a global scale. The parameter β_t controls the local appearance of the increment process, the smaller β_t the more pronounced irregularity on a local scale.

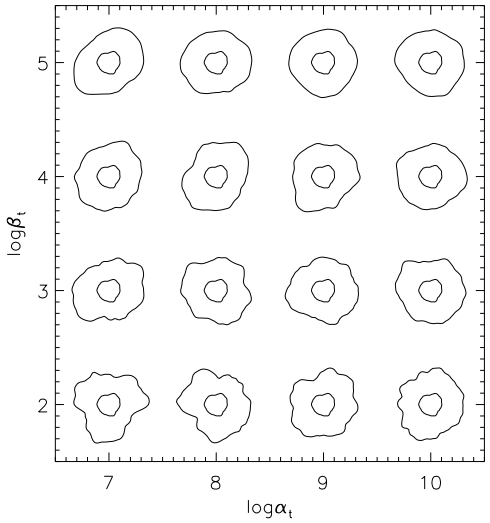

Figure 2: Simulated objects under the second-order growth model. The object at time t is fixed while the object at time $t+1$ is simulated under the indicated values of α_t and β_t.

3 Distributional results

In this section, we study the induced distribution of object size and shape under the p-order growth model. The limiting shape may be circular but, as we shall see, there is a whole range of possibilities.

Unless otherwise explicitly stated, we assume that $R_0 \equiv 0$. We then have for $\theta \in [0, 2\pi)$

$$R_T(\theta) = \rho_T + \sum_{k=2}^{\infty} [A_k^T \cos(k\theta) + B_k^T \sin(k\theta)], \tag{6}$$

where $A_k^T \sim B_k^T \sim N(0, \lambda_k^T)$ are all independent,

$$\rho_T = \sum_{t=0}^{T-1} \mu_t, \tag{7}$$

and

$$\lambda_k^T = \sum_{t=0}^{T-1} \lambda_{t,k}. \tag{8}$$

The shape of the object at time T will be represented by its normalised radius vector function

$$\frac{R_T}{\mathrm{E}(R_T(0))} = \frac{R_T}{\rho_T},$$

which can be regarded as a continuous analogue of the standardised vertex transformation vector in shape theory, cf. Hobolth et al. (2002).

Under the assumption of independent increments, the distribution of the area of the object at time T, $A(Y_T)$, is known, provided that the radius-vector function R_T is positive.

Proposition 3.1. Assume that the radius vector function R_T of the object Y_T is positive and that it satisfies (6)–(8). Then,

$$\mathrm{A}(Y_T) \sim \pi\rho_T^2 + \pi \sum_{k=2}^{\infty} \lambda_k^T V_k,$$

where V_k, $k = 2, 3, \ldots$, are mutually independent exponentially distributed random variables with mean 1.

Proof. The area of the object at time T is

$$\mathrm{A}(Y_T) = \frac{1}{2} \int_0^{2\pi} R_T(\theta)^2 \mathrm{d}\theta.$$

Note that since

$$\sum_{k=2}^{\infty} (A_k^T)^2 + (B_k^T)^2 < \infty, \text{ almost surely,}$$

we have that $\mathrm{A}(Y_T) < \infty$, almost surely. Using equation (6) and Parseval's equation, we get that

$$\begin{aligned} \mathrm{A}(Y_T) &= \pi\rho_T^2 + \frac{\pi}{2} \sum_{k=2}^{\infty} [(A_k^T)^2 + (B_k^T)^2] \\ &= \pi\rho_T^2 + \pi \sum_{k=2}^{\infty} \lambda_k^T V_k, \end{aligned}$$

where V_k, $k = 2, 3, \ldots$, are mutually independent exponentially distributed random variables with mean 1. □

The distribution of the area of Y_T is thus a sum of independent Gamma distributed random variables. The saddlepoint approximation of such a distribution is easily derived, cf. Jensen (1992).

It does not seem possible to get a correspondingly simple result for the distribution of the boundary length of Y_T. This seems apparent from the expression for the boundary length of Y_T

$$\int_0^{2\pi} \sqrt{R_T'(\theta)^2 + R_T(\theta)^2} d\theta,$$

which is valid in the case where R_T is differentiable.

As we shall see now, the class of p-order growth models is quite rich in the sense that the shape of the limiting object, represented by its normalised radius vector function,

may be distributed according to any p-order model $G_p(1, \alpha, \beta)$ with mean 1. For large values of α and β, the shape is close to circular.

Let us consider the p-order growth model with proportional parameters, i.e. $\alpha_t = \gamma\beta_t$. Equivalently, we assume that there exists a sequence $\{\tau_t\}$ of positive real numbers such that

$$Z_t = \mu_t + \tau_t X_t \tag{9}$$

and $\{X_t\}$ are independent and identically $G_p(0, \alpha, \beta)$ distributed. If $\sigma^2 = \mathrm{Var}(X_t(\theta))$, then $Z_t(\theta) \sim N(\mu_t, \tau_t^2\sigma^2)$ under (9).

Examples of choices of τ_t are $\tau_t = 1$, $\sqrt{\mu_t}$ or ρ_{t+1}, cf. (7). If $\tau_t = 1$, the variance of the increment $Z_t(\theta)$ is constant in time. If $\tau_t = \sqrt{\mu_t}$, we obviously need that $\mu_t \geq 0$ for all t and we have that $\mathrm{Var}(Z_t(\theta)) \propto \mathrm{E}(Z_t(\theta))$ such that the variance of the increment $Z_t(\theta)$ is proportional to the average increase in the radius at time t. If $\tau_t = \rho_{t+1}$, then the distribution of the shape of the object defined by the radius vector function

$$\{\rho_t + Z_t(\theta) : \quad \theta \in [0, 2\pi)\}$$

is constant in time, i.e. the distribution of

$$\frac{\rho_t + Z_t(\theta)}{\mathrm{E}(\rho_t + Z_t(\theta))}$$

does not depend on t.

In the proposition below, we show that under (9) the shape of Y_t is distributed according to a p-order model.

Proposition 3.2. Suppose that $Z = \{Z_t\}$ satisfies (9) where X_t, $t = 0, 1, 2, \ldots$, are independent and identically $G_p(0, \alpha, \beta)-$distributed. Then, the normalised radius vector function of Y_T is distributed as

$$\frac{R_T}{\mathrm{E}(R_T(0))} \sim G_p(1, \bar{\alpha}_T, \bar{\beta}_T)$$

where

$$\bar{\alpha}_T = \alpha\rho_T^2 / \sum_{t=0}^{T-1} \tau_t^2, \quad \bar{\beta}_T = \beta\rho_T^2 / \sum_{t=0}^{T-1} \tau_t^2.$$

Proof. It suffices to show that

$$\frac{\mathrm{Cov}(R_T(0), R_T(\theta))}{[\mathrm{E}(R_T(0))]^2} = \sum_{k=2}^{\infty} \frac{\cos(k\theta)}{\bar{\alpha}_T + \bar{\beta}_T(k^{2p} - 2^{2p})}.$$

Using (6) and (9), we find

$$\begin{aligned}
&\frac{\mathrm{Cov}(R_T(0), R_T(\theta))}{[\mathrm{E}(R_T(0)]^2]} \\
&\quad = \frac{1}{\rho_T^2} \sum_{k=2}^{\infty} \lambda_k^T \cos(k\theta) \\
&\quad = \frac{1}{\rho_T^2} \sum_{k=2}^{\infty} \sum_{t=0}^{T-1} \tau_t^2 \frac{\cos(k\theta)}{\alpha + \beta(k^{2p} - 2^{2p})} \\
&\quad = \sum_{k=2}^{\infty} \frac{\cos(k\theta)}{\bar{\alpha}_T + \bar{\beta}_T(k^{2p} - 2^{2p})}.
\end{aligned}$$

□

Below, we study examples of different limiting shapes under the model (9).

Example 3.3. (Constant increment growth) Let the situation be as in Proposition 3.2 with $\mu_t = \mu$ and $\tau_t = 1$ in (9). The increment processes Z_t are thereby independent and identically distributed. It follows from Proposition 3.2 that

$$\frac{R_T}{\mathrm{E}R_T(0)} \sim G_p(1, \bar{\alpha}_T, \bar{\beta}_T),$$

where $\bar{\alpha}_T = T\mu^2\alpha$ and $\bar{\beta}_T = T\mu^2\beta$. Since $\bar{\alpha}_T \to \infty$ and $\bar{\beta}_T \to \infty$ for $T \to \infty$, the boundary of the object becomes more circular and smooth as T increases. An example is shown in Figure 3. The limiting object has circular shape.

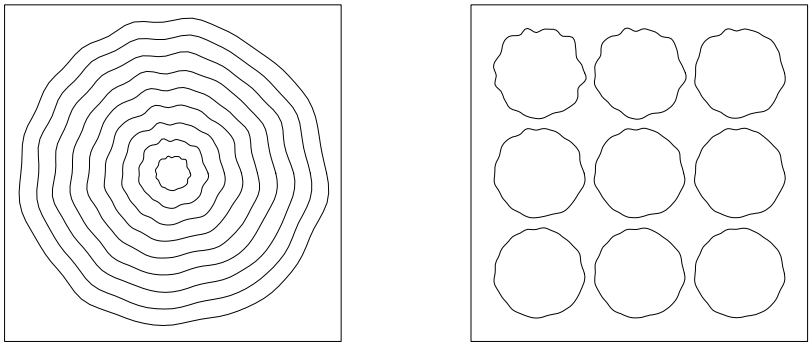

Figure 3: Right: Simulated growth pattern under the constant increment second-order growth model. Left: The corresponding normalised profiles, representing the shape of the object.

Example 3.4. (Wiener growth) Let the situation be as in Proposition 3.2 with μ_t arbitrary and $\tau_t = \sqrt{\mu_t}$ in (9). This special case is called a Wiener growth model since $\mathrm{Var}(R_T) \propto \mathrm{E}(R_T)$. If $\mu_t = \mu$ such that $\rho_T = T\mu$, the process is called a Wiener process with linear drift. If $\rho_T = \delta T^\psi$ for some $\delta, \psi > 0$, then $R_T - \rho_T$ satisfies

$$R_{at} - \rho_{at} \sim a^H (R_t - \rho_t), \quad a \geq 0, \tag{10}$$

with parameter $H = \frac{\psi}{2}$, which is a discrete analogue of self-similarity, cf. Sato (1999). Notice that

$$\frac{R_T}{\mathrm{E}R_T(0)} \sim G_p(1, \alpha\rho_T, \beta\rho_T).$$

If $\rho_T \to \rho < \infty$, the limiting object can have any stochastic shape determined by $G_p(1, \alpha\rho, \beta\rho)$.

Example 3.5. Let the situation be as in Proposition 3.2 with μ_t arbitrary and $\tau_t = \rho_{t+1}$ in (9). The normalised radius vector function is distributed as

$$\frac{R_T}{\mathrm{E}R_T(0)} \sim G_p(1, \alpha\frac{\rho_T^2}{\sum_{t=1}^T \rho_t^2}, \beta\frac{\rho_T^2}{\sum_{t=1}^T \rho_t^2}).$$

If $\rho_T^2 / \sum_{t=1}^T \rho_t^2 \to 0$ as $T \to \infty$, the objects become more irregular both globally and locally as T increases. An example is shown in Figure 4.

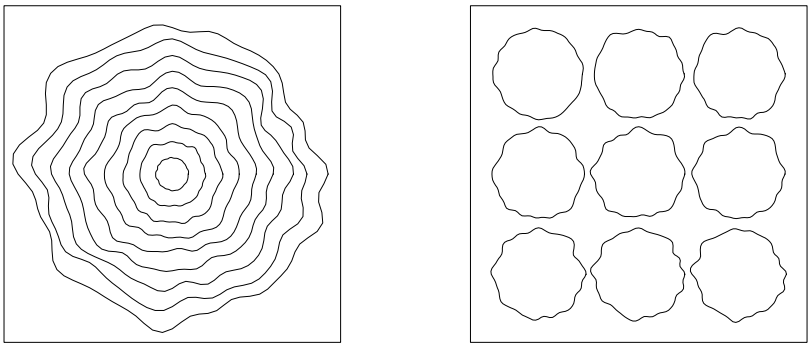

Figure 4: Right: Simulated growth pattern under the model described in Example 3.5. Left: The corresponding normalised profiles, representing the shape of the object.

4 An application

For illustrative purposes, we consider a data set consisting of human breast cancer cell islands, which have been observed in vitro in a nutrient medium on a flat dish. This data set has earlier been analysed in Cressie and Hulting (1992). Three profiles of cancer cell islands are available. The data set is presented in the upper left corner of Figure 5.

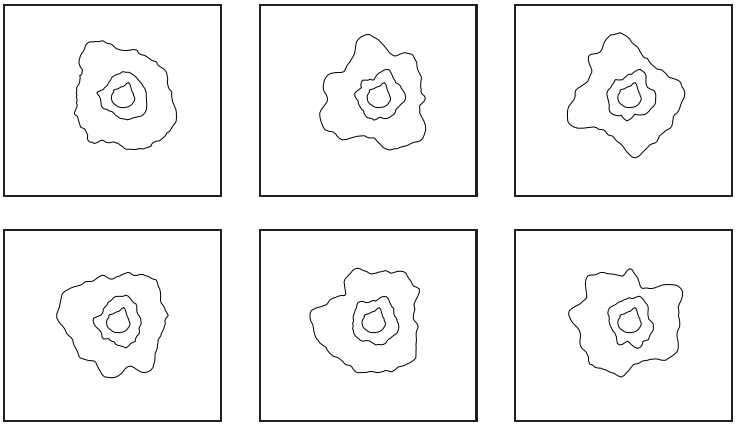

Figure 5: The tumour growth data (upper left corner) and simulations under the second-order growth model with μ_t, α_t and β_t replaced by the maximum likelihood estimates.

The centre of mass of Y_0 is used as reference point. The data consist of increments

$$z_t\Big(\frac{2\pi i}{n_t}\Big), \quad i = 0, 1, \ldots, n_t - 1,$$

in n_t directions, equidistant in angle, $t = 0, 1$. For convenience, z_t is normalised with the average radius of Y_0. Only digitised images are available. As n_t, we have used approximately 25% of the number of pixels on the boundary of the digitised image of Y_t, $t = 0, 1$.

Under the p-order growth model, the mean value parameters μ_t can be estimated by the average observed increment at time t. The variance parameters can be estimated

using the likelihood function

$$L(\alpha_0, \beta_0, \alpha_1, \beta_1) = \prod_{t=0,1} L_t(\alpha_t, \beta_t),$$

where $L_t(\alpha_t, \beta_t)$ is the likelihood function based on the Fourier coefficients $A_{t,k}$ and $B_{t,k}$ of Z_t of order $k \leq K_t$, say. Since $A_{t,k} \sim B_{t,k} \sim N(0, \lambda_{t,k})$ are all independent and

$$\lambda_{t,k}^{-1} = \alpha_t + \beta_t(k^{2p} - 2^{2p}), \quad k = 2, 3, \ldots,$$

the likelihood becomes

$$L_t(\alpha_t, \beta_t) = \prod_{k=2}^{K_t} [\alpha_t + \beta_t(k^{2p} - 2^{2p})] \exp(-c_{t,k}[\alpha_t + \beta_t(k^{2p} - 2^{2p})]), \tag{11}$$

where $c_{t,k} = [a_{t,k}^2 + b_{t,k}^2]/2$ are the observed phase amplitudes. In applications, $a_{t,k}$ and $b_{t,k}$ are replaced by discrete versions of the integrals in (4).

The choice of the cut-off value K_t is very important. Clearly, K_t must not be too large in order to avoid that the estimates are influenced by the digitisation effects. On the other hand, if the cut-off value K_t is too small information about the growth pattern is lost. The choice of K_t should be an intermediate value for which the estimate of the local parameter β_t is stable. Whether a specific choice of K_t is appropriate can also be judged from visual inspection of simulated growth patterns under the estimated model.

For the two increments z_0 and z_1, we used $(n_0, K_0) = (60, 25)$ and $(n_1, K_1) = (120, 30)$, respectively. The maximum likelihood estimates under the second-order growth model are

$$\hat{\mu}_0 = 1.04, \log(\hat{\alpha}_0) = 5.29, \log(\hat{\beta}_0) = -1.88,$$
$$\hat{\mu}_1 = 2.53, \log(\hat{\alpha}_1) = 3.18, \log(\hat{\beta}_1) = -3.54.$$

The estimated regression curves

$$\hat{\lambda}_{t,k} = \frac{1}{\hat{\alpha}_t + \hat{\beta}_t(k^4 - 2^4)}, \quad t = 0, 1 \quad k = 2, 3, \ldots$$

are shown in Figure 6, together with 95% confidence limits for the logarithm of the phase amplitudes. The model fits the data well which can also be seen from the fractile diagrams (QQ plots) for the normalised Fourier coefficients, also shown in Figure 6.

Simulations under the second-order growth model with μ_t, α_t and β_t replaced by the maximum likelihood estimates are shown in Figure 5.

Since the data set only contains two increments, it is not meaningful to try to evaluate the Markov assumption. Note also that the Z_ts are assumed independent but not necessarily identically distributed. If

$$\alpha_t = \gamma\beta_t, \tag{12}$$

we have that

$$\sqrt{\beta_t}(Z_t - \mu_t) \sim G_p(0, \gamma, 1)$$

are independent and identically distributed. Thus, under the assumption (12) of proportionality and with sufficient number T of time points, we can examine the independence of

$$\sqrt{\beta_t}(Z_t(\theta) - \mu_t), \quad t = 0, 1, \ldots, T-1,$$

for selected values of $\theta \in [0, 2\pi)$, using a runs test, for instance.

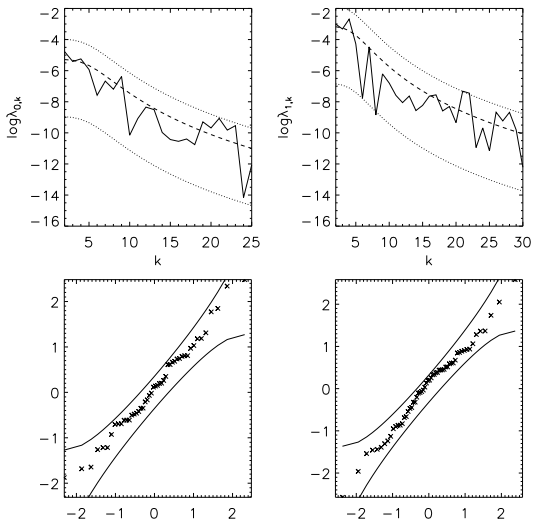

Figure 6: The two upper figures show the observed phase amplitudes (full-drawn lines) together with the estimated regression curves (stippled) and 95% confidence limits, $t = 0, 1$. The two lower figures show fractile diagrams (QQ plots) for the normalised Fourier coefficients $a_{t,k}/\sqrt{\hat{\lambda}_{t,k}}$, $b_{t,k}/\sqrt{\hat{\lambda}_{t,k}}$ together with 95% confidence limits, $t = 0, 1$.

5 A time series extension

Let us suppose that

$$Z_t = \mu_t + \tau_t X_t,$$

where $X = \{X_t\}$ is a stationary time series of cyclic Gaussian processes satisfying the ARMA model equation

$$X_t - \phi_1 X_{t-1} - \cdots - \phi_r X_{t-r} = W_t - \psi_1 W_{t-1} - \cdots - \psi_s W_{t-s}. \tag{13}$$

We assume that $W = \{W_t\}$ is a sequence of i.i.d. stationary cyclic Gaussian processes on $[0, 2\pi)$ with

$$W_t \sim G_p(0, \alpha, \beta).$$

If $\phi_i = 0$, $i = 1, \ldots, r$, and $\psi_j = 0$, $j = 1, \ldots, s$, Z follows the p-order growth model with independent increments, treated in the previous sections.

Under the general ARMA model (13), the Fourier coefficients of X and W of a given order follow a one-dimensional ARMA model. Furthermore, for fixed $\theta \in [0, 2\pi)$, $X_t(\theta)$ follows a one-dimensional ARMA model. Aspects of this time series approach has earlier been discussed in Alt (1999). An early example concerning year ring widths is discussed in Kronborg (1981).

Note that in the special case of a MA model ($\phi_1 = \cdots = \phi_r = 0$), the marginal distribution of Z_t belongs to the class of p-order models

$$Z_t \sim G_p(\mu_t, \alpha_t, \beta_t),$$

where

$$\alpha_t = \frac{\alpha}{\tau_t^2[1+\psi_1^2+\cdots+\psi_s^2]},$$
$$\beta_t = \frac{\beta}{\tau_t^2[1+\psi_1^2+\cdots+\psi_s^2]}.$$

Note also that in this case Z_t and $Z_{t'}$ are independent if $|t-t'|>s$.

6 Extension to three dimensions

The p-order growth model for planar objects can easily be extended to three dimensions. Consider a spatial compact object $Y_t \subset \mathbb{R}^3$ which is star-shaped for all t with respect to $z \in \mathbb{R}^3$. Clearly the boundary of the object can be determined by

$$\{z + R_t(\theta,\varphi) : \ \theta \in [0,2\pi), \ \ \varphi \in [0,\pi]\},$$

where $R_t(\theta,\varphi)$ is the distance from z to the boundary of Y_t in direction

$$\omega(\theta,\varphi) = (\sin\varphi\cos\theta, \sin\varphi\sin\theta, \cos\varphi).$$

In the same way as in the planar case we let the object Y_{t+1} be a stochastic transformation of the object Y_t, such that

$$R_{t+1}(\theta,\varphi) = R_t(\theta,\varphi) + Z_t(\theta,\varphi),$$

$\theta \in [0,2\pi)$, $\varphi \in [0,\pi]$, where $\{Z_t\}$ is a time series of Gaussian processes on $[0,2\pi)\times[0,\pi]$. Writing the stochastic process Z_t in terms of its Fourier-Legendre series expansion we get, cf. Hobolth (2003),

$$Z_t(\theta,\varphi) = \sum_{n=0}^{\infty}\sum_{m=-n}^{m=n} A_{t,n,m}\phi_{n,m}(\theta,\varphi),$$

where $\phi_{n,m}$ are the spherical harmonics and $A_{t,n,m}$ are random coefficients. Using a similar reasoning as in Hobolth (2003) it can be seen that $A_{t,0,0}$ determines the overall growth from Y_t to Y_{t+1}. The coefficients $A_{t,1,m}$, $m=-1,0,1$, control the asymmetry of growth, and the remaining coefficients $A_{t,n,m}$ for $n \geq 2$, $m=-n,\ldots,n$, affect how the growth appears globally for small n and locally for large n. A p-order growth model can be defined by assuming that $A_{t,0,0}=\mu_t$, $A_{t,1,m}=0$ for $m=-1,0,1$ and

$$A_{t,n,m} \sim N(0,\lambda_{t,n}),$$

$n=2,3,\ldots$, $m=-n,\ldots,n$, independent, where

$$\lambda_{t,n}^{-1} = \alpha_t + \beta_t(n^{2p}-2^{2p}).$$

As in the planar case, the increment processes may be chosen to be normal after a transformation. A simulation from such a model, where $\{Z_t\}$ is a series of log-Gaussian processes, is shown in Figure 7.

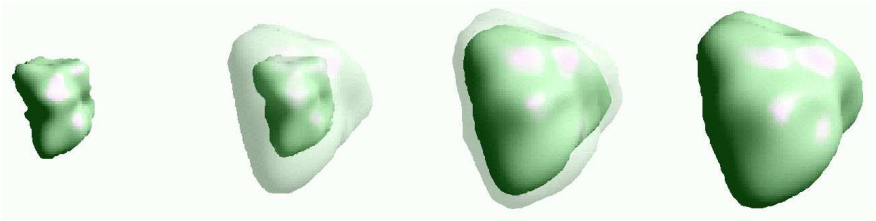

Figure 7: Simulation from a 3D log-Gaussian radial growth model.

7 Discussion

The $p-$order growth model has mainly been suggested as a general tool for analysing observed radial growth patterns. The model may, however, also be of interest as a building block in other modelling situations, for instance in models for tessellations where cells are created by radial growth from each point of a point process.

The $p-$order growth model can be extended in various ways. It is obviously easy to modify the model such that the increments are Gaussian after a transformation. An example is log-Gaussian increments. If the number of increments observed is not too small it is also of interest to try to model the dependency in the series $Z = \{Z_t\}$. We have discussed a time series approach. Another alternative is to look at Lévy based models,

$$Z_t(\theta) = \int_{A_t(\theta)} h_t(a;\theta) Z(da),$$

$A_t(\theta) \in \mathcal{B}$, where $\mathcal{B}$ is the Borel field of $[0, 2\pi) \times \mathbb{R}$ and Z is a Lévy basis on $[0, 2\pi) \times \mathbb{R}$. A detailed study of the Lévy based growth models is ongoing research in our group, cf. Schmiegel et al. (2005). These models can also be formulated in continuous time.

The likelihood used in the application is correct if the increments are independent. If the marginal distributions of the Z_ts belong to the class of p-order models but the Z_ts are dependent, the likelihood may still be used as a pseudo-likelihood.

In relation to tumour growth in particular, it will also be of interest in the future to try to embed specific mathematical models in a stochastic framework. A starting point could here be a study of dynamic point process models with a specified time-dependent intensity function.

8 Acknowledgements

Dr. G.C. Buehring, University of California, Berkeley, is the source of the tumour growth data in Figure 5. Sławomir Rażniewski is thanked for designing the 3D simulation program used in Figure 7. This work was supported in part by MaPhySto – Network in Mathematical Physics and Stochastics, funded by The Danish National Research Foundation and a grant from the Danish Natural Science Research Council.

References

Alt, W. (1999). Statistics and dynamics of cellular shape changes. In Chaplain, M. A. J., Singh, G. D., and McLachlan, J. C., editors, *On Growth and Form: Spatio-temporal*

Pattern Formation in Biology, pages 287–307. Wiley, Chichester.

Chaplain, M. A. J., Singh, G. D., and McLachlan, J. C. (1999). *On Growth and Form: Spatio-temporal Pattern Formation in Biology*. Wiley, Chichester.

Cressie, N. and Hulting, F. L. (1992). A spatial statistical analysis of tumor growth. *J. Amer. Statist. Assoc.*, 87:272–283.

Deijfen, M. (2003). Asymptotic shape in a continuum growth model. *Advances in Applied Probability (SGSA)*, 35:303–318.

Gardner, R. (1995). *Geometric Tomography*. Cambridge University Press, New York.

Hobolth, A. (2003). The spherical deformation model. *Biostatistics*, 4:583–595.

Hobolth, A. and Jensen, E. B. V. (2000). Modelling stochastic changes in curve shape, with an application to cancer diagnostics. *Advances in Applied Probability (SGSA)*, 32:344–362.

Hobolth, A., Kent, J. T., and Dryden, I. L. (2002). On the relation between edge and vertex modelling in shape analysis. *Scandinavian Journal of Statistics*, 29:355–374.

Hobolth, A., Pedersen, J., and Jensen, E. B. V. (2003). A continuous parametric shape model. *Ann. Inst. Statist. Math.*, 55:227–242.

Jensen, J. L. (1992). A note on a conjecture of H.E. Daniels. *Revista Brasileira de Probabilidade e Estatística*, 6:85–95.

Kansal, A. R., Torquato, S., Harsh, G. R., Chiocca, E. A., and Deisboeck, T. S. (2000). Simulated brain tumor growth dynamics using a three-dimensional cellular automaton. *J. Theor. Biol.*, 203:367–382.

Kent, J. T., Dryden, I. L., and Anderson, C. R. (2000). Using circulant symmetry to model featureless objects. *Biometrika*, 87:527–544.

Kronborg, D. (1981). Distribution of crosscorrelations in two-dimensional time series, with application to dendrochronology. Research report no. 72, Department of Theoretical Statistics, Institute of Mathematics, University of Aarhus.

Marusic, M., Bajzer, Z., Freyer, J. P., and Vuk-Pavlovic, S. (1994). Analysis of growth of multicellular tumour spheroids by mathematical models. *Cell Prolif.*, 27:73–94.

Murray, J. D. (2003). *Mathematical Biology. II: Spatial Models and Biomedical Applications*. Springer-Verlag, Berlin.

Qi, A. S., Zheng, X., Du, C. Y., and An, B. S. (1993). A cellular automaton model of cancerous growth. *J. Theor. Biol.*, 161:1–12.

Sato, K. (1999). *Lévy Processes and Infinitely Divisable Distributions.* Cambridge University Press, Cambridge.

Schmiegel, J., Jónsdóttir, K. Ý., Barndorff-Nielsen, O. E., and Jensen, E. B. V. (2005). Lévy based growth models. In preparation.

Steel, G. G. (1977). *Growth kinetics of tumours*. Clarendon Press, Oxford.

Swan, G. W. (1987). Tumour growth models and cancer therapy. In Thompson, J. R. and Brown, B. R., editors, *Cancer Modeling*, pages 91–104. Marcel Dekker, New York.

Thompson, D. W. (1917). *On Growth and Form*. Cambridge University Press, Cambridge.

Paper B

Jensen, E.B.V., Jónsdóttir, K.Ý., Schmiegel, J.
and Barndorff-Nielsen, O. (2006).
Spatio-temporal modelling
– with a view to biological growth.

To appear in *Statistics of Spatio-Temporal Systems*,
Monographs on Statistics and Applied Probability,
Chapman & Hall/CRC

Spatio-temporal modelling - with a view to biological growth

Eva B. Vedel Jensen, Kristjana Ýr Jónsdóttir,
Jürgen Schmiegel and Ole E. Barndorff-Nielsen
University of Aarhus

1 Introduction

Modelling of biological growth patterns is a field of mathematical biology that has attracted much attention in recent years, see e.g. Chaplain et al. (1999) and Capasso et al. (2002). The biological systems modelled are diverse and comprise growth of plant populations, year rings of trees, capillary networks, bacteria colonies, and tumours. This chapter deals with spatio-temporal models for such random growing objects, using spatio-temporal point processes or the theory of Lévy bases. For both type of models, the Poisson process will play a key role, either as a reference process or more directly in the model construction.

The first main group of models to be discussed are based on spatio-temporal point processes. We let $Z = \{(t_i, \xi_i)\}$ be a spatio-temporal point process on $S = \mathbb{R}_+ \times \mathcal{X}$ where $\mathcal{X}$ is a bounded subset of $\mathbb{R}^d$ with positive volume $|\mathcal{X}|$. The object at time t is given by

$$X_t = \{\xi_i \in \mathcal{X} : (t_i, \xi_i) \in Z, t_i \leq t\}.$$

Note that $X_{t'} \subseteq X_t$ for $t' \leq t$. The object X_t is called the cumulative spatial point process at time t. Figure 1 shows an example of a growth pattern that may be modelled using this framework. The data come from an experiment on a Danish barley field and show the development in a subregion of the field of a particular type of weed plant (Trifolium, clover) at six different dates. Such point patterns show clustering compared to a Poisson pattern and have been the inspiration for developing important new models of Cox type, cf. Brix (1998, 1999), Brix and Diggle (2001), Brix and Møller (2001), Møller (2003) and references therein. The points ξ_i may also be used as centres of 'cells' $\Xi(\xi_i) \subset \mathbb{R}^d$, modelled as random compact sets, see Molchanov (2005). An important early example of such a model, describing tumour growth, can be found in Cressie and Hulting (1992), see also Cressie and Laslett (1987) and Cressie (1991a,b).

A second main group of models describes how the boundary of a full-dimensional object expands in time. We will mainly discuss growth models based on Lévy bases, cf. Barndorff-Nielsen et al. (2003), Barndorff-Nielsen and Schmiegel (2004) and references therein. One example of such a model describes the growth of a star-shaped object, using its radial function. In the planar case, the radial function of an object Y_t at time t gives the distance $R_t(\phi)$ from a reference point z to the boundary of Y_t in direction

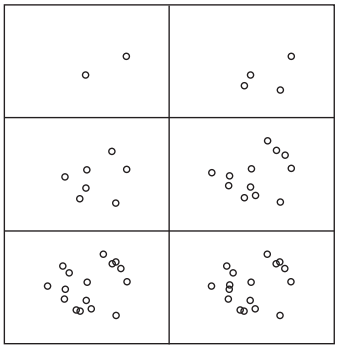

Figure 1: The development of a particular type of weed plant (Trifolium, clover) at six different time points. See Brix (1998, 1999) and Brix and Møller (2001).

$\phi \in [-\pi, \pi)$. For such objects, we study model specifications of the type

$$R_t(\phi) = \exp\left(\int_{A_t(\phi)} f_t(\xi, \phi) Z(\mathrm{d}\xi)\right),$$

where Z is a factorisable or a normal Lévy basis, $A_t(\phi)$ is an ambit set (a concept introduced in Barndorff-Nielsen and Schmiegel (2004)) and $f_t(\xi, \phi)$ is a deterministic weight function. As we shall see, it is possible for such a model to derive an explicit expression for

$$\mathrm{Cov}(R_t(\phi), R_{t'}(\phi'))$$

in terms of the three components of the model. Figure 2 shows an example of a growth pattern that may be modelled using this framework. These data are part of a larger data set that has been discussed in Brú et al. (1998). Notice that the boundary of the growing tumour cell island is very irregular.

In Section 2, models based on spatio-temporal point processes are presented while models based on Lévy bases are dealt with in Section 3. Basic results for spatio-temporal point processes are briefly reviewed in Appendix A.

2 Models based on spatio-temporal point processes

We will start by giving a short and fairly self-contained introduction to the theory of spatio-temporal point processes. For a more detailed treatment, cf. Daley and Vere-Jones (2002). Expositions with emphasis on purely spatial point processes can be found in Stoyan et al. (1995), Van Lieshout (2000), Diggle (2003), and Møller and Waagepetersen (2003).

2.1 Set-up

Let $Z = \{(t_i, \xi_i)\}$ be a spatio-temporal point process on $S = \mathbb{R}_+ \times \mathcal{X}$. We assume that the projections of Z on $\mathcal{X}$ and $\mathbb{R}_+$ are both simple point processes (no multiple points). In the following we let

$$Z_t = \{(t_i, \xi_i) \in Z : t_i \leq t\}$$

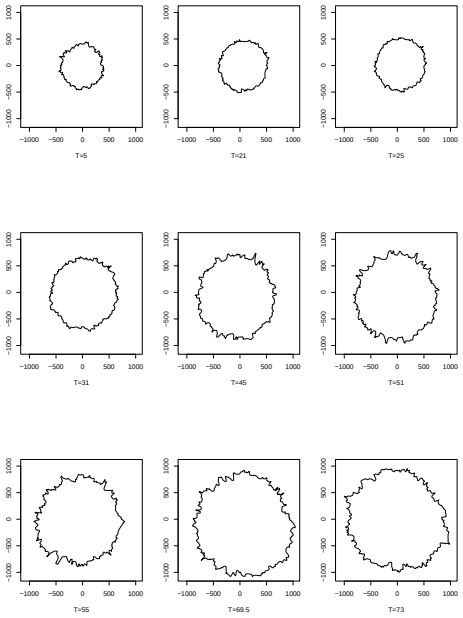

Figure 2: Contours of a brain tumour cell island at nine different time points. See Brú et al. (1998).

be the restriction of Z to $S_t = (0, t] \times \mathcal{X}$. Note that since Z is locally finite and S_t is bounded, Z_t is a finite random subset of S_t. The corresponding cumulative spatial processes are denoted

$$X = \{\xi_i : (t_i, \xi_i) \in Z\}, \quad X_t = \{\xi_i : (t_i, \xi_i) \in Z_t\}.$$

Note that X and X_t are the projections of Z and Z_t, respectively, on $\mathcal{X}$, see also Figure 3.

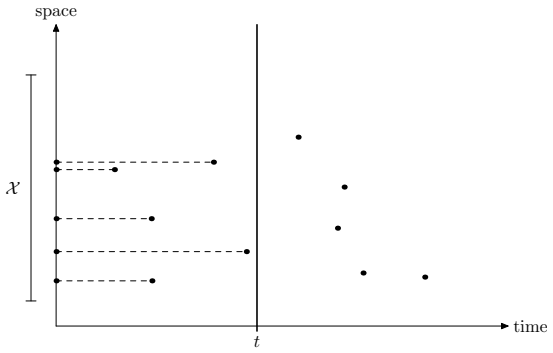

Figure 3: An illustration of the set-up. The points constitute the spatio-temporal point process Z and the dashed lines indicate the projections on $\mathcal{X}$ of points arrived before or at time t. The projected points in $\mathcal{X}$ constitute X_t.

Since the projection of Z on $\mathbb{R}_+$ is simple, the temporal part of the process gives a natural ordering of the points that does not exist in general for a spatial point process.

This feature will be used at various places in the following. Unless stated otherwise, the numbering of the points of Z is such that

$$t_1 < t_2 < \cdots < t_n < \cdots .$$

It will be assumed that Z_t has a density g_{Z_t} with respect to the unit rate Poisson point process on S_t. Because of the natural ordering of the time axis, there are also alternative and perhaps more natural ways of specifying the distribution of Z. Thus, the process can be defined by two families of conditional probability densities

$$\big\{p_n(t \mid t_{(n-1)}, \xi_{(n-1)}) : n \in \mathbb{N}\big\} \tag{1}$$

and

$$\big\{f_n(\xi \mid t_{(n-1)}, \xi_{(n-1)}, t_n) : n \in \mathbb{N}\big\} \tag{2}$$

with respect to the Lebesgue measure on $\mathbb{R}$ and $\mathbb{R}^d$, respectively. Here and in what follows we use the short notation $t_{(n)}, \xi_{(n)}$ for

$$(t_1, \xi_1), \ldots, (t_n, \xi_n).$$

The density $p_n(\cdot \mid t_{(n-1)}, \xi_{(n-1)})$ describes the distribution of the n-th time point given the history of the whole process up to time t_{n-1}, whereas the density $f_n(\cdot \mid t_{(n-1)}, \xi_{(n-1)}, t_n)$ describes the distribution of the spatial point at time t_n given the history up to time t_{n-1} and the arrival time of the n-th point. The density $p_n(\cdot \mid t_{(n-1)}, \xi_{(n-1)})$ has support (t_{n-1}, ∞) while the density $f_n(\cdot \mid t_{(n-1)}, \xi_{(n-1)}, t_n)$ has support $\mathcal{X}$.

In Appendix A, it is shown for a general spatio-temporal point process how the density of the process Z_t can be expressed in terms of conditional densities. A proof of this well-known result can be found in Daley and Vere-Jones (2002) on conditional intensities and likelihoods for marked point processes. An alternative proof may be found in Appendix A. Here, we just present the result. The density of Z_t with respect to the unit rate Poisson point process on S_t can be expressed as

$$\begin{aligned} g_{Z_t}(z) = \exp(t|\mathcal{X}|) \prod_{i=1}^{n} [p_i(t_i \mid t_{(i-1)}, \xi_{(i-1)}) f_i(\xi_i \mid t_{(i-1)}, \xi_{(i-1)}, t_i)] \\ \times S_{n+1}(t \mid t_{(n)}, \xi_{(n)}), \end{aligned}$$

where

$$z = \{(t_1, \xi_1), \ldots, (t_n, \xi_n)\}, \quad t_1 < \cdots < t_n.$$

Here

$$S_{n+1}(t \mid t_{(n)}, \xi_{(n)}) = \int_t^\infty p_{n+1}(u \mid t_{(n)}, \xi_{(n)}) \mathrm{d}u, \quad t > t_n,$$

is the survival function of $p_{n+1}(\cdot \mid t_{(n)}, \xi_{(n)})$.

For spatio-temporal point processes it is of particular interest to study the conditional intensities. For a sequence $\{(t_i, \xi_i)\}$ with

$$0 = t_0 < t_1 < \cdots < t_n < \cdots ,$$

the conditional intensity is

$$\lambda^\star(t, \xi) = \lambda_g(t) f^\star(\xi \mid t), \quad \text{if } t_{n-1} < t \leq t_n,$$

where

$$\lambda_g(t) = \frac{p_n(t \mid t_{(n-1)}, \xi_{(n-1)})}{S_n(t \mid t_{(n-1)}, \xi_{(n-1)})}, \quad \text{if } t_{n-1} < t \leq t_n,$$
$$f^\star(\xi \mid t) = f_n(\xi \mid t_{(n-1)}, \xi_{(n-1)}, t), \quad \text{if } t_{n-1} < t \leq t_n.$$

The conditional intensity $\lambda^\star$ has a simple intuitive interpretation. Thus,

$$\lambda^\star(t, \xi)\mathrm{d}t\mathrm{d}\xi$$

can be interpreted as the conditional probability of observing a point at (t, ξ) given the previous history of the process and a waiting time for the $n-$th point at least up till t. It can be shown that the density of Z_t can be written as

$$g_{Z_t}(z) = \exp\left(-\int_{S_t}[\lambda^\star(s,\xi) - 1]\mathrm{d}s\mathrm{d}\xi\right)\prod_{i=1}^{n}\lambda^\star(t_i, \xi_i), \tag{3}$$

where

$$z = \{(t_1, \xi_1), \ldots, (t_n, \xi_n)\}, \quad t_1 < \cdots < t_n.$$

For further details, see Appendix A.

2.2 The Poisson case

The process Z is Poisson with intensity function λ if the number $Z(A)$ of points falling in any Borel subset $A \in \mathcal{B}(S)$ is Poisson distributed with parameter

$$\int_A \lambda(s, \xi)\mathrm{d}s\mathrm{d}\xi.$$

For a Poisson process, $Z(A_1)$ and $Z(A_2)$ are independent if A_1 and A_2 are disjoint.

If Z is Poisson, the conditional intensity function $\lambda^\star$ is equal to the unconditional intensity function λ, and the density of Z_t with respect to the unit rate Poisson point process on S_t is given by

$$g_{Z_t}(z) = \exp(-\int_{S_t}[\lambda(s,\xi) - 1]\mathrm{d}\xi\mathrm{d}s)\prod_{i=1}^{n}\lambda(t_i, \xi_i).$$

The distribution of the cumulative spatial process X_t is also Poisson with intensity function

$$\lambda^t(\xi) = \int_0^t \lambda(s, \xi)\mathrm{d}s.$$

If the intensity function can be written as $\lambda(t, \xi) = \lambda_1(t)\lambda_2(\xi)$, then

$$\lambda^t(\xi) = a(t)\lambda_2(\xi),$$

where

$$a(t) = \int_0^t \lambda_1(s)\mathrm{d}s.$$

Thus, if the intensity function is of product form, the cumulative point pattern at time t is a scaled version of a spatial template Poisson point process with intensity function $\lambda_2(\xi)$.

In the Poisson case, the conditional densities (1) and (2) are

$$p_n(t \mid t_{(n-1)}, \xi_{(n-1)}) = \lambda_g(t) \exp(-\int_{t_{n-1}}^{t} \lambda_g(s)\mathrm{d}s), \quad t > t_{n-1},$$

and

$$f_n(\xi \mid t_{(n-1)}, \xi_{(n-1)}, t_n) = \frac{\lambda(t_n, \xi)}{\lambda_g(t_n)}, \quad \xi \in \mathcal{X},$$

where

$$\lambda_g(t) = \int_{\mathcal{X}} \lambda(t, \xi)\mathrm{d}\xi.$$

These results hold under the assumption

$$\int_t^{\infty} \lambda_g(s)\mathrm{d}s = \infty \text{ for all } t \geq 0.$$

The conditional densities can be given simple interpretations. Thus, let T_n be the arrival time of the $n-$th point. Then, given $(t_{(n-1)}, \xi_{(n-1)})$,

$$\int_{t_{n-1}}^{T_n} \lambda_g(s)\mathrm{d}s$$

is exponentially distributed with parameter 1. The density of the position Ξ_n of the $n-$th point, given $(t_{(n-1)}, \xi_{(n-1)}, t_n)$, is proportional to $\lambda(t_n, \cdot)$.

Poisson point processes play a fundamental role in stochastic geometry, see Stoyan et al. (1995) and references therein. In relation to growth modelling, an important model class is the class of Boolean models. In a purely spatial context, a Boolean model is defined by

$$Y = \cup_i \Xi(\eta_i),$$

where $\{\eta_i\}$ is a Poisson point process on $\mathcal{X}$ and $\{\Xi(\eta_i)\}$ is a sequence of independent and identically distributed random sets, independent of the points $\{\eta_i\}$ and centred at the points of the point process. In particular, Boolean models have been used in the modelling of tumour growth by Cressie and coworkers, see Cressie and Laslett (1987), Cressie (1991a,b) and Cressie and Hulting (1992). Their model can be described as a sequence of Boolean models such that the tumour Y_t at time t is a union of balls placed at uniform random positions inside the tumour Y_{t-1} at time $t-1$. Formally this means

$$Y_t = \cup\{B_d(\xi_i, R) : \xi_i \in Y_{t-1}\},$$

where $\{\xi_i\}$ is a homogeneous Poisson point process in $\mathcal{X}$. They also consider more regular point patterns than Poisson and, in the planar case, rectangular cells instead of circular cells in the growth process and establish the relation to interacting particle systems. Suitable transformations are introduced in order to be able to model a higher growth rate at parts of the boundary with higher curvature.

More recently, Deijfen (2003) has studied a random object Y_t defined as a connected union of randomly sized balls constructed from a spatio-temporal Poisson point process. It is shown that the asymptotic shape of the object is spherical. Other stochastic models of tumour growth also have asymptotic spherical growth, cf. Richardson (1973),

Schurger (1979), Bramson and Griffeath (1980), Bramson and Griffeath (1981) and Durret and Liggett (1981).

The model suggested in Cressie and Hulting (1992) has been the inspiration for the discrete Markov growth model studied recently in Jónsdóttir and Jensen (2005). The increments follow a cyclic Gaussian $p-$order process on the circle, see also Hobolth et al. (2003).

2.3 Cox processes

A spatio-temporal Cox process Z on S is a spatio-temporal Poisson point process with a *random* intensity function Λ, cf. Cox (1955), Møller and Waagepetersen (2003) and references therein. Such a process exhibits clustering between the points. The intensity function of a spatio-temporal Cox process is given by $\lambda(t,\xi) = \mathbb{E}\Lambda(t,\xi)$ and the pair correlation function by

$$\rho((t,\xi),(s,\eta)) = \frac{\mathbb{E}(\Lambda(t,\xi)\Lambda(s,\eta))}{\mathbb{E}\Lambda(t,\xi)\mathbb{E}\Lambda(s,\eta)}.$$

Note that

$$\rho((t,\xi),(s,\eta))\mathbb{E}\Lambda(t,\xi)\mathbb{E}\Lambda(s,\eta)\mathrm{d}t\mathrm{d}\xi\mathrm{d}s\mathrm{d}\eta$$

can be interpreted as the probability that Z contains points simultaneously in two infinitesimal regions around (t,ξ) and (s,η).

It is clear that Z_t is a spatio-temporal Cox process on S_t driven by the restriction Λ_t of Λ to S_t. The cumulative spatial process X_t is a Cox process on $\mathcal{X}$ driven by

$$\Lambda^t(\xi) = \int_0^t \Lambda(s,\xi)\mathrm{d}s.$$

The intensity function of X_t is $\lambda^t(\xi) = \mathbb{E}\Lambda^t(\xi)$. It can be shown that for $t' \leq t$, $X_{t'}$ has the same distribution as a process obtained by independent thinning of the points in X_t with retention probability for a point located at $\xi \in \mathcal{X}$ given by

$$p_{t',t}(\xi) = \frac{\lambda^{t'}(\xi)}{\lambda^t(\xi)}.$$

A spatio-temporal Cox process with log-Gaussian intensity function has been used with success in the analysis of weed data of the type shown in Figure 1, see Møller et al. (1998) or Brix and Møller (2001). More specifically, the model considered is of the following form

$$\log\Lambda(t,\xi) = m(t,\xi) + W(\xi),$$

where m is a mean function satisfying

$$m(t',\xi) \leq m(t,\xi) \text{ for } t' \leq t, \xi \in \mathcal{X},$$

and W is a zero mean Gaussian process on $\mathcal{X}$. In fact, a bivariate model of Cox type is considered for the modelling of two types of weed plants. An extension of this approach, involving an Ornstein-Uhlenbeck stochastic differential equation, is discussed in Brix and Diggle (2001).

Another important class of spatio-temporal Cox processes is the class of spatio-temporal shot noise Cox processes. As an example, consider a Cox process Z driven by

$$\Lambda(t,\xi) = \sum_{(u,c,\gamma)\in\Phi} \gamma k((u,c),(t,\xi)),$$

where $k((u,c),\cdot)$ is a kernel (i.e. a probability density on S) and Φ is a Poisson point process on $S\times\mathbb{R}_+$. A comprehensive treatment of the purely spatial case can be found in Møller (2003). See also the recent paper by Møller and Torrisi (2005). The process can be viewed as a cluster process since

$$Z|\Phi \sim \cup_{(u,c,\gamma)\in\Phi} U_{u,c,\gamma},$$

where $U_{u,c,\gamma}$, $(u,c,\gamma)\in\Phi$, are independent spatio-temporal Poisson processes with intensity functions

$$\gamma k((u,c),(\cdot,\cdot)).$$

The cumulative spatial process X_t is also a cluster process of Cox-type since

$$X_t|\Phi \sim \cup_{(u,c,\gamma)\in\Phi} V_{u,c,\gamma},$$

where $V_{u,c,\gamma}$, $(u,c,\gamma)\in\Phi$, are independent Poisson point processes on $\mathcal{X}$ with intensity function

$$\gamma\int_0^t k((u,c),(s,\cdot))\mathrm{d}s.$$

Another important model class is that of shot noise G Cox processes, also suggested for the analysis of the weeds data, cf. Brix (1998, 1999) and Brix and Chadoeuf (2002). These processes are defined through the class of $G-$measures, which originates from the so-called $G-$family of probability distributions, extending gamma and inverse Gaussian distributions.

2.4 Markov point processes

In recent years, Markov models for inhomogeneous spatial point processes have been studied quite intensively, see Stoyan and Stoyan (1998), Baddeley et al. (2000), Jensen and Nielsen (2000), Hahn et al. (2003) and references therein. The majority of the inhomogeneous models has been constructed by introducing inhomogeneity into a homogeneous Markov point process X, defined on a bounded subset $\mathcal{X}$ of $\mathbb{R}^d$. In this section, we will discuss extensions of these inhomogeneous point process models to a spatio-temporal framework. Extensions can be constructed in an *empirical* fashion, writing down a density for the spatio-temporal point pattern or in a *mechanistic* fashion, using conditional intensities.

We start by giving a short review of recently suggested inhomogeneous spatial Markov point processes. It should be noted that Markov models are primarily appropriate for describing inhibition between the points.

2.4.1 Inhomogeneous spatial point processes

In principle, any given homogeneous template point process can be turned into an inhomogeneous point process by independent thinning with a retention probability

$p(\xi)$ that depends on the location $\xi \in \mathcal{X}$. As Baddeley et al. (2000) show, second order functions such as Ripley's K-function can be defined for thinned point processes such that they are identical to the corresponding second order functions of the original process. However, thinning changes the interaction structure. Thus, if a very regular point process is subjected to inhomogeneous thinning, regions of low intensity seem to exhibit almost no interaction and look similar to a realisation of a Poisson process while regions with high intensity will show the original very regular pattern.

Another method that is applicable to any template process is to generate inhomogeneity by a nonlinear transformation of the spatial coordinates. Jensen and Nielsen (2000) prove that the process resulting from transformation of a Markov point process is again Markov. Transformation does in general not preserve (local) isotropy of the template process. See also Jensen and Nielsen (2004).

Ogata and Tanemura (1986) and Stoyan and Stoyan (1998) suggest to introduce inhomogeneity into Markov or Gibbs models by location dependent first order interactions. As an example, consider a Strauss template X on $\mathcal{X}$ with parameters $\beta > 0$, $\gamma \in [0, 1]$ and $R > 0$, which is defined by a density

$$f_X(x) \propto \beta^{n(x)} \gamma^{s(x)}, \quad s(x) = \sum_{\{\eta,\xi\} \subseteq x} \mathbf{1}_{[0,R]}(\|\eta - \xi\|), \tag{4}$$

with respect to the unit rate Poisson process on $\mathcal{X}$. In (4), the sum is over all pairs of different points in x. The resulting inhomogeneous process has density

$$f_X(x) \propto \prod_{\eta \in x} \beta(\eta) \gamma^{s(x)}, \quad s(x) = \sum_{\{\eta,\xi\} \subseteq x} \mathbf{1}_{[0,R]}(\|\eta - \xi\|) \tag{5}$$

with respect to the unit rate Poisson process on $\mathcal{X}$. For such an inhomogeneous process, the degree of regularity in the resulting process depends on the intensity as in the case of thinning, described above.

An approach that preserves locally the geometry of the template model, in particular the degree of regularity and also isotropy, was introduced in Hahn et al. (2003). It can be applied to models that are specified by a density with respect to the unit rate Poisson process. The idea of the approach is that a location dependent scale factor $c(\xi) > 0$ changes the local specification of the model such that in a neighbourhood of any point $\xi \in \mathcal{X}$, the inhomogeneous process behaves like the template process scaled by the factor $c(\xi)$. This is achieved by defining the locally scaled process X_c by a density $f_{X_c}^{(c)}$ with respect to an inhomogeneous Poisson process of rate $c(\xi)^{-d}$. The density $f_{X_c}^{(c)}$ is obtained (up to a normalising constant) from the template density f_X by replacing all k-dimensional volume measures ν^k, $k = 0, 1, \ldots, d$, that occur in the definition of f_X by their locally scaled counterparts ν_c^k, where $\nu_c^k(A) := \int_A c(u)^{-k} \nu^k(du)$ for all $A \in \mathcal{B}_d$. Note that according to previous notation $\nu^d(\cdot) = |\cdot|$.

A locally scaled version of the Strauss process has thereby the density

$$f_{X_c}^{(c)}(x) \propto \beta^{n(x)} \gamma^{s_c(x)}, \quad s_c(x) = \sum_{\{\eta,\xi\} \subseteq x} \mathbf{1}_{[0,R]}(\nu_c^1([\eta, \xi])), \tag{6}$$

where

$$\nu_c^1([\eta, \xi]) := \int_{[\eta,\xi]} c(u)^{-1} \nu^1(\mathrm{d}u)$$

is the locally scaled length of the segment $[\eta, \xi]$. This modification applies to all Markov point processes where the higher order interaction is a function of pairwise distances. The resulting inhomogeneous point process is again Markov, now with respect to the neighbour relation

$$\eta \sim \xi \quad \Longleftrightarrow \quad \nu_c^1([\eta, \xi]) \leq R.$$

Since evaluation of the integral in the locally scaled length measure may be computationally expensive in the general case, the scaled distance of two points may be approximated by

$$\nu_c^1([\eta, \xi]) \approx \frac{\|\eta - \xi\|}{(c(\eta) + c(\xi))/2}. \tag{7}$$

Using (7) in (6), and adjusting the first order term in (6), we get the density f_{X_c} of X_c with respect to the unit rate Poisson process as

$$f_{X_c}(x) \propto \beta^{n(x)} \gamma^{s_c(x)} \prod_{\eta \in x} c(\eta)^{-d}, \quad s_c(x) = \sum_{\{\eta,\xi\} \subseteq x} \mathbf{1}_{[0, \frac{c(\eta)+c(\xi)}{2} R]}(\|\eta - \xi\|). \tag{8}$$

As shown in Hahn et al. (2003), if the scaling function is slowly varying compared to the interaction radius, the local intensity in a point ξ of such a locally scaled process is in good approximation proportional to $c(\xi)^{-d}$. Figure 4 and 5 show realisations of locally scaled Strauss processes. Notice that locally these processes look like a scaled version of a homogeneous Strauss process.

The statistical analysis of local scaling models is discussed in Prokesova et al. (2005).

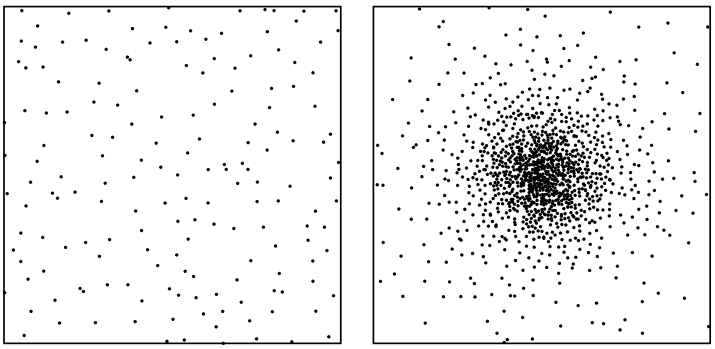

Figure 4: (Left) Homogeneous template Strauss process X on $[-1, 1]^2$ with parameters $\beta = 200$, $\gamma = 0.1$, $R = 0.1$. (Right) Inhomogeneous Strauss process X_c with $c(\xi) = \|\xi\|^2 + 0.1$. (Reprinted from Hahn et al. (2003).)

2.4.2 Spatio-temporal extensions

How can we construct spatio-temporal extensions of these inhomogeneous Markov point processes? An *empirical* approach is to write down an expression for the density g_{Z_t} of Z_t with respect to the unit rate Poisson point process on S_t. If the interactions are purely spatial, an obvious suggestion is

$$g_{Z_t}(z) \propto \prod_{i=1}^{n} \lambda(t_i, \xi_i) \cdot \prod_{y \subseteq_2 x} \varphi(y),$$

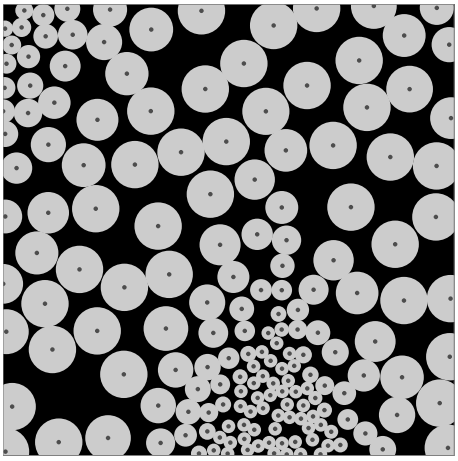

Figure 5: Inhomogeneous Strauss process obtained by local scaling. The value of the interaction parameter is $\gamma = 0$, corresponding to a hardcore model. To each point ξ, a circular disc of radius $\frac{c(\xi)}{2}R$ is attached.

where

$$z = \{(t_1, \xi_1), \ldots, (t_n, \xi_n)\},$$
$$x = \{\xi_1, \ldots, \xi_n\},$$

and $\subseteq_2$ indicates that only subsets with at least two elements are considered. If

$$\lambda(t, \xi) = \lambda_1(t)\lambda_2(\xi),$$

then it can be shown that the density of X_t is of the form

$$f_{X_t}(x) \propto a(t)^{n(x)} \prod_{\xi \in x} \lambda_2(\xi) \prod_{y \subseteq_2 x} \varphi(y),$$

where

$$a(t) = \int_0^t \lambda_1(s)\mathrm{d}s.$$

Furthermore, $X_{t'}$ can be obtained from X_t by independent thinning, $t' \leq t$.

Inspired by these results, we may consider backwards temporal thinning of a spatial Markov point process X with intensity function λ, say. Let the resulting spatio-temporal point process be denoted by

$$Z = \{(T_\xi, \xi) : \xi \in X\}.$$

If, conditionally on X,

$$T_\xi, \xi \in X,$$

are independent and T_ξ has density p_ξ, then the cumulative process X_t has intensity function

$$\lambda^t(\xi) = \lambda(\xi) \int_0^t p_\xi(s)\mathrm{d}s.$$

Furthermore, for all $t' \leq t$, $X_{t'}$ can be obtained from X_t by independent thinning, with retention probability for a point located at ξ given by

$$p_{t',t}(\xi) = \int_0^{t'} p_\xi(s)\mathrm{d}s / \int_0^t p_\xi(s)\mathrm{d}s.$$

Note that the special $K-$function defined in Baddeley et al. (2000) will be the same for all processes X_t. Note also that the thinning, backwards in time, implies that X_t may look Poisson-like for small t.

Below, we study thinning of a locally scaled Strauss process.

Example 2.1 *Temporal thinning of a locally scaled Strauss process.* Let $c_1 : \mathbb{R}_+ \to \mathbb{R}$ and $c_2 : \mathbb{R}^d \to \mathbb{R}$ be positive and bounded local scaling functions for time and space, respectively. Let the density of X be a locally scaled Strauss process

$$f_X(x) \propto \beta^{n(x)} \gamma^{s_{c_2}(x)} \prod_{\eta \in x} c_2(\eta)^{-d},$$

where

$$s_{c_2}(x) = \sum_{\{\eta,\xi\} \subseteq x} \mathbf{1}_{[0,R]}(\nu^1_{c_2}([\eta, \xi])).$$

A birth time at ξ is distributed with a density which does not depend on ξ

$$p_\xi(t) \propto c_1(t)^{-1}, \tag{9}$$

if $t \in [0, T]$, and $p_\xi(t) = 0$, otherwise.

Figure 6 shows the result of a simulation of a temporal thinning of such a locally scaled Strauss process on $[-1, 1]^2$ with $\beta = 100$, $\gamma = 0.01$, $R = 0.1$ and local scaling function $c_2(\xi) = 0.2 + 4\|\xi\|^2$. The birth times have density given in (9) with $c_1(t) = 0.2 + 0.05t$ and $T = 12$. The figure shows the corresponding cumulative point patterns $X_{t'}$ for $t' = 2, 4, 8, 12$. Note that for small t', $X_{t'}$ appears Poisson-like.

Another possibility is specification of a spatio-temporal point process model in terms of conditional intensities, see e.g. Hawkes (1971) or Schoenberg et al. (2002) and references therein. This approach could be characterised as *mechanistic*. Here, the form of the conditional intensity may be motivated by the form of the Papangelou conditional intensity for a purely spatial point process. A local scaling example is given below.

Example 2.2 Let $c_1 : \mathbb{R}_+ \to \mathbb{R}$ and $c_2 : \mathbb{R}^d \to \mathbb{R}$ be positive and bounded scaling functions for time and space, respectively. We define the spatio-temporal point process Z by its conditional intensities,

$$\lambda^\star(t, \xi) = \frac{\beta \gamma^{s_{c_2}(\xi | \xi_{(n-1)})}}{c_1(t) c_2(\xi)^d}, \quad t_{n-1} < t \leq t_n, \ \ \xi \in \mathcal{X},$$

where

$$s_{c_2}(\xi \mid \xi_{(n-1)}) = \sum_{i=1}^{n-1} \mathbf{1}_{[0,R]}(\nu^1_{c_2}([\xi, \xi_i])).$$

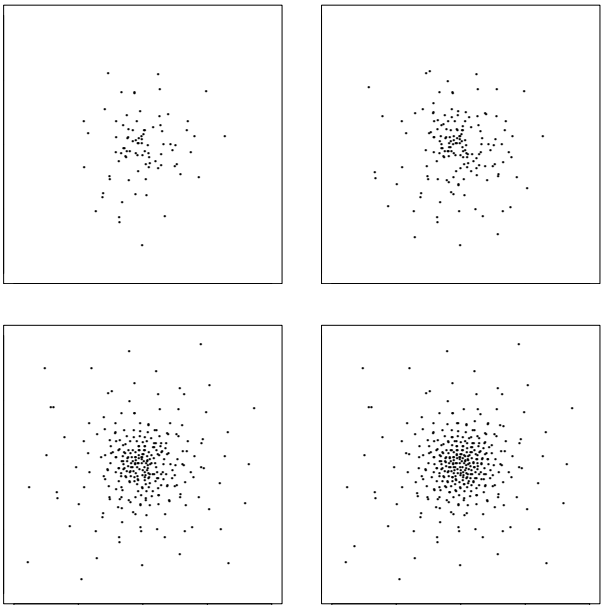

Figure 6: Result of a simulation of a backwards thinning of a locally scaled Strauss process on $[-1,1]^2$. For details, see Example 2.1.

In this case, the density of Z_t is of the following form

$$\begin{aligned} g_{Z_t}(z) &= \exp\Big(-\sum_{i=1}^{n}\int_{t_{i-1}}^{t_i}\int_{\mathcal{X}}\Big(\frac{\beta\gamma^{s_{c_2}(\xi|\xi_{(i-1)})}}{c_1(t)c_2(\xi)^d}-1\Big)\mathrm{d}t\mathrm{d}\xi\Big)\prod_{i=1}^{n}\frac{\beta\gamma^{s_{c_2}(\xi_i|\xi_{(i-1)})}}{c_1(t_i)c_2(\xi_i)^d} \\ &= \exp\Big(-\sum_{i=1}^{n}\int_{t_{i-1}}^{t_i}\int_{\mathcal{X}}\Big(\frac{\beta\gamma^{s_{c_2}(\xi|\xi_{(i-1)})}}{c_1(t)c_2(\xi)^d}-1\Big)\mathrm{d}t\mathrm{d}\xi\Big)\beta^{n(z)}\gamma^{\sum_{i=1}^{n}s_{c_2}(\xi_i|\xi_{(i-1)})} \\ &\quad\times\prod_{i=1}^{n}\frac{1}{c_1(t_i)c_2(\xi_i)^d}. \end{aligned}$$

Figure 7 shows the result of a simulation on $[-1,1]^2$ of this type of spatio-temporal extension of the locally scaled Strauss process, with $\beta = 3.61$, $\gamma = 0.01$, $R = 0.1$, $c_1(t) = 0.2+0.05t$ and $c_2(\xi) = 0.2+4\|\xi\|^2$. The parameter values are thereby identical to those chosen in the previous example, except for the value of β which has been chosen so that the number of points are expected to be the same in the two examples.

3 Lévy based growth models

In this section, we will discuss an alternative approach to modelling of random growing objects. We will concentrate on the case of random planar star-shaped objects. The model describes how the boundary of the growing object expands in time. The basic notion of this approach is that of Lévy bases.

3.1 Set-up

This subsection provides a very brief overview of the theory of Lévy bases, in particular, the theory of integration with respect to a Lévy basis. For a more detailed account,

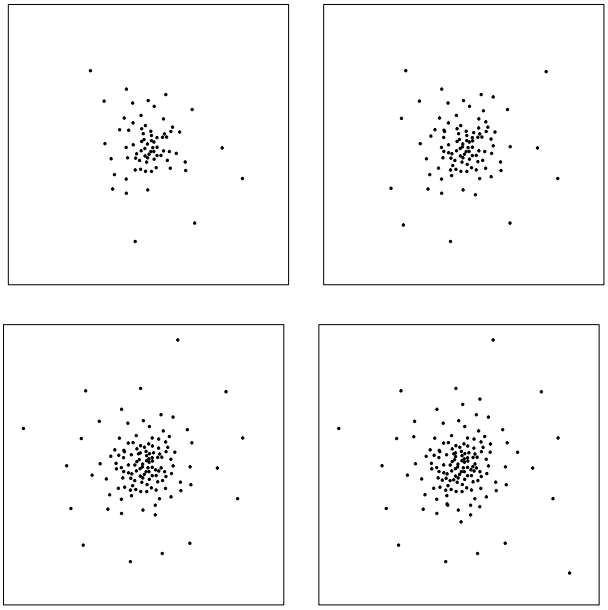

Figure 7: Result of a simulation on $[-1,1]^2$ of the spatio-temporal extension of the locally scaled Strauss process described in Example 2.2. For details, see the text.

see Barndorff-Nielsen and Schmiegel (2004) and references therein. We will use the following notation for the cumulant function of a random variable X,

$$C\{\lambda \ddagger X\} = \log \mathbb{E}(e^{i\lambda X}).$$

Let $(\mathcal{R}, \mathcal{A})$ be a measurable space. In what follows, we will assume that $\mathcal{R}$ is a Borel subset of $\mathbb{R}^n$. Let $\mathcal{A} = \mathcal{B}(\mathcal{R})$ be the $\sigma-$algebra of Borel subsets of $\mathcal{R}$ and let $\mathcal{A}_b$ denote the class of bounded elements of $\mathcal{A}$. A collection of random variables $Z = \{Z(A) : A \in \mathcal{A}\}$ or $Z = \{Z(A) : A \in \mathcal{A}_b\}$ is said to be an *independently scattered random measure*, if for every sequence $\{A_n\}$ of disjoint sets in $\mathcal{A}$, respectively $\mathcal{A}_b$, the random variables $Z(A_n)$ are independent and $Z(\bigcup A_n) = \sum Z(A_n)$ a.s., where in case $Z = \{Z(A) : A \in \mathcal{A}_b\}$ we furthermore require $\cup A_n \in \mathcal{A}_b$. If, in addition, $Z(A)$ is *infinitely divisible* for all $A \in \mathcal{A}$, Z will be called a *Lévy basis*. (The need to distinguish between the two cases $\mathcal{A}$ and $\mathcal{A}_b$ comes from the possible difficulty in controlling the countable sum $\sum Z(A_n)$ if Z can take both positive and negative values. When that is the case Z should strictly speaking be referred to as an independently scattered signed random measure.)

When Z is a Lévy basis, the cumulant function of $Z(A)$ can be written as

$$C\{\lambda \ddagger Z(A)\} = i\lambda a(A) - \frac{1}{2}\lambda^2 b(A) + \int_{\mathbb{R}} (e^{i\lambda x} - 1 - i\lambda x \mathbf{1}_{[-1,1]}(x)) U(\mathrm{d}x, A), \qquad (10)$$

where a is a signed measure on $\mathcal{A}$ or $\mathcal{A}_b$, b is a positive measure on $\mathcal{A}$ or $\mathcal{A}_b$, $U(\mathrm{d}x, A)$ is a Lévy measure on $\mathbb{R}$ for fixed A and a measure on $\mathcal{A}$ or $\mathcal{A}_b$ for fixed $\mathrm{d}x$. The Lévy basis is said to have characteristic triplet (a, b, U) and the measure U is referred to as the generalised Lévy measure.

The cumulant function (10) can also be expressed in an infinitesimal form

$$C\{\lambda \ddagger Z(\mathrm{d}\xi)\} = i\lambda a(\mathrm{d}\xi) - \frac{1}{2}\lambda^2 b(\mathrm{d}\xi) + \int_{\mathbb{R}} (e^{i\lambda x} - 1 - i\lambda x \mathbf{1}_{[-1,1]}(x)) U(\mathrm{d}x, \mathrm{d}\xi).$$

Without essential loss of generality we can assume that the measure U factorises as

$$U(\mathrm{d}x, \mathrm{d}\xi) = V(\mathrm{d}x, \xi)\mu(\mathrm{d}\xi),$$

where μ is some measure on $\mathcal{R}$ and $V(\mathrm{d}x, \xi)$ is a Lévy measure for fixed ξ. A Lévy basis is called *factorisable*, if the Lévy measure $V(\cdot; \xi)$ does not depend on ξ. If a Lévy basis is factorisable, then one can write

$$C\{\lambda \ddagger Z(\mathrm{d}\xi)\} = i\lambda a(\mathrm{d}\xi) - \frac{1}{2}\lambda^2 b(d\xi) + C\{\lambda \ddagger Z'\}\mu(\mathrm{d}\xi),$$

where Z' is an infinitely divisible random variable with cumulant function

$$C\{\lambda \ddagger Z'\} = \int_{\mathbb{R}} (e^{i\lambda x} - 1 - i\lambda x \mathbf{1}_{[-1,1]}(x)) V(\mathrm{d}x).$$

We will now give examples of Lévy bases.

Example 3.1 *Poisson Lévy basis.* The Poisson basis has characteristic triplet $(\mu, 0, U)$, where $U(\mathrm{d}x, \mathrm{d}\xi) = \delta_1(\mathrm{d}x)\mu(\mathrm{d}\xi)$ and δ_1 is Dirac's delta function at 1, so Z is factorisable. Clearly the cumulant function of $Z(A)$ is

$$C\{\lambda \ddagger Z(A)\} = (e^{i\lambda} - 1)\mu(A).$$

We have $Z(A) \sim \mathrm{P}ois(\mu(A))$. The Poisson point process was dealt with in more detail in Section 2.2. □

Example 3.2 *Normal Lévy basis.* The normal Lévy basis has characteristic triplet $(\alpha\mu, \sigma^2\mu, 0)$ and the cumulant function is

$$C\{\lambda \ddagger Z(A)\} = i\lambda\alpha\mu(A) - \frac{1}{2}\lambda^2\sigma^2\mu(A).$$

Note that $Z(A) \sim N(\alpha\mu(A), \sigma^2\mu(A))$. □

Example 3.3 *Gamma Lévy basis.* The gamma Lévy basis has characteristic triplet $(a, 0, U)$ where

$$a(\mathrm{d}\xi) = \frac{1 - e^{-\alpha(\xi)}}{\alpha(\xi)}\mu(\mathrm{d}\xi),$$
$$U(\mathrm{d}x, \mathrm{d}\xi) = \mathbf{1}_{\mathbb{R}_+}(x)x^{-1}e^{-\alpha(\xi)x}\mathrm{d}x\mu(\mathrm{d}\xi),$$

and $\alpha(\xi) > 0$. If $\alpha(\xi)$ does not depend on ξ, $\alpha(\xi) = \alpha$, say, $Z(A) \sim G(\mu(A), \alpha)$, $A \in \mathcal{A}$. □

Example 3.4 *Inverse Gaussian Lévy basis.* When Z has characteristic triplet $(a, 0, U)$ where

$$a(\mathrm{d}\xi) = \frac{1}{\sqrt{2\pi}} \int_0^1 u^{-\frac{1}{2}} e^{-\frac{1}{2}\gamma^2(\xi)u} \mathrm{d}u\mu(\mathrm{d}\xi),$$
$$U(\mathrm{d}x, \mathrm{d}\xi) = \frac{1}{\sqrt{2\pi}} \mathbf{1}_{\mathbb{R}_+}(x) x^{-\frac{3}{2}} e^{-\frac{1}{2}\gamma^2(\xi)x} \mathrm{d}x\mu(\mathrm{d}\xi),$$

and $\gamma(\xi) > 0$, Z constitutes an inverse Gaussian Lévy basis. If $\gamma(\xi)$ does not depend on ξ, $\gamma(\xi) = \gamma$, say, then $Z(A) \sim IG(\mu(A), \gamma)$, $A \in \mathcal{A}$. □

The Poisson, gamma and inverse Gaussian Lévy bases are examples of the random $G-$measures introduced in Brix (1999). These measures are purely discrete and can be represented as

$$Z(A) = a_0(A) + \int_0^\infty y\tilde{Z}(A \times \mathrm{d}y),$$

where $\tilde{Z}$ is a Poisson measure on $\mathcal{R} \times [0, \infty)$. This result is an example of a Lévy-Ito representation.

The usefulness of the definitions above becomes clear in connection with the integration of measurable functions f with respect to a Lévy basis Z. We consider the integral of a measurable function f on $\mathcal{R}$ with respect to a factorisable Lévy basis Z. For simplicity we denote this integral by $f \bullet Z$. For the theory of integration with respect to independently scattered random measures, see Kallenberg (1989) and Kwapien and Woyczynski (1992). A key result for many calculations is (subject to minor regularity conditions)

$$C\{\lambda \ddagger f \bullet Z\} = i\lambda(f \bullet a) - \frac{1}{2}\lambda^2(f^2 \bullet b) + \int_{\mathcal{R}} C\{\lambda f(\xi) \ddagger Z'\}\mu(\mathrm{d}\xi). \tag{11}$$

Similarly, for the logarithm of the Laplace transform of $f \bullet Z$,

$$K\{\lambda \ddagger f \bullet Z\} = C\{-i\lambda \ddagger f \bullet Z\},$$

we have

$$K\{\lambda \ddagger f \bullet Z\} = \lambda(f \bullet a) + \frac{1}{2}\lambda^2(f^2 \bullet b) + \int_{\mathcal{R}} K\{\lambda f(\xi) \ddagger Z'\}\mu(\mathrm{d}\xi). \tag{12}$$

If Z is a normal Lévy basis, $Z(A) \sim N(\alpha\mu(A), \sigma^2\mu(A))$, we have

$$C\{\lambda \ddagger f \bullet Z\} = \int_{\mathcal{R}} C\{\lambda f(\xi) \ddagger Z'\}\mu(\mathrm{d}\xi), \tag{13}$$

and

$$K\{\lambda \ddagger f \bullet Z\} = \int_{\mathcal{R}} K\{\lambda f(\xi) \ddagger Z'\}\mu(\mathrm{d}\xi), \tag{14}$$

where $Z' \sim N(\alpha, \sigma^2)$. Note that (13) and (14) also hold for a factorisable Lévy basis with $a \equiv b \equiv 0$.

3.2 Lévy based growth models

Let us consider a planar compact object with size and shape changing over time, where the object at time t is denoted by $Y_t \subset \mathbb{R}^2$. In the following we will assume that Y_t is star-shaped with respect to a point $z \in \mathbb{R}^2$ for all t. Then the boundary of the object Y_t can be determined by its radial function $R_t = \{R_t(\phi) : \phi \in [-\pi, \pi)\}$, where

$$R_t(\phi) = \max\{r : z + r(\cos\phi, \sin\phi) \in Y_t\}, \quad \phi \in [-\pi, \pi).$$

In the following we will let

$$\mathcal{R} = [-\pi, \pi) \times [0, \infty)$$

and $\mathcal{A}$ the Borel σ-algebra of $\mathcal{R}$. The idea behind the following definitions is based on the intuitive picture of an ambit set $A_t(\phi)$, associated to each point (ϕ, t), which defines the causal correlation cone. The ambit set satisfies

$$A_t(\phi) \subseteq [-\pi, \pi) \times [0, t].$$

Examples are shown in Figure 8. The radial process $R_t(\phi)$ is defined as the integral of some weight function over the attached ambit set, with respect to a positive factorisable Lévy basis or as the exponential of such an integral with respect to a factorisable or normal Lévy basis.

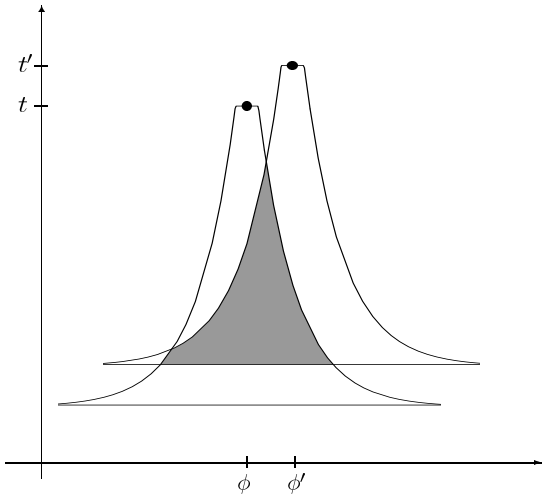

Figure 8: Examples of ambit sets $A_t(\phi)$ and $A_{t'}(\phi')$, respectively. Their intersection (shown hatched) determines the dependence structure of the growth process.

Definition 3.5 Let Z be a factorisable positive Lévy basis on $\mathcal{R}$. The field of radial functions $R = \{R_t(\phi)\}$ follows a *linear Lévy growth model* if

$$R_t(\phi) = \int_{A_t(\phi)} f_t(\xi; \phi) Z(\mathrm{d}\xi).$$

The ambit set $A_t(\phi) \in \mathcal{A}$ and the positive deterministic weight function $f_t(\xi; \phi)$, which is assumed to be suitable for the integral to exist, must be defined cyclically such that $R_t(\cdot)$ is cyclic.

Definition 3.6 Let Z be a factorisable or normal Lévy basis. The field of radial functions $R = \{R_t(\phi)\}$ follows an *exponential Lévy growth model* if

$$R_t(\phi) = \exp\left(\int_{A_t(\phi)} f_t(\xi;\phi) Z(\mathrm{d}\xi)\right).$$

The ambit set $A_t(\phi) \in \mathcal{A}$ and the deterministic weight function $f_t(\xi;\phi)$, assumed to be suitable for the integrals to exist, must be defined cyclically such that $R_t(\cdot)$ is cyclic.

There are many interesting problems to study within this model framework. Basically, it is the Lévy basis Z, the ambit sets $A_t(\phi)$ and the weight functions $f_t(\xi;\phi)$, which determine the growth dynamics. These three ingredients can be chosen arbitrarily so that a great variety of different growth dynamics can be obtained.

Below, we study linear and exponential growth models separately.

3.2.1 Linear Lévy growth models

Let us assume that R follows a linear Lévy growth model and that the Lévy basis has no Gaussian part, i.e. $b \equiv 0$. Using the key relation (12), we get that

$$\mathbb{E}(R_t(\phi)) = \int_{A_t(\phi)} f_t(\xi;\phi) a(\mathrm{d}\xi) + \mathbb{E}(Z') \int_{A_t(\phi)} f_t(\xi;\phi) \mu(\mathrm{d}\xi) \tag{15}$$

$$\mathbb{V}(R_t(\phi)) = \mathbb{V}(Z') \int_{A_t(\phi)} f_t(\xi;\phi)^2 \mu(\mathrm{d}\xi), \tag{16}$$

where $\mathbb{V}$ is the notation used for variance. Using (16) and the independence properties of a Lévy basis, we furthermore have

$$\mathrm{Cov}(R_t(\phi), R_{t'}(\phi')) = \mathbb{V}(Z') \int_{A_t(\phi)\cap A_{t'}(\phi')} f_t(\xi;\phi) f_{t'}(\xi;\phi') \mu(\mathrm{d}\xi). \tag{17}$$

The proof of (17) goes as follows. Let $A = A_t(\phi)$ and $A' = A_{t'}(\phi')$. Then,

$$\begin{aligned}
&\mathrm{Cov}(R_t(\phi), R_{t'}(\phi')) \\
&\quad = \mathrm{Cov}\left(\int_A f_t(\xi;\phi) Z(\mathrm{d}\xi), \int_{A'} f_{t'}(\xi;\phi') Z(\mathrm{d}\xi)\right) \\
&\quad = \mathrm{Cov}\left(\int_{A\cap A'} f_t(\xi;\phi) Z(\mathrm{d}\xi), \int_{A\cap A'} f_{t'}(\xi;\phi') Z(\mathrm{d}\xi)\right) \\
&\quad = \frac{1}{2}\Bigg[\mathbb{V}\left(\int_{A\cap A'} (f_t(\xi;\phi) + f_{t'}(\xi;\phi')) Z(\mathrm{d}\xi)\right) \\
&\qquad\quad - \mathbb{V}\left(\int_{A\cap A'} f_t(\xi;\phi) Z(\mathrm{d}\xi)\right) - \mathbb{V}\left(\int_{A\cap A'} f_{t'}(\xi;\phi') Z(\mathrm{d}\xi)\right)\Bigg].
\end{aligned}$$

Modelling of a given covariance structure reduces to solving (17) for the weight-function f and the shape and size of the ambit sets $A_t(\phi)$. In practise this might be a complicated task, but for special applications it is possible. Equation (17) also provides some useful geometric interpretation of the covariance structure. This can most easily be seen for the simple case of a constant weight-function $f_t(\xi;\phi) \equiv f$ for all $\xi, (\phi, t) \in \mathcal{R}$. In this case (17) reduces to

$$\mathrm{Cov}(R_t(\phi), R_{t'}(\phi')) \propto \mu(A_t(\phi) \cap A_{t'}(\phi')). \tag{18}$$

For a constant weight function the modelling of spatio-temporal covariances thus reduces to the problem of finding ambit sets $A_t(\phi)$ whose measure of overlap

$$\mu(A_t(\phi) \cap A_{t'}(\phi'))$$

fulfills (18) (see Figure 8 for an illustration). Note that only the measure of the overlap is involved and not the shape of the overlap.

In some growth examples it might be more natural to specify the model in terms of the time derivative of $R_t(\phi)$. For instance, as

$$R'_t(\phi) = \int_{A_t(\phi)} f_t(\xi;\phi) Z(\mathrm{d}\xi).$$

The induced model for $R_t(\phi)$ is again a linear Lévy growth model. We thus have

$$\begin{aligned} R_t(\phi) &= \int_0^t \int_{\mathcal{R}} \mathbf{1}_{A_s(\phi)}(\xi) f_s(\xi;\phi) Z(\mathrm{d}\xi)\mathrm{d}s \\ &= \int_{\mathcal{R}} \int_0^t \mathbf{1}_{A_s(\phi)}(\xi) f_s(\xi;\phi)\mathrm{d}s Z(\mathrm{d}\xi) \\ &= \int_{\bar{A}_t(\phi)} \bar{f}_t(\xi;\phi) Z(\mathrm{d}\xi), \end{aligned} \tag{19}$$

where

$$\bar{A}_t(\phi) = \cup_{0\leq s\leq t} A_s(\phi)$$

and

$$\bar{f}_t(\xi;\phi) = \int_0^t \mathbf{1}_{A_s(\phi)}(\xi) f_s(\xi;\phi)\mathrm{d}s.$$

The representation (19) is, of course, not unique. If the ambit sets are of the form

$$A_t(\phi) = B_t \cap C_\phi,$$

where $B_t \subseteq [-\pi,\pi)\times[0,t]$, we may instead choose

$$\bar{A}_t(\phi) = C_\phi \cap ([-\pi,\pi)\times[0,t])$$

and

$$\bar{f}_t(\xi;\phi) = \int_0^t \mathbf{1}_{B_s}(\xi) f_s(\xi;\phi)\mathrm{d}s.$$

3.2.2 Exponential Lévy growth models

In the following we will assume that we have a factorisable Lévy basis with $b \equiv 0$ or a normal Lévy basis. Equation (14) allows us to calculate arbitrary n-point correlations in an exponential Lévy growth model. If we assume the correlations are finite, i.e. $\mathbb{E}\{R_{t_1}(\phi_1)\cdot\ldots\cdot R_{t_n}(\phi_n)\} < \infty$, we have

$$\frac{\mathbb{E}\{\prod_{j=1}^n R_{t_j}(\phi_j)\}}{\prod_{j=1}^n \mathbb{E}\{R_{t_j}(\phi_j)\}} = \frac{\exp\left\{\int_{\mathcal{R}} \mathrm{K}\left\{\sum_{j=1}^n f_{t_j}(\xi,\phi_j)\mathbf{1}_{A_{t_j}(\phi_j)}(\xi) \ddagger Z'\right\}\mu(\mathrm{d}\xi)\right\}}{\exp\left\{\sum_{j=1}^n \int_{\mathcal{R}} \mathrm{K}\left\{f_{t_j}(\xi,\phi_j)\mathbf{1}_{A_{t_j}(\phi_j)}(\xi) \ddagger Z'\right\}\mu(\mathrm{d}\xi)\right\}}. \tag{20}$$

In the proof of (20) the following reformulation can be used

$$\mathbb{E}\left\{\prod_{j=1}^{n} R_{t_j}(\phi_j)\right\} = \mathbb{E}\exp\left\{\int_{\mathcal{R}}\left[\sum_{j=1}^{n} f_{t_j}(\xi;\phi_j)\mathbf{1}_{A_{t_j}(\phi_j)}(\xi)\right]Z(\mathrm{d}\xi)\right\}$$
$$= \exp\left(K\left\{1 \ddagger \int_{\mathcal{R}}\left[\sum_{j=1}^{n} f_{t_j}(\xi;\phi_j)\mathbf{1}_{A_{t_j}(\phi_j)}(\xi)\right]Z(\mathrm{d}\xi)\right\}\right).$$

For a constant weight function $f_t(\xi;\phi) \equiv f$ for all ξ, $(\phi,t) \in \mathcal{R}$, it follows that

$$\frac{\mathbb{E}\{R_{t_1}(\phi_1)R_{t_2}(\phi_2)\}}{\mathbb{E}\{R_{t_1}(\phi_1))\mathbb{E}(R_{t_2}(\phi_2)\}} = \exp\{\overline{\mathrm{K}}\,\mu(A_{t_1}(\phi_1)\cap A_{t_1}(\phi_2))\} \tag{21}$$

where $\overline{\mathrm{K}} = \mathrm{K}\{2f \ddagger Z'\} - 2\mathrm{K}\{f \ddagger Z'\}$.

In some cases, it may be natural to formulate a linear model for the time derivative of $\ln R_t(\phi)$

$$(\ln R_t(\phi))' = \int_{A_t(\phi)} f_t(\xi;\phi)Z(\mathrm{d}\xi).$$

The resulting model for $R_t(\phi)$ is an exponential Lévy growth model

$$R_t(\phi) = \exp(\int_{\bar{A}_t(\phi)} \bar{f}_t(\xi;\phi)Z(\mathrm{d}\xi)),$$

where $\bar{A}_t(\phi)$ and $\bar{f}_t(\xi;\phi)$ are specified as in the previous subsection.

Figure 9a shows a simulation from an exponential Lévy growth model with

$$A_t(\phi) = \{(\theta,s) : t - T(t) \le s \le t, |\theta - \phi| \le \Theta(s)\},$$

$(\phi,t) \in \mathcal{R}$, $f_t(\xi;\phi) = f$ and Z a normal Lévy basis. Here, $T(t)$ and $\Theta(s)$ represent the temporal and spatial dependencies, respectively. The similarities between the simulation and the observed in vitro growth pattern in Figure 9b are striking. A detailed analysis of these data will be presented elsewhere.

It still remains to fully explore the flexibility of the Lévy growth models. In particular, relations like (18) and (21) describe the correlation structure as a function of the measure of overlap between pairs of ambit sets. These relations can be used to create covariance models for processes defined on the circle. On the other hand, it will be interesting to investigate if a given covariance model can be obtained using the ambit set approach.

4 Acknowledgements

The authors thank Ute Hahn from the Department of Mathematics, University of Augsburg, for fruitful discussions on models based on spatio-temporal point processes. This work was supported in part by grants from the Danish Natural Science Research Council and the Carlsberg Foundation.

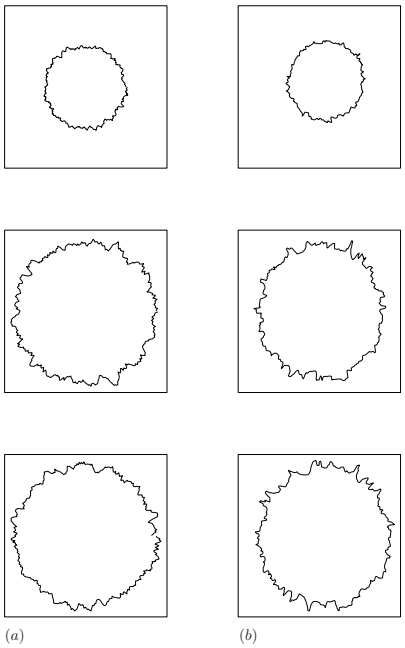

Figure 9: Comparison of a simulation of a log-normal model (a) with in vitro tumour growth (b) at times $t = 25, 45, 51$ (arbitrary units). Parameters of the simulation are $\mu = 0.11$, $\sigma = 0.01$, $T(t) = t/20$, $\Theta(\phi) = \pi/90$ and $f_t(\phi) = 1$. For details, see the text.

Appendix A: Conditional densities and conditional intensities

Let Π be the unit rate Poisson point process on S and Π_t the restriction of Π to S_t. We let Ω be the set of all locally finite subsets of S and Ω_t the set of finite subsets of S_t. On Ω_t, we use the $\sigma-$algebra $\mathcal{A}_t$ generated by

$$\{z \in \Omega_t : n(z \cap B) = k\}, \quad k \in \mathbb{N}_0, B \in \mathcal{B}_t,$$

where $\mathcal{B}_t$ is the Borel σ-algebra on S_t.

We will first state the following basic result for the Poisson point process.

Lemma A.1 Let π_t be the distribution of Π_t and $g_t : (\Omega_t, \mathcal{A}_t) \to (\mathbb{R}, \mathcal{B}(\mathbb{R}))$ be a Borel function. Then

$$\begin{aligned} &\int_{\Omega_t} g_t(z)\pi_t(\mathrm{d}z) \qquad (22)\\ &\quad = \sum_{n=0}^{\infty} \exp(-t|\mathcal{X}|) \int_{\mathcal{X}} \cdots \int_{\mathcal{X}} \int_0^t \int_{t_1}^t \cdots \int_{t_{n-1}}^t g_t(\{(t_1,\xi_1),\ldots,(t_n,\xi_n)\}) \\ &\qquad\qquad \times \mathrm{d}t_n \cdots \mathrm{d}t_1 \mathrm{d}\xi_n \cdots \mathrm{d}\xi_1, \end{aligned}$$

where $|\cdot|$ denotes the Lebesgue measure on $\mathbb{R}^d$.

Proof of Lemma A.1. For the restriction Π_t of the unit rate Poisson point process to S_t, the number N of points (t_i, ξ_i) in S_t is Poisson distributed with parameter $t|\mathcal{X}|$

and conditionally on $N = n$, Π_t is distributed as

$$\{(t_1, \xi_1), \ldots, (t_n, \xi_n)\}$$

where $(t_i, \xi_i), i = 1, \ldots, n$, are independent and uniform in S_t. It follows that

$$\begin{aligned}
&\int_{\Omega_t} g_t(z)\pi_t(\mathrm{d}z) \\
&\quad = \sum_{n=0}^{\infty} \exp(-t|\mathcal{X}|)\frac{(t|\mathcal{X}|)^n}{n!} \int_{\mathcal{X}} \cdots \int_{\mathcal{X}} \int_0^t \cdots \int_0^t g(\{(t_1, \xi_1), \ldots, (t_n, \xi_n)\}) \\
&\qquad\qquad \times \frac{1}{(t|\mathcal{X}|)^n} \mathrm{d}t_n \cdots \mathrm{d}t_1 \mathrm{d}\xi_n \cdots \mathrm{d}\xi_1 \\
&\quad = \sum_{n=0}^{\infty} \exp(-t|\mathcal{X}|) \int_{\mathcal{X}} \cdots \int_{\mathcal{X}} \int_0^t \int_{t_1}^t \cdots \int_{t_{n-1}}^t g(\{(t_1, \xi_1), \ldots, (t_n, \xi_n)\}) \\
&\qquad\qquad \times \mathrm{d}t_n \cdots \mathrm{d}t_1 \mathrm{d}\xi_n \cdots \mathrm{d}\xi_1.
\end{aligned}$$

□

If Z_t has density

$$g_{Z_t}(z), \quad z \in \Omega_t$$

with respect to the unit rate Poisson point process Π_t on S_t, then for $A \in \mathcal{A}_t$,

$$\mathrm{P}(Z_t \in A) = \int_A g_{Z_t}(z)\pi_t(\mathrm{d}z) = \int_{\Omega_t} \mathbf{1}[z \in A] g_{Z_t}(z)\pi_t(\mathrm{d}z)$$

and Lemma A.1 can be used to calculate the integral.

The density of Z_t can be expressed in terms of the two families of conditional densities (1) and (2) presented in the main text, see the proposition below.

Proposition A.2 Let

$$g_n(t_{(n)}, \xi_{(n)}) = \prod_{i=1}^{n} p_i(t_i \mid t_{(i-1)}, \xi_{(i-1)}) f_i(\xi_i \mid t_{(i-1)}, \xi_{(i-1)}, t_i)$$

be the density of the first n points of Z. Then, the density of Z_t with respect to Π_t is

$$g_{Z_t}(z) = \exp(t|\mathcal{X}|) g_n(t_{(n)}, \xi_{(n)}) S_{n+1}(t \mid t_{(n)}, \xi_{(n)}), \tag{23}$$

if $z \in \Omega_t$ is of the form

$$z = \{(t_1, \xi_1), \ldots, (t_n, \xi_n)\}, \quad t_1 < \cdots < t_n.$$

Here

$$S_{n+1}(t \mid t_{(n)}, \xi_{(n)}) = \int_t^{\infty} p_{n+1}(u \mid t_{(n)}, \xi_{(n)}) \mathrm{d}u, \quad t > t_n,$$

is the survival function of $p_{n+1}(\cdot \mid t_{(n)}, \xi_{(n)})$.

Proof of Proposition A.2. For $A \in \mathcal{A}_t$, we find

$$\begin{aligned}
&\mathrm{P}(Z_t \in A) \\
&\quad = \sum_{n=0}^{\infty} \mathrm{P}(Z_t \in A, n(Z_t) = n) \\
&\quad = \sum_{n=0}^{\infty} \int_{\mathbb{R}_+ \times \mathcal{X}} \cdots \int_{\mathbb{R}_+ \times \mathcal{X}} \mathbf{1}[\{(t_1,\xi_1),\ldots,(t_n,\xi_n)\} \in A] \mathbf{1}[t_{n+1} > t] \\
&\qquad\qquad g_{n+1}(t_{(n+1)}, \xi_{(n+1)}) \mathrm{d}t_{n+1} \mathrm{d}\xi_{n+1} \cdots \mathrm{d}t_1 \mathrm{d}\xi_1 \\
&\quad = \sum_{n=0}^{\infty} \int_{\mathcal{X}} \cdots \int_{\mathcal{X}} \int_0^t \int_{t_1}^t \cdots \int_{t_{n-1}}^t \mathbf{1}[\{(t_1,\xi_1),\ldots,(t_n,\xi_n)\} \in A] g_n(t_{(n)}, \xi_{(n)}) \\
&\qquad\qquad S_{n+1}(t \mid t_{(n)}, \xi_{(n)}) \mathrm{d}t_n \cdots \mathrm{d}t_1 \mathrm{d}\xi_n \cdots \mathrm{d}\xi_1.
\end{aligned}$$

Now Lemma A.1 implies the result. □

Another possibility is specification of the model in terms of the conditional intensities. For an increasing sequence

$$(t_1,\xi_1),\ldots,(t_n,\xi_n),\ldots, \quad t_1 < \cdots < t_n < \cdots, \tag{24}$$

we define the conditional intensity at (t,ξ) by

$$h_n(t,\xi \mid t_{(n-1)}, \xi_{(n-1)}) = \frac{p_n(t \mid t_{(n-1)}, \xi_{(n-1)}) f_n(\xi \mid t_{(n-1)}, \xi_{(n-1)}, t)}{S_n(t \mid t_{(n-1)}, \xi_{(n-1)})}, \tag{25}$$

for $t_{n-1} < t \leq t_n$ ($t_0 = 0$). Note that the conditional intensity h_n is the product of the hazard function

$$\frac{p_n(t \mid t_{(n-1)}, \xi_{(n-1)})}{S_n(t \mid t_{(n-1)}, \xi_{(n-1)})}$$

for the n-th time point given the history $(t_{(n-1)}, \xi_{(n-1)})$ and the density

$$f_n(\xi \mid t_{(n-1)}, \xi_{(n-1)}, t)$$

of the n-th spatial point given the history $(t_{(n-1)}, \xi_{(n-1)})$ and the n-th time point t.

References

Baddeley, A. J., Møller, J., and Waagepetersen, R. P. (2000). Non- and semiparametric estimation of interaction in inhomogeneous point patterns. *Statistica Neerlandica*, 54:329–350.

Barndorff-Nielsen, O. E. and Schmiegel, J. (2004). Lévy based spatial-temporal modelling, with applications to turbulence. *Russian Math. Surveys*, 59(1):65–95.

Barndorff-Nielsen, O. E., Schmiegel, J., Eggers, H. C., and Greiner, M. (2003). A class of spatio-temporal and causal stochastic processes, with application to multiscaling and multifractality. Technical report, MaPhySto Research Report no. 33, University of Aarhus.

Bramson, M. and Griffeath, D. (1980). The Asymptotic Behavior of a Probabilistic Model for Tumour Growth. In Jager, W., Rost, H., and Tautu, P., editors, *Biological Growth and Spread*, number 38 in Springer Lecture Notes in Biomathematics, pages 165–172.

Bramson, M. and Griffeath, D. (1981). On the Williams–Bjerknes tumour growth model, I. *Ann. Prob.*, 9:173–185.

Brix, A. (1998). *Spatial and Spatio-temporal Models for Weed Abundance*. PhD thesis, Royal Veterinary and Agricultural University, Copenhagen.

Brix, A. (1999). Generalized gamma measures and shot-noise Cox processes. *Adv. Appl. Prob.*, 31:929–953.

Brix, A. and Chadoeuf, J. (2002). Spatio-temporal modelling of weeds by shot-noise G Cox processes. *Biom. J.*, 44:83–99.

Brix, A. and Diggle, P. J. (2001). Spatiotemporal prediction for log-Gaussian Cox processes. *J. R. Statist. Soc. B.*, 63:823–841.

Brix, A. and Møller, J. (2001). Space-time multitype log Gaussian Cox processes with a view to modelling weeds. *Scand. J. Statist.*, 28:471–488.

Brú, A., Pastor, J. M., Fernaud, I., Brú, I., Melle, S., and Berenguer, C. (1998). Super-rough dynamics on tumour growth. *Phys. Rev. Lett.*, 81:4008–4011.

Capasso, V., Agur, Z., Arino, O., Chaplain, M., Gyllenbarg, M., Heesterbeek, J. A. P., Kaufman, M., Krivan, V., Stevens, A., and Tracqui, P. (2002). Book of abstracts, 5th Conference of the European Society of Mathematical and Theoretical Biology. Milano.

Chaplain, M. A. J., Singh, G. D., and McLachlan, J. C. (1999). *On Growth and Form: Spatio-temporal Pattern Formation in Biology*. Wiley, Chichester.

Cox, D. R. (1955). Some statistical models realted with series of events. *J. R. Statist. Soc. B.*, 17:129–164.

Cressie, N. (1991a). Modelling growth with random sets. In Possolo, A. and Hayward, C. A., editors, *Spatial Statistics and Imaging*, pages 31–45. IMS Lecture Notes, Proceedings of the 1988 AMS-IMS-SIAM Joint Summer Research Conference.

Cressie, N. (1991b). *Statistics for Spatial Data*. Wiley, New York.

Cressie, N. and Hulting, F. L. (1992). A spatial statistical analysis of tumor growth. *J. Amer. Statist. Assoc.*, 87:272–283.

Cressie, N. and Laslett, G. M. (1987). Random set theory and problems of modelling. *SIAM Review*, 29:557–574.

Daley, D. J. and Vere-Jones, D. (2002). *An Introduction to the Theory of Point Processes. Volume I: Elementary Theory and Methods*. Springer, New York, second edition.

Deijfen, M. (2003). Asymptotic shape in a continuum growth model. *Adv. Appl. Prob. (SGSA)*, 35:303–318.

Diggle, P. J. (2003). *Statistical Analysis of Spatial Point Patterns*. Edward Arnold, London, second edition.

Durret, R. and Liggett, T. (1981). The shape of the limit set in Richardsons growth model. *Ann. Prob.*, 9:186–193.

Hahn, U., Jensen, E. B. V., van Lieshout, M. N. M., and Nielsen, L. S. (2003). Inhomogeneous point processes by location dependent scaling. *Adv. Appl. Prob. (SGSA)*, 35(2):319–336.

Hawkes, A. G. (1971). Point spectra of some mutually exciting point processes. *J. R. Statist. Soc. B*, 33:438–443.

Hobolth, A., Pedersen, J., and Jensen, E. B. V. (2003). A continuous parametric shape model. *Ann. Inst. Statist. Math.*, 55:227–242.

Jensen, E. B. V. and Nielsen, L. S. (2000). Inhomogeneous Markov point processes by transformation. *Bernoulli*, 6:761–782.

Jensen, E. B. V. and Nielsen, L. S. (2004). Statistical inference for transformation inhomogeneous point processes. *Scand. J. Statist.*, 31:131–142.

Jónsdóttir, K. Ý. and Jensen, E. B. V. (2005). Gaussian radial growth. *Image Anal. Stereol.*, 24:117–126.

Kallenberg, O. (1989). *Random Measures*. Akademie Verlag, Berlin, 4 edition.

Kwapien, S. and Woyczynski, W. A. (1992). *Random Series and Stochastic Integrals: Single and Multiple*. Birkhäuser, Basel.

Molchanov, I. S. (2005). *Theory of Random Sets*. Springer, London.

Møller, J. (2003). Shot noise Cox processes. *Adv. Appl. Prob. (SGSA)*, 35:614–640.

Møller, J., Syversveen, A. R., and Waagepetersen, R. P. (1998). Log Gaussian Cox processes. *Scand. J. Statist.*, 25:451–482.

Møller, J. and Torrisi, G. L. (2005). Generalised shot noise Cox processes. *Adv. Appl. Prob. (SGSA)*, 37:48–74.

Møller, J. and Waagepetersen, R. P. (2003). *Statistical Inference and Simulation for Spatial Point Processes*. Chapman and Hall/CRC, Boca Raton.

Ogata, Y. and Tanemura, M. (1986). Likelihood estimation of interaction potentials and external fields of inhomogeneous spatial point patterns. In Francis, I., Manly, B., and Lam, F., editors, *Proc. Pacific Statistical Congress*, pages 150–154. Elsevier.

Prokesova, M., Hahn, U., and Jensen, E. B. V. (2005). Statistics for locally scaled point processes. To appear in special issue of Springer Lecture Notes on Statistics.

Richardson, D. (1973). Random growth in a tessellation. *Proc. Camb. Phil. Soc.*

Schoenberg, F. P., Brillinger, D. R., and Guttorp, P. (2002). Point processes, spatial-temporal. In El-Shaarawi, A. and W.W., P., editors, *Encyclopedia of Environmetrics,*, pages 1573–1577. John Wiley & Sons, Ltd, Chichester.

Schurger, K. (1979). On the asymptotic geometrical behavior of a class of contact interaction processes with a monotone infection rate. *Zeitschrift fur Wahrscheinlichkeitstherorie and verwand Gebiete*, 48:35–48.

Stoyan, D., Kendall, S. W., and Mecke, J. (1995). *Stochastic Geometry and its Applications*. John Wiley & Sons, Chichester.

Stoyan, D. and Stoyan, H. (1998). Non homogeneous Gibbs process models for forestry – a case study. *Biometrical J.*, 40:521–531.

Van Lieshout, M. N. M. (2000). *Markov Point Processes and their Applications.* Imperial College Press, London.

Paper C

Jónsdóttir, K.Ý., Schmiegel, J. and Jensen, E.B.V. (2006).
Lévy based growth models.
To appear as a Thiele Research report. To be submitted.

Lévy based growth models

Kristjana Ýr Jónsdóttir, Jürgen Schmiegel
and Eva B. Vedel Jensen
University of Aarhus

Abstract

We introduce a class of spatio-temporal models based on Lévy theory, in particular on Lévy bases and integration with respect to those. We will focus on how these models can be used to describe how the boundary of a star-shaped planar object expands in time, using its radius vector function R_t at time $t \geq 0$. We study both linear and exponential Lévy based models, i.e.

$$R_t(\phi) = \mu_t(\phi) + \int_{A_t(\phi)} f_t(\xi;\phi) Z(d\xi), \phi \in [-\pi, \pi),$$

and

$$R_t(\phi) = \exp\left(\mu_t(\phi) + \int_{A_t(\phi)} f_t(\xi;\phi) Z(d\xi)\right), \phi \in [-\pi, \pi),$$

where Z is a Lévy basis, $A_t(\phi)$ is a so-called ambit set, $f_t(\xi;\phi)$ is a deterministic weight function and $\mu_t(\phi)$ a deterministic function. A great advantage of these models is the possibility of controlling the spatial and temporal correlation structure, since it is possible to derive explicit expression for

$$\mathrm{Cov}(R_t(\phi), R_{t'}(\phi')),$$

in terms of the components of the model. An application to tumour growth will be presented.

Keywords: Lévy basis, spatio-temporal modelling, growth models, tumor growth.

1 Introduction

Stochastic spatio-temporal modelling is of great importance in a variety of disciplines of the natural sciences, including biology (Cantalapiedra et al. (2001), Brix and Chadoeuf (2002), Fewster (2003) and Gratzer et al. (2004)), image analysis (Feideropoulou and Pesquet-Popescu (2004)), atmospheric sciences (Pérez-Muñuzuri et al. (2003)), geophysics (Calder (1986), Lovejoy et al. (1992) and Sornette and Ouillon (2005)) and turbulence (Barndorff-Nielsen et al. (2006)), just to name a few. In particular, modelling of tumour growth dynamics has been a very active research area in recent years (Delsanto et al. (2000), Peirolo and Scalerandi (2004), Pang and Tzeng (2004), Schmiegel (2006)).

The purpose of the present paper is to study growth modelling in a Lévy based framework, i.e. stochastic spatio-temporal modelling based on the integration with respect to a Lévy basis. The paper is thereby a natural continuation of the work initiated

in Schmiegel (2006) which was mainly directed towards an audience of physicists. The advantage of a Lévy based growth modelling approach is that the resulting models are at the same time flexible and mathematically tractable. This type of modelling has earlier been used with success in the field of turbulence, cf. Barndorff-Nielsen et al. (2006) and references therein.

The organisation of the paper is as follows. Section 2 provides some background on Lévy basis which is the essential component in our approach. In Section 3, Lévy based spatio-temporal models are discussed in general. In Section 4, Lévy based growth models for star-shaped planar objects are introduced and some qualitative examples of different growth dynamics are given. Section 5 contains a description of different covariance structures which can be obtained under the Lévy growth models. Finally, Section 6 contains an application of the Lévy based growth models to tumour growth.

2 Background

This section provides a brief overview of the theory of Lévy bases, in particular, the theory of integration with respect to a Lévy basis.

We focus on results which are prerequisites for subsequent sections, without proofs. For a more detailed study of independently scattered random measures and their integration, cf. Kallenberg (1989), Rajput and Rosinski (1989), Kwapien and Woyczynski (1992) and Barndorff-Nielsen and Schmiegel (2003). We will use the following notation $C(\lambda \ddagger X) = \log \mathbb{E}(e^{i\lambda X})$ for the cumulant function of a random variable X .

2.1 Basic definitions

Let $(\mathcal{R}, \mathfrak{A})$ be a measurable space. A collection of random variables $Z = \{Z(A) : A \in \mathfrak{A}\}$ on $(\mathcal{R}, \mathfrak{A})$ is said to be an *independently scattered random measure*, if for every sequence $\{A_n\}$ of disjoint sets in $\mathfrak{A}$, the random variables $Z(A_n)$ are independent and $Z(\bigcup A_n) = \sum Z(A_n)$ a.s. Moreover, if $Z(A)$ is *infinitely divisible* for all $A \in \mathfrak{A}$, Z is called a *Lévy basis*.

When Z is a Lévy basis, the cumulant function of $Z(A)$ can be written as

$$C(\lambda \ddagger Z(A)) = i\lambda a(A) - \frac{1}{2}\lambda^2 b(A) + \int_{\mathbb{R}} (e^{i\lambda u} - 1 - i\lambda u \mathbf{1}_{[-1,1]}(u)) U(du, A), \qquad (1)$$

where a is a signed measure on $\mathfrak{A}$, b is a positive measure on $\mathfrak{A}$, $U(du, A)$ is a Lévy measure on $\mathbb{R}$ for fixed $A \in \mathfrak{A}$ and a measure on $\mathfrak{A}$ for fixed du. The result (1) is the famous Lévy-Khintchine representation. The Lévy basis Z is said to have characteristics (a, b, U). The measure U is referred to as the generalised Lévy measure.

It may be useful to express the cumulant function (1) in infinitesimal form

$$C(\lambda \ddagger Z(d\xi)) = i\lambda a(d\xi) - \frac{1}{2}\lambda^2 b(d\xi) + \int_{\mathbb{R}} (e^{i\lambda u} - 1 - i\lambda u \mathbf{1}_{[-1,1]}(u)) U(du, d\xi).$$

In this paper, we will consider Lévy bases with characteristics (a, b, U), where the measure U factorises as

$$U(du, d\xi) = V(du, \xi)\mu(d\xi).$$

Here, μ is some measure on $\mathfrak{A}$ and $V(du, \xi)$ is a Lévy measure for fixed ξ. Furthermore, the measures a and b are absolutely continuous with respect to the measure μ and satisfy

$$a(d\xi) = \tilde{a}(\xi)\mu(d\xi), \quad b(d\xi) = \tilde{b}(\xi)\mu(d\xi).$$

Under these assumptions we may think of

$$C(\lambda \ddagger Z'(\xi)) = i\lambda\tilde{a}(\xi) - \frac{1}{2}\lambda^2\tilde{b}(\xi) + \int_{\mathbb{R}} \{e^{i\lambda u} - 1 - i\lambda u \mathbf{1}_{[-1,1]}(u)\} V(du, \xi),$$

as a cumulant function of a random variable $Z'(\xi)$ satisfying

$$C(\lambda \ddagger Z(d\xi)) = C(\lambda \ddagger Z'(\xi))\mu(d\xi). \tag{2}$$

If $\tilde{a}(\xi)$, $\tilde{b}(\xi)$ and the Lévy measure $V(\cdot; \xi)$ do not depend on ξ, we call Z a *factorisable* Lévy basis and then $Z'(\xi) = Z'$ does also not depend on ξ. If, moreover, $\mathcal{R} = \mathbb{R}^n$ and μ is proportional to the Lebesgue measure, then Z is called a *homogeneous* Lévy basis.

Let us now consider the integral of a measurable function f on $\mathcal{R}$ with respect to a Lévy basis Z. For simplicity we denote this integral by $f \bullet Z$. Key results for many calculations are the following equations for the cumulant function of the stochastic integral $f \bullet Z$ (subject to minor regularity conditions, cf. Barndorff-Nielsen and Thorbjørnsen (2003)). Using equation (2) we get

$$C(\lambda \ddagger f \bullet Z) = \int C(\lambda f(\xi) \ddagger Z'(\xi))\mu(d\xi). \tag{3}$$

A similar result holds for the logarithm of the Laplace transform of $f \bullet Z$,

$$K(\lambda \ddagger f \bullet Z) = C(-i\lambda \ddagger f \bullet Z),$$

i.e.

$$K(\lambda \ddagger f \bullet Z) = \int K(\lambda f(\xi) \ddagger Z'(\xi))\mu(d\xi). \tag{4}$$

We will now give a few examples of Lévy bases. Here we assume that $\mathcal{R} = \mathbb{R}^n$ and $\mathfrak{A} = \mathcal{B}(\mathbb{R}^n)$.

Example 1. (Gaussian Lévy basis) If Z is a Lévy basis on $\mathcal{R}$, such that $Z(A) \sim N(a(A), b(A))$, where a is a signed measure on $\mathcal{R}$ and b is a positive measure on $\mathcal{R}$, we call Z a Gaussian Lévy basis. The Gaussian Lévy basis has characteristics $(a, b, 0)$ and the cumulant function is

$$C(\lambda \ddagger Z(A)) = i\lambda a(A) - \frac{1}{2}\lambda^2 b(A).$$

We have that $Z'(\xi) \sim N(\tilde{a}(\xi), \tilde{b}(\xi))$, i.e. $C(\lambda \ddagger Z'(\xi)) = i\lambda\tilde{a}(\xi) - \frac{1}{2}\lambda^2\tilde{b}(\xi)$. Then

$$C(\lambda \ddagger f \bullet Z) = \int C(\lambda f(\xi) \ddagger Z'(\xi))\mu(d\xi) = i\lambda(f \bullet a) - \frac{1}{2}\lambda^2(f^2 \bullet b), \tag{5}$$

where μ is a positive measure. Note that $f \bullet Z \sim N(f \bullet a, f^2 \bullet b)$. □

	$V(du,\xi)$	$\tilde{a}(\xi)$
Poisson	$\delta_1(du)$	1
Gamma	$\mathbf{1}_{\mathbb{R}_+}(u)\beta u^{-1}e^{-\alpha(\xi)}du$	$\beta\left(\frac{1-e^{-\alpha(\xi)}}{\alpha(\xi)}\right)$
Inverse Gaussian	$\frac{\eta}{\sqrt{2\pi}}\mathbf{1}_{\mathbb{R}_+}(u)u^{-\frac{3}{2}}e^{-\frac{1}{2}\gamma^2(\xi)u}du$	$\frac{\eta}{\sqrt{2\pi}}\int_0^1 u^{-\frac{1}{2}}e^{-\frac{1}{2}\gamma^2(\xi)u}du$

Table 1: The definition of three Lévy jump bases, the Poisson basis, the Gamma basis and the Inverse Gaussian basis.

	$Z'(\xi)$	$C(\lambda \ddagger Z'(\xi))$	$\mathbb{E}(Z'(\xi))$	$\mathbb{V}(Z'(\xi))$
Poisson	Po(1)	$(e^{i\lambda}-1)$	1	1
Gamma	$\Gamma(\beta,\alpha(\xi))$	$-\beta\log\left(1-\frac{i\lambda}{\alpha(\xi)}\right)$	$\frac{\beta}{\alpha(\xi)}$	$\frac{\beta}{\alpha^2(\xi)}$
Inverse Gaussian	$\mathrm{IG}(\eta,\gamma(\xi))$	$\eta\gamma(\xi)\left(1-\sqrt{1-\frac{2i\lambda}{\gamma^2(\xi)}}\right)$	$\frac{\eta}{\gamma(\xi)}$	$\frac{\eta}{\gamma^3(\xi)}$

Table 2: Distribution of $Z'(\xi)$, with the corresponding cumulant function, mean and variance.

Example 2. (Lévy jump basis) A Lévy basis is called a Lévy jump basis if the characteristics of the basis is $(a,0,U)$. In Table 1 we give three examples of Lévy jump bases, the Poisson basis, the Gamma basis and the Inverse Gaussian basis.

The distribution of the random variable $Z'(\xi)$, its cumulant function, mean and variance are given in Table 2, for the three types of Lévy bases. Note that if Z is a Poisson basis, $Z(A) \sim \mathrm{Po}(\mu(\mathrm{A}))$, for all $A \in \mathfrak{A}$. If $\alpha(\xi) \equiv \alpha$, $\gamma(\xi) \equiv \gamma$, then we have for all $A \in \mathfrak{A}$, that $Z(A) \sim \Gamma(\beta\mu(A),\alpha)$ and $Z(A) \sim \mathrm{IG}(\eta\mu(\mathrm{A}),\gamma)$, respectively. □

Note that any Lévy basis Z is the sum of a Lévy jump basis Z_1 and an independent Gaussian basis Z_2 such that

$$C(\lambda \ddagger f \bullet Z) = C(\lambda \ddagger f \bullet Z_1) + C(\lambda \ddagger f \bullet Z_2).$$

Finally, we would like to mention an important representation of positive Lévy bases, the Lévy-Ito representation,

$$Z(A) = a_0(A) + \int_{\mathbb{R}_+} xN(dx,A), \tag{6}$$

where N is a Poisson basis on $\mathbb{R}_+ \times \mathcal{R}$, with intensity measure U and

$$a_0(A) = a(A) - \int_0^1 xU(dx,A).$$

Note that equation (6) can also be written as

$$Z(A) = a_0(A) + \sum_{(u,\xi)\in N} u\mathbf{1}_A(\xi), \tag{7}$$

where N is a Poisson point process on $\mathbb{R}_+ \times \mathcal{R}$ with intensity measure U. If f is a measurable function on $\mathbb{R}$ with respect to the Lévy basis Z, we get that

$$f \bullet Z = f \bullet a_0 + \sum_{(u,\xi)\in N} uf(\xi).$$

2.2 Extension to multivariate Lévy bases

The above theory can easily be extended to higher dimensions. If $Z = (Z_1, \ldots, Z_m)$ is a multivariate Lévy basis, the Lévy-Khintchine representation takes the form

$$C(\lambda \ddagger Z(A)) = i\langle a(A), \lambda\rangle - \frac{1}{2}\langle \lambda b(A), \lambda\rangle + \int_{\mathbb{R}^m} \{e^{i\langle \lambda, u\rangle} - 1 - i\langle \lambda, u\rangle \mathbf{1}_E(u)\} U(du, A),$$

where $\langle \cdot, \cdot \rangle$ is the vector product in $\mathbb{R}^m$, $E = [-1, 1]^m$, λ is a m-dimensional vector, a is a m-dimensional measure and b is a $m \times m$ matrix valued measure. In Sato (1999), the theory of multivariate Lévy processes is discussed in details.

3 Lévy based spatio-temporal models

Let us consider a random variable $X_t(\sigma)$, depending on time t and a position in space σ. In the following we will assume that $(\sigma, t) \in \mathcal{R} = \mathcal{S} \times \mathbb{R}$, i.e. $\mathcal{R}$ is a product of the space $\mathcal{S} \subset \mathbb{R}^d$ and the time space $\mathbb{R}$. We let $\mathfrak{A}$ be the Borel σ-algebra of $\mathcal{R}$.

We will consider models for the spatio-temporal process $X = \{X_t(\sigma) : (\sigma, t) \in \mathcal{R}\}$ based on the theory of Lévy bases and integration with respect to those, discussed in Section 2.

The idea behind the following definitions is based on the intuitive picture of an *ambit set* $A_t(\sigma)$ associated with each point $(\sigma, t) \in \mathcal{R}$, which defines the dependency on the past at time t and position σ. The ambit set $A_t(\sigma)$ is of the following form

$$A_t(\sigma) = \{(\rho, s) \in \mathcal{R} : \rho \in \Delta_s(\sigma), s \leq t\},$$

where $\Delta_s(\sigma) \subseteq \mathcal{S}$ is a neighbourhood of σ, consisting of the set of positions at time s that influence the process at position σ and time t, cf. Figure 1. The spatio-temporal process $X = \{X_t(\sigma) : (\sigma, t) \in \mathcal{R}\}$ is then defined as

$$X_t(\sigma) = \int_{A_t(\sigma)} f_t(\xi; \sigma) Z(d\xi), \tag{8}$$

where Z is a Lévy basis and $f_t(\xi; \sigma)$ is a deterministic weight function (assumed to be suitable for the integral to exist). We will refer to the spatio-temporal process

$$X = \{X_t(\sigma) : (\sigma, t) \in \mathcal{R}\}$$

as a *linear spatio-temporal Lévy model* and to

$$\tilde{X} = \{\exp(X_t(\sigma)) : (\sigma, t) \in \mathcal{R}\}$$

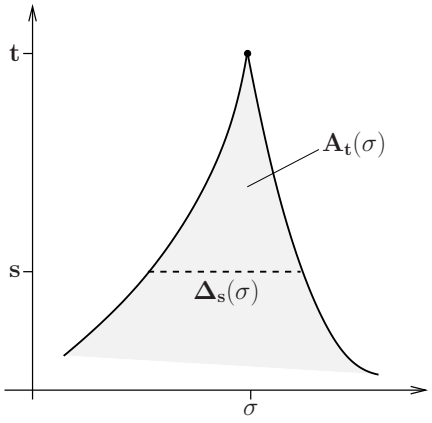

Figure 1: The ambit set $A_t(\sigma)$.

as an *exponential spatio-temporal Lévy model*.

There are many interesting problems to study within this framework, both theoretical and in connection with various applications of spatio-temporal processes. In this paper we focus on spatio-temporal processes modelling growth, cf. Section 4 and onwards. The main application has until now been in spatio-temporal modelling of turbulence, cf. Barndorff-Nielsen and Schmiegel (2003), Barndorff-Nielsen et al. (2003) and Schmiegel et al. (2004).

3.1 Linear spatio-temporal Lévy models

Let us assume that X follows a linear spatio-temporal Lévy model. Using the key relation (4), we get that

$$\begin{aligned}\mathbb{E}(X_t(\sigma)) &= \int_{A_t(\sigma)} f_t(\xi;\sigma)\mathbb{E}(Z'(\xi))\mu(d\xi) \\ \mathbb{V}(X_t(\sigma)) &= \int_{A_t(\sigma)} f_t(\xi;\sigma)^2\mathbb{V}(Z'(\xi))\mu(d\xi).\end{aligned} \tag{9}$$

It is also clear that the covariances are of the form

$$\mathrm{Cov}(X_t(\sigma), X_{t'}(\sigma')) = \int_{A_t(\sigma)\cap A_{t'}(\sigma')} f_t(\xi;\sigma) f_{t'}(\xi;\sigma')\mathbb{V}(Z'(\xi))\mu(d\xi). \tag{10}$$

If the weight function is constant, $f_t(\xi;\sigma) \equiv f$ and if the Lévy basis Z is factorisable, then (10) reduces to

$$\mathrm{Cov}(X_t(\sigma), X_{t'}(\sigma')) = f\mathbb{V}(Z')\mu(A_t(\sigma) \cap A_{t'}(\sigma')). \tag{11}$$

In this case the covariance structure only depends on the μ-measure of the intersection of the two ambit sets.

The mean value and covariance structure of the linear spatio-temporal Lévy models, using the different underlying Lévy jump bases given in Example 2 of the previous section, can easily be obtained using Table 2. For an underlying Gaussian basis we refer to Example 1.

3.2 Exponential spatio-temporal Lévy models

Let us assume that $\tilde{X}$ follows an exponential spatio-temporal Lévy model. Equation (4) enables us to calculate arbitrary n-point correlations. Here n-point correlations for arbitrary spatial positions $\sigma_1, \ldots, \sigma_n$ and times $t_1, \ldots, t_n$ are defined as

$$m_n(\sigma_1, t_1; \ldots; \sigma_n, t_n) \equiv \mathbb{E}\left(\tilde{X}_{t_1}(\sigma_1) \cdot \ldots \cdot \tilde{X}_{t_n}(\sigma_n)\right).$$

If we assume that the correlations are finite, i.e. $\mathbb{E}(\tilde{X}_{t_1}(\sigma_1) \cdot \ldots \cdot \tilde{X}_{t_n}(\sigma_n)) < \infty$, we get from (4) the expression

$$m_n(\sigma_1, t_1; \ldots; \sigma_n, t_n) = \exp\left(\int_{\mathcal{R}} K(\sum_{j=1}^{n} f_{t_j}(\xi; \sigma_j)\mathbf{1}_{A_{t_j}(\sigma_j)}(\xi) \ddagger Z'(\xi))\mu(d\xi)\right). \quad (12)$$

Given an underlying Lévy basis, (12) gives an explicit expression of the n-point correlations $m_n(\sigma_1, t_1; \ldots; \sigma_n, t_n)$ in terms of weight functions and ambit sets.

Now let us consider 2-point correlators of the form

$$\mathrm{Corr}(Y_1, Y_2) = \frac{\mathbb{E}(Y_1 Y_2)}{\mathbb{E}(Y_1)\mathbb{E}(Y_2)},$$

where Y_1 and Y_2 are some random variables. An attractive geometric interpretation of the 2-point correlators can be obtained by using equation (12). We get that

$$\begin{aligned} c_{t,t'}(\sigma, \sigma') &:= \mathrm{Corr}(\tilde{X}_t(\sigma), \tilde{X}_{t'}(\sigma')) \\ &= \exp\left(\int_{A_t(\sigma)\cap A_{t'}(\sigma')} \log\left(\mathrm{Corr}(e^{f_t(\xi;\sigma)Z'(\xi)}, e^{f_{t'}(\xi;\sigma')Z'(\xi)})\right)\mu(d\xi)\right). \quad (13) \end{aligned}$$

Note that

$$\begin{aligned} &\log \mathrm{Corr}(e^{f_t(\xi;\sigma)Z'(\xi)}, e^{f_{t'}(\xi;\sigma')Z'(\xi)}) \\ &\quad = K((f_t(\xi;\sigma) + f_{t'}(\xi;\sigma')) \ddagger Z'(\xi)) - K(f_t(\xi;\sigma) \ddagger Z'(\xi)) - K(f_{t'}(\xi;\sigma') \ddagger Z'(\xi)). \end{aligned}$$

In the simple case where the weight functions are constant, i.e. $f_t(\xi;\sigma) \equiv f$ for all $(\sigma, t) \in \mathcal{R}$ and where the underlying Lévy basis is factorisable, $Z'(\xi) = Z'$, we get that

$$c_{t,t'}(\sigma, \sigma') = \exp\left(\overline{K}\mu(A_t(\sigma) \cap A_{t'}(\sigma'))\right) \quad (14)$$

where $\overline{K} = K(2f \ddagger Z') - 2K(f \ddagger Z')$. For a factorisable Lévy basis Z and a constant weight function, one can express the higher order correlators in terms of different overlaps of the corresponding ambit sets.

We refer to Example 1 and Table 2, to obtain the mean value and covariance structure for the exponential spatio-temporal models using the different types of underlying Lévy bases.

4 Lévy based growth models

From now on we will study how the Lévy setup can be used to construct flexible stochastic models for growing objects. We focus on planar objects but generalisations

to higher dimensions are straight forward. We denote the object at time t by $Y_t \subset \mathbb{R}^2$ and we will assume that Y_t is compact and star-shaped with respect to a point $z \in \mathbb{R}^2$ for all t. For the cancer growth data discussed in Section 6, this is essentially no restriction. The boundary of a star-shaped object Y_t can be determined by its radius vector function $R_t = \{R_t(\phi) : \phi \in [-\pi, \pi)\}$, where

$$R_t(\phi) = \max\{r : z + r(\cos\phi, \sin\phi) \in Y_t\}, \;\; \phi \in [-\pi, \pi),$$

cf. Figure 2. We will consider both linear and exponential spatio-temporal Lévy

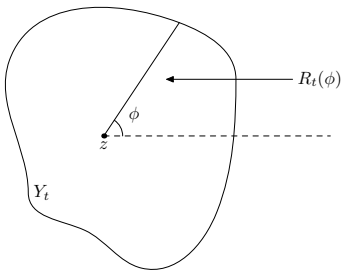

Figure 2: The star-shaped object Y_t is determined by its radius-vector function R_t at time t.

models for the radius vector function. The underlying Lévy basis is a random measure on $\mathcal{R} = \mathcal{S} \times \mathbb{R}$, where $\mathcal{S} = [-\pi, \pi)$. In order to obtain enough flexibility in the modelling, we allow for arbitrary adjustment in the mean value of the radius vector function. The linear Lévy growth model is then defined by the following equation

$$R_t(\phi) = \mu_t(\phi) + \int_{A_t(\phi)} f_t(\xi; \phi) Z(d\xi). \tag{15}$$

We assume that the ingredients of the model have been chosen such that $R_t(\phi) > 0$ almost surely. Under an exponential Lévy growth model, the radius vector function satisfies the following equation

$$R_t(\phi) = \exp\left(\mu_t(\phi) + \int_{A_t(\phi)} f_t(\xi; \phi) Z(d\xi)\right). \tag{16}$$

For both model types, the weight functions $f_t(\xi; \phi)$ and the ambit sets $A_t(\phi)$ are assumed to be suitable for the integral to exist. Furthermore, the weight functions and ambit sets must be defined cyclically such that the radius-vector function $R_t(\phi)$ is cyclic. In the following, all angular calculations are regarded as cyclic.

One can also consider models for the time derivative of $R_t(\phi)$, i.e.

$$\frac{\partial}{\partial t} R_t(\phi) = \mu_t(\phi) + \int_{A_t(\phi)} f_t(\xi; \phi) Z(d\xi). \tag{17}$$

If $\frac{\partial}{\partial t} R_t(\phi) > 0$, then the boundary of Y_t will always expand. This may not be the case for the earlier specified models but the ingredients of the earlier models may be chosen such that strict growth is present with very high probability. Under (17), the induced

model for $R_t(\phi)$ will also be a linear Lévy growth model since

$$\begin{aligned} R_t(\phi) &= r_0(\phi) + \bar{\mu}_t(\phi) + \int_0^t \int_{A_s(\phi)} f_s(\xi;\phi) Z(d\xi) ds \\ &= r_0(\phi) + \bar{\mu}_t(\phi) + \int_{\bar{A}_t(\phi)} \bar{f}_t(\xi;\phi) Z(d\xi), \end{aligned}$$

where r_0 is the radius-vector function at time $t = 0$,

$$\bar{\mu}_t(\phi) = \int_0^t \mu_s(\phi) ds,$$

$$\bar{A}_t(\phi) = \cup_{0 \le s \le t} A_s(\phi),$$

and

$$\bar{f}_t(\xi;\phi) = \int_0^t \mathbf{1}_{A_s(\phi)}(\xi) f_s(\xi;\phi) ds.$$

In Barndorff-Nielsen and Schmiegel (2003), a model of this type is discussed in relation to turbulence. A discrete version of (17) with a Gaussian Lévy basis is discussed in detail in Jónsdóttir and Jensen (2005).

In some cases it might be more natural to formulate the model in terms of the time derivative of $\ln(R_t(\phi))$,

$$\frac{\partial}{\partial t}(\ln(R_t(\phi)) = \mu_t(\phi) + \int_{A_t(\phi)} f_t(\xi;\phi) Z(d\xi).$$

In this case the induced model is an exponential Lévy growth model of the type

$$R_t(\phi) = r_0(\phi) \exp\left(\bar{\mu}_t(\phi) + \int_{\bar{A}_t(\phi)} \bar{f}_t(\xi;\phi) Z(d\xi) \right).$$

The choice of the Lévy basis Z, the ambit sets $A_t(\phi)$, the weight functions $f_t(\xi;\phi)$ and $\mu_t(\xi;\phi)$ completely determines the growth dynamics. These four ingredients can be chosen arbitrarily and independently which results in a great variety of different growth dynamics. We will now give a number of examples.

Example 3. The size of the ambit sets plays an important role in the control of the local and global fluctuations of the boundary of the object Y_t. As an example, let us consider a linear Lévy growth model with $\mu_t(\phi) \equiv \mu_t$ and $f_t(\xi;\phi) \equiv 1$ such that

$$R_t(\phi) = \mu_t + Z(A_t(\phi)). \tag{18}$$

The ambit set

$$A_t(\phi) = \{(\theta, s) :| \theta - \phi | \le \Theta(t), t - T(t) \le s \le t\}$$

has angular extension $2\Theta(t)$ and temporal extension $T(t)$. In Figure 3, simulations are shown under this model, using a normal Lévy basis with

$$Z(A) \sim N(0, \sigma^2 \mu(A)), \quad A \in \mathfrak{A},$$

and μ equal to the Lebesgue measure on $\mathcal{R}$. The simulations are based on a discretisation of Z on a grid with $\Delta t = 1$ and $\Delta\phi = \frac{2\pi}{1000}$. The upper and lower row of Figure 3 show simulations for two choices of angular extension of the ambit set at three different time points. The angular extension of the ambit set is $\Theta(t) = \frac{\pi}{100}$ for the upper row, while $\Theta(t) = \frac{\pi}{5}$ for the lower row. For the smaller angular extension we observe localised fluctuations of the profiles, but the global appearance appears circular. For the larger angular extension the fluctuations are on a much larger scale and the global appearance is more variable. □

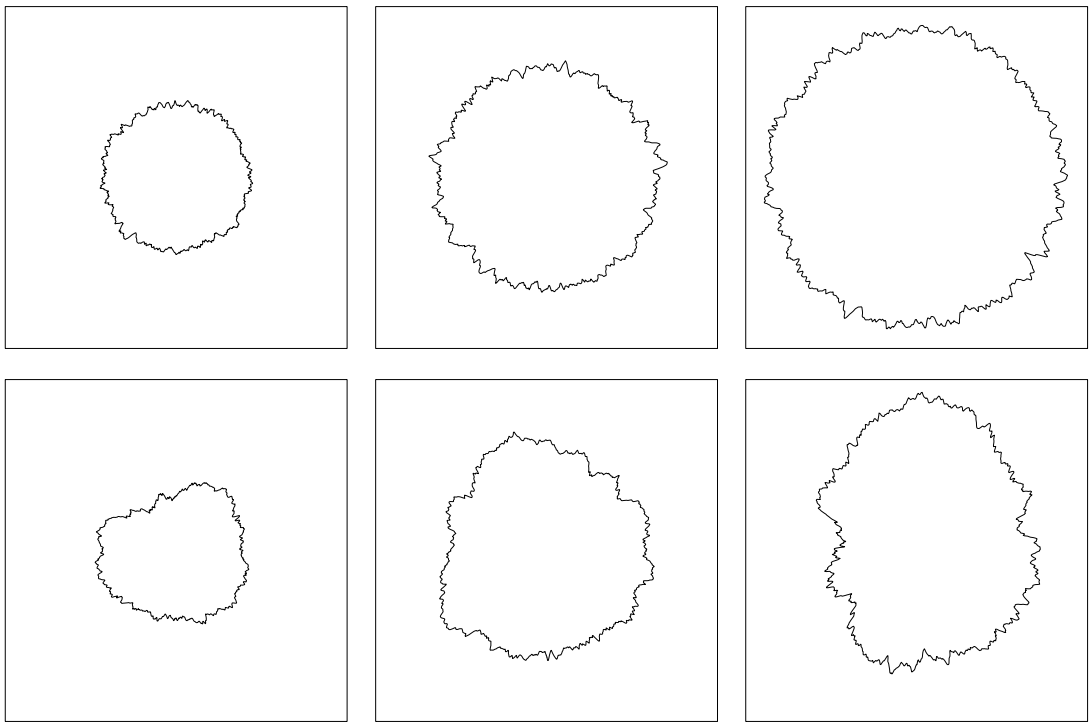

Figure 3: Simulation of the linear Lévy growth model (18) at time points $t = 20, 45, 80$, using a Gaussian Lévy basis. The upper row and lower row show simulations of two choices of the angular extension of the ambit set $\Theta(t) = \frac{\pi}{100}$ and $\Theta(t) = \frac{\pi}{5}$, respectively. Otherwise the parameters of the simulation are $\mu_{20} = 16$, $\mu_{45} = 24$, $\mu_{80} = 32$, $\sigma^2 = 1$ and $T(t) = t/5$.

Example 4. In this example, we study a model as the one described in Example 3, but now with a Gamma Lévy basis. The model equation is

$$R_t(\phi) = \tilde{\mu}_t + Z(A_t(\phi)), \tag{19}$$

where $A_t(\phi)$ is defined as in Example 3,

$$Z(A) \sim \Gamma(\beta\mu(A), \alpha), \quad A \in \mathfrak{A},$$

and μ is the Lebesgue measure on $\mathcal{R}$. Note that $\mu(A_t(\phi))$ does not depend on ϕ. The parameters α, β and $\tilde{\mu}_t$ are chosen such that $\mathbb{E}(R_t(\phi))$ and $\mathbb{V}(R_t(\phi))$ are the same as

in the previous example. Accordingly, the parameters are chosen such that

$$\tilde{\mu}_t = \mu_t - \sigma\sqrt{\beta}\mu(A_t(0)),$$
$$\alpha = \sqrt{\frac{\beta}{\sigma^2}}.$$

The resulting simulations for $\beta = 1$ are shown in the upper and lower row of Figure 4 for the two choices of angular extension of the ambit set, $\Theta(t) = \frac{\pi}{100}$ and $\Theta(t) = \frac{\pi}{5}$, respectively. Note that more sudden outbursts are seen compared to the previous example. □

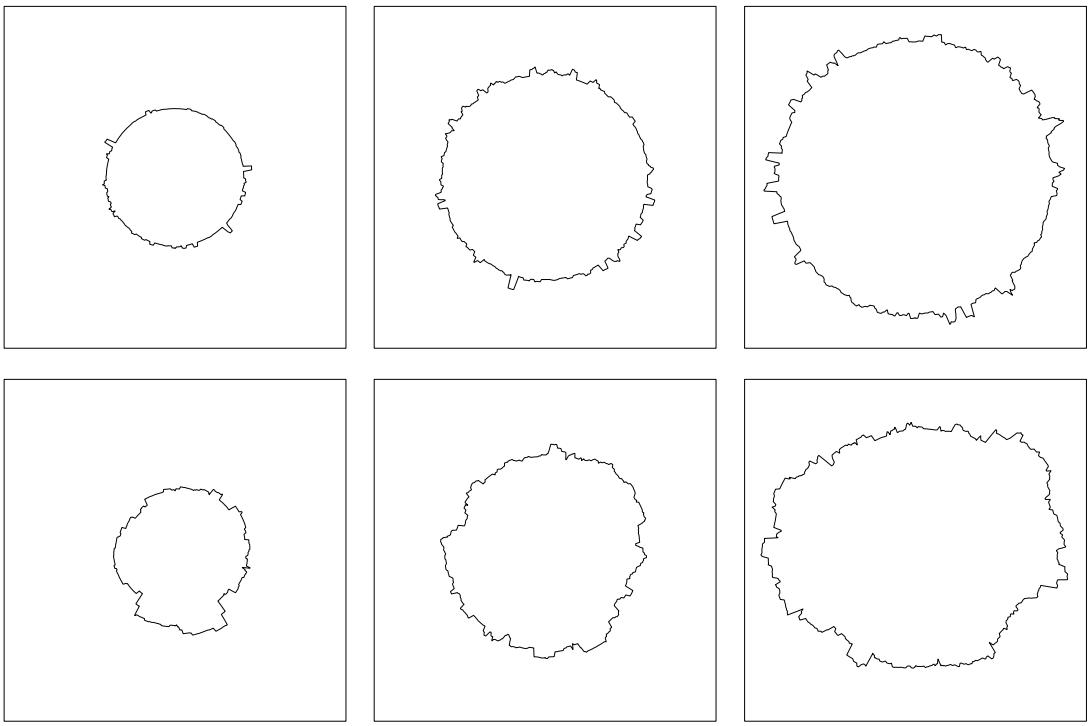

Figure 4: Simulation of the linear Lévy growth model (19) at time points $t = 20, 45, 80$, using a Gamma Lévy basis. The upper row and lower row show simulations of two choices of the angular extension of the ambit set $\Theta(t) = \frac{\pi}{100}$ and $\Theta(t) = \frac{\pi}{5}$, respectively. Otherwise, $\beta = 1$ and the remaining parameters are specified as in Example 3.

Example 5. In Figure 5, we show simulations from the linear growth model

$$R_t(\phi) = f(\phi)\big(\mu_t + Z(A_t(\phi))\big), \tag{20}$$

where μ_t, $A_t(\phi)$ and Z are specified as in Example 3 and

$$f_t(\phi) = 0.35\exp(\frac{\mid \phi - \pi \mid}{\pi}).$$

Clearly the growth of the object is asymmetric. The weight function puts more weight on the angle $\phi_0 = 0$. □

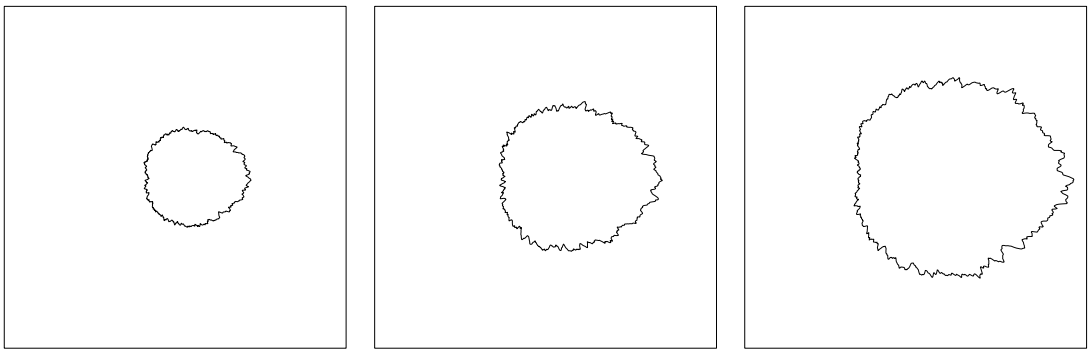

Figure 5: Simulation of the model (20) at time points $t = 20, 45, 80$, using a Gaussian Lévy basis. The weight function is given by $f_t(\phi) = 0.35 \exp(\frac{|\phi-\pi|}{\pi})$.

Example 6. Consider a linear Lévy growth model for the time derivative of the radius vector function

$$\frac{\partial}{\partial t} R_t(\phi) = Z(A_t(\phi)),$$

where Z is a Poisson basis with intensity measure

$$\mu(A) = \lambda_0 \int_A s ds d\theta.$$

The ambit set is of the form

$$A_t(\phi) = \{(\theta, s) : |\theta - \phi| \leq \frac{\Theta}{s}, \max(0, t-T) \leq s \leq t\}.$$

We can write the ambit set as

$$A_t(\phi) = B_t \cap C_\phi,$$

where

$$B_t = \{(\theta, s) : \max(0, t-T) \leq s \leq t\},$$

and

$$C_\phi = \left\{(\theta, s) : s \geq \frac{\Theta}{\pi},\ |\theta - \phi| \leq \frac{\Theta}{s}\right\} \cup \left\{(\theta, s) : 0 \leq s \leq \frac{\Theta}{\pi}\right\}.$$

The induced model for $R_t(\phi)$ is

$$R_t(\phi) = \int_{\bar{A}_t(\phi)} \bar{f}_t(\xi) Z(d\xi),$$

where

$$\bar{A}_t(\phi) = C_\phi \cap ([-\pi, \pi) \times [0, t])$$

and

$$\begin{aligned} \bar{f}_t(\xi) &= \int_0^t 1_{B_s}(\xi) ds \\ &= \begin{cases} t - s, & \text{if } t \leq T \text{ or } (t > T, s > t - T) \\ T, & \text{if } t > T, s \leq t - T. \end{cases} \end{aligned}$$

Here, $\xi = (\theta, s)$. The simulations shown in Figure 6 have been performed with $\lambda_0 = 10$, $T = 1$ and $\Theta = 1/2$. □

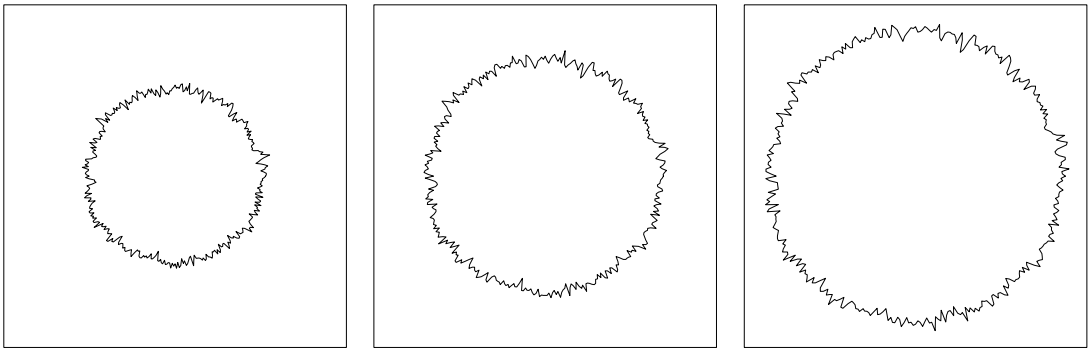

Figure 6: Simulation of a Lévy growth model for the derivative of the radius vector function. The underlying Lévy basis is Poisson.

5 The induced covariance structure

In this section we will derive expressions for $\mathrm{Cov}(R_t(\phi), R_{t'}(\phi'))$ under various assumptions on the Lévy basis Z, the ambit sets $A_t(\phi)$ and the weight functions $f_t(\xi;\phi)$. We will concentrate on linear Lévy growth models. The covariance structure of $R_t(\phi)$ is then given by

$$\mathrm{Cov}(R_t(\phi), R_{t'}(\phi)) = \int_{A_t(\phi)\cap A_{t'}(\phi')} f_t(\xi;\phi) f_{t'}(\xi';\phi) \mathbb{V}(Z'(\xi))\mu(d\xi). \tag{21}$$

For exponential growth models, (21) holds for the log-transformed radius vector function. Throughout the section, we will assume that

$$\begin{aligned} A_t(\phi) &= (\phi, 0) + A_t(0), \\ f_t(\xi;\phi) &= f_t((|\theta - \phi|, s); 0), \\ \mathbb{V}(Z'(\xi))\mu(d\xi) &= g(s)dsd\theta \end{aligned} \tag{22}$$

for all $\xi = (\theta, s) \in \mathcal{R}$ and $(\phi, t) \in \mathcal{R}$. These conditions ensure that $\mathrm{Cov}(R_t(\phi), R_{t'}(\phi))$ only depends on the cyclic difference between ϕ and ϕ'.

We will first consider the case where the angular extension of the ambit set is the full angular space but the weight functions are quite arbitrary. Secondly, we consider the case of constant weight functions but quite arbitrary ambit sets.

5.1 Ambit sets with full angular range

In this subsection we consider ambit sets of the form

$$A_t(\phi) = [-\pi, \pi) \times [t - T(t), t].$$

In order to make the formulae as compact as possible, we use in the proposition below the notation $t \cap t'$ for the time points shared by $A_t(\cdot)$ and $A_{t'}(\cdot)$, i.e.

$$t \cap t' = \begin{cases} [\tilde{t}_1, \tilde{t}_2] & \text{if } \tilde{t}_1 \leq \tilde{t}_2 \\ \emptyset & \text{otherwise,} \end{cases}$$

where

$$\tilde{t}_1 = \max(t - T(t), t' - T(t')) \text{ and } \tilde{t}_2 = \min(t, t').$$

Proposition 7. Let us assume that the ambit set is of the form $A_t(\phi) = [-\pi, \pi) \times [t - T(t), t]$ for all $(\phi, t) \in \mathcal{R}$ and let

$$f_t(\xi; \phi) = a_0^t(s) + \sum_{k=1}^{\infty} a_k^t(s) \cos(k(\theta - \phi)), \tag{23}$$

where $\xi = (\theta, s)$, be the Fourier expansion of the weight function. Then, the spatial covariances are

$$\mathrm{Cov}(R_t(\phi), R_t(\phi')) = 2\lambda_0^t + \sum_{k=1}^{\infty} \lambda_k^t \cos k(\phi - \phi'), \tag{24}$$

where

$$\lambda_k^t = \pi \int_{t-T(t)}^{t} (a_k^t(s))^2 g(s) ds, \;\; k = 0, 1, \ldots.$$

Furthermore, the temporal covariances are given by

$$\mathrm{Cov}(R_t(\phi), R_{t'}(\phi)) = 2\tau_0(t, t') + \sum_{k=1}^{\infty} \tau_k(t, t'), \tag{25}$$

where

$$\tau_k(t, t') = \pi \int_{t \cap t'} a_k^t(s) a_k^{t'}(s) g(s) ds.$$

Proof. The proof is straightforward. First note that the actual form (23) of the Fourier expansion is a consequence of (22). We get that

$$\begin{aligned}
&\mathrm{Cov}(R_t(\phi), R_t(\phi')) \\
&\quad = \int_{A_t(\phi) \cap A_t(\phi')} f_t(\xi; \phi) f_t(\xi; \phi') \mathrm{Var}(Z'(\xi)) \mu(d\xi) \\
&\quad = \pi \left[2 \int_{t-T(t)}^{t} (a_0^t(s))^2 g(s) ds + \sum_{k=1}^{\infty} \left(\int_{t-T(t)}^{t} (a_k^t(s))^2 g(s) ds \right) \cos k(\phi - \phi') \right],
\end{aligned}$$

and

$$\begin{aligned}
&\mathrm{Cov}(R_t(\phi), R_{t'}(\phi)) \\
&\quad = \int_{A_t(\phi) \cap A_{t'}(\phi)} f_t(\xi; \phi) f_{t'}(\xi; \phi) \mathrm{Var}(Z'(\xi)) \mu(d\xi) \\
&\quad = \pi \left[2 \int_{t \cap t'} a_k(t) a_k(t') g(s) ds + \sum_{k=1}^{\infty} \int_{t \cap t'} a_k(t) a_k(t') g(s) ds \right].
\end{aligned}$$

□

Note that the angular covariance $\mathrm{Cov}(R_t(\phi), R_t(\phi'))$ only depends on $|\phi - \phi'|$ and the temporal covariance $\mathrm{Cov}(R_t(\phi), R_{t'}(\phi))$ does not depend on the angle ϕ at all.

Corollary 8. Let the assumptions be as in Proposition 7. Assume that $a_k^t(s) = a_k^t$. Then, the spatial correlations are determined by the weight function f

$$\rho(R_t(\phi), R_t(\phi')) = \frac{2(a_0^t)^2 + \sum_{k=1}^{\infty}(a_k^t)^2 \cos k(\phi - \phi')}{2(a_0^t)^2 + \sum_{k=1}^{\infty}(a_k^t)^2}.$$

If, in addition, $a_k^t = b_t c_k$, then $\rho(R_t(\phi), R_t(\phi'))$ does not depend on t, while the temporal correlations are determined by $T(t)$ and the function g,

$$\rho(R_t(\phi), R_{t'}(\phi)) = \int_{t\cap t'} g(s)ds \Big/ \left[\int_{t-T(t)}^{t} g(s)ds \cdot \int_{t'-T(t')}^{t'} g(s)ds\right]^{1/2}.$$

□

Example 9. A dynamic version of the p-order model described in Hobolth et al. (2003) is easily obtained, using this framework. We let

$$a_k^t(s) = \left[\alpha_t + \beta_t(k^{2p} - 2^{2p})\right]^{-1/2}, \quad k = 2, 3, \ldots,$$

and $a_0^t(s) = a_1^t(s) = 0$. If α_t and β_t are proportional, the simplifying assumptions of Corollary 8 is fulfilled. In Jónsdóttir and Jensen (2005), this model has been used for the time derivative of the radius vector function. Only Gaussian Lévy bases are considered and neighbour time points are assumed to be so far apart that the increments can be regarded as independent. □

In some applications of growth where the shape of the object at any specific time is important, Fourier expansions of the radius-vector function is useful, cf. Alt (1999) and Jónsdóttir and Jensen (2005). Let us consider the Fourier coefficients of $R_t(\phi)$,

$$\begin{aligned} A_0^t &= \frac{1}{2\pi}\int_{-\pi}^{\pi} R_t(\phi)d\phi, \\ A_k^t &= \frac{1}{\pi}\int_{-\pi}^{\pi} R_t(\phi)\cos(k\phi)d\phi, \\ B_k^t &= \frac{1}{\pi}\int_{-\pi}^{\pi} R_t(\phi)\sin(k\phi)d\phi, \end{aligned}$$

$k = 1, 2, \ldots$, and consider the Fourier expansion

$$R_t(\phi) = A_0^t + \sum_{k=1}^{\infty}(A_k^t\cos(k\phi) + B_k^t\sin(k\phi)).$$

Under the assumptions of Proposition 7 it can be shown that

$$A_k^t = \int_{-\pi}^{\pi}\int_{t-T(t)}^{t} a_k^t(s)\cos(k\theta)Z(d\theta \times ds), \quad B_k^t = \int_{-\pi}^{\pi}\int_{t-T(t)}^{t} b_k^t(s)\sin(k\theta)Z(d\theta \times ds),$$

for $k = 0, 1, \ldots$, so the Fourier coefficients follow also a linear Lévy model. It can also be shown that for $k \neq j$, $t, t' \geq 0$,

$$\mathrm{Cov}(A_k^t, A_j^{t'}) = \mathrm{Cov}(B_k^t, B_j^{t'}) = \mathrm{Cov}(A_k^t, B_j^{t'}) = 0,$$

and

$$\mathrm{Cov}(A_k^t, A_k^{t'}) = \mathrm{Cov}(B_k^t, B_k^{t'}) = \tau_k(t,t'), \quad \mathrm{Cov}(A_0^t, A_0^{t'}) = 2\tau_0(t,t'),$$

$k = 1, 2, \ldots$, where $\tau_k(t,t')$ is given in Proposition 7.

In the case where Z is a Gaussian Lévy basis, this means that $A_0 = \{A_0^t\}_{t\in\mathbb{R}_+}$, $A_k = \{A_k^t\}_{t\in\mathbb{R}_+}$ and $B_k = \{B_k^t\}_{t\in\mathbb{R}_+}$, $k = 1, 2, \ldots$, are all independent Gaussian stochastic processes. A_0 has covariance function $2\tau_0(t,t')$ and $A_k \sim B_k$ has covariance function $\tau_k(t,t')$, $k = 1, 2, \ldots$. If one observes A_k^t and B_k^t, for some time points $t = t_1, \ldots, t_n$, $k = 1, \ldots, K_t$, the likelihood function is very tractable.

5.2 Constant weight functions

In this subsection, we consider the case of constant weight functions. Without loss of generality, we assume that $f_t(\xi;\phi) \equiv 1$ and (21) reduces to

$$\begin{aligned}\mathrm{Cov}(R_t(\phi), R_{t\prime}(\phi')) &= \int_{A_t(\phi)\cap A_{t'}(\phi')} \mathbb{V}(Z'(\xi))\mu(d\xi) \\ &= \mathbb{V}(Z')\mu(A_t(\phi)\cap A_{t'}(\phi')),\end{aligned} \tag{26}$$

where the last equality holds if the Lévy basis is factorisable.

It is not difficult (but sometimes tedious) to find explicit expressions for $\mathrm{Cov}(R_t(\phi), R_{t\prime}(\phi'))$ for specific sets. In the Appendix, ambit sets of the form

$$A_t(\phi) = B_t \cap C_\phi,$$

where

$$\begin{aligned}B_t &= \{(\theta, s) : \max(0, t - T(t)) \le s \le t\}, \\ C_\phi &= \{(\theta, s) :\mid \phi - \theta \mid \le \Theta(s)\},\end{aligned}$$

are considered.

Evidently, (26) implies that $\mathrm{Cov}(R_t(\phi), R_{t\prime}(\phi')) \ge 0$ which is a severe restriction for the spatial covariances. In the proposition below, the spatial covariances are expressed in terms of the function delimiting the ambit set. We assume here that μ is the Lebesgue measure on $\mathcal{R}$.

Proposition 10. Let us suppose that there exists a continuous function $g_t : [-\pi, \pi) \to \mathbb{R}_+$ with the properties

$$\begin{aligned}&g_t(\phi) = g_t(-\phi) \\ &g_t \text{ is decreasing on } [0, \pi] \\ &g_t(0) = t\end{aligned} \tag{27}$$

such that

$$A_t(0) = \{(\theta, s) : g_t(\pi) \le t' \le g_t(\phi')\}.$$

Then, if the Fourier expansion of g_t is ($g_t(\phi) = g_t(-\phi)$)

$$g_t(\phi) = \sum_{k=0}^{\infty} \gamma_k^t \cos(k\phi), \tag{28}$$

then

$$\mu(A_t(0) \cap A_t(\phi)) = \sum_{k=0}^{\infty} \lambda_k^t \cos(k\phi), \tag{29}$$

where

$$\lambda_0^t = \sum_{k \text{ odd}} [\pi - \frac{8}{\pi k^2}]\gamma_k^t - \pi \sum_{k \text{ even}} \gamma_k^t$$
$$\lambda_j^t = \frac{16}{\pi} \sum_{k \text{ odd}} \frac{1}{(2j)^2 - k^2} \gamma_k^t, \quad j = 1, 2, \ldots.$$

□

Proof. It is not difficult to show that

$$\mu(A_t(0) \cap A_t(\phi)) = 2 \int_{-\pi}^{-\pi+\frac{\phi}{2}} g_t(\theta) d\theta + 2 \int_{\frac{\phi}{2}}^{\pi} g_t(\theta) d\theta - \pi g_t(\pi), \quad \phi \in [0, \pi). \tag{30}$$

Using (28), we find the following alternative expression for the intersection areas

$$\mu(A_t(0) \cap A_t(\phi)) = \begin{cases} -4 \sum_{k \text{ odd}} \frac{\gamma_k^t}{k} \sin(k\frac{\phi}{2}) + \pi \sum_{k \text{ odd}} \gamma_k^t - \pi \sum_{k \text{ even}} \gamma_k^t & \text{if } \phi \in [0, \pi] \\ 4 \sum_{k \text{ odd}} \frac{\gamma_k^t}{k} \sin(k\frac{\phi}{2}) + \pi \sum_{k \text{ odd}} \gamma_k^t - \pi \sum_{k \text{ even}} \gamma_k^t & \text{if } \phi \in [-\pi, 0]. \end{cases}$$

The result is now obtained by deriving a Fourier expansion of the latter expression and comparing with (29). □

Example 11. In the particular case where

$$g_t(\phi) = \gamma_0^t + \gamma_1^t \cos \phi$$

we find

$$\lambda_0^t = [\pi - \frac{8}{\pi}]\gamma_1^t - \pi\gamma_0^t$$
$$\lambda_j^t = \frac{16}{\pi} \frac{1}{(2j)^2 - 1} \gamma_1^t, \quad j = 1, 2, \ldots.$$

It follows that

$$(\lambda_j^t)^{-1} = \alpha_t + \beta_t j^2, \quad j = 1, 2, \ldots, \tag{31}$$

where $\alpha_t = -\pi/(16\gamma_1^t)$ and $\beta_t = \pi/(4\gamma_1^t)$. Under the assumption of a normal Lévy basis, (31) is a special case of the $p-$order model considered in Jónsdóttir and Jensen (2005) with $p = 1$ and α proportional to β. Note that the requirements (27) implies that $\gamma_0^t = t - \gamma_1^t$ and $\gamma_1^t > 0$. It does not seem to be possible to obtain p-order models with $p > 1$, using this approach. □

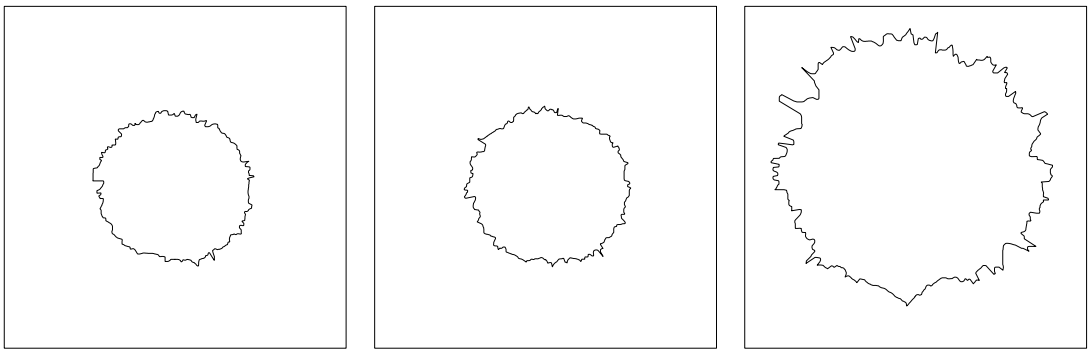

Figure 7: Profiles of a growing brain tumor in vitro at time points $t = 21, 25, 55$.

6 An application to cancer growth

In Schmiegel (2006), snapshots of a growing brain tumor in vitro have been analysed, using the approach described in this paper. The data were first studied in Brú et al. (1998). The data are reproduced in Figure 7 for time points $t = 21, 25, 55$.

A detailed initial analysis showed negative spatial covariances and a need for modelling both small and large scale fluctuations in the growth process. The model used was an exponential Lévy growth model of the form

$$R_t(\phi) = \exp\Bigg(\mu_t + \alpha(t)\int_{t-T(t)}^{t-t_0(t)}\int_{-\pi}^{\pi}\cos(\phi-\theta)Z(ds\times d\theta) + \beta(t)\int_{t-t_0(t)}^{t}\int_{\phi-h_t(s-t+t_0(t))}^{\phi+h_t(s-t+t_0(t))}Z(ds\times d\theta)\Bigg). \tag{32}$$

Here h_t is a deterministic and monotonically decreasing function defined on $[0, t_0(t)]$, satisfying $h_t(t_0(t)) = 0$. Accordingly, the weight function is on the form

$$f_t(\xi;\phi) = \alpha(t)\cos(\phi-\theta)\mathbf{1}_{[t-T(t),t-t_0(t)]}(s) + \beta(t)\mathbf{1}_{[t-t_0(t),t]}(s)\mathbf{1}_{[0,h_t(s-t+t_0(t))]}(|\phi-\theta|).$$

The associated ambit set is shown in Figure 8. In Schmiegel (2006), a Gaussian Lévy

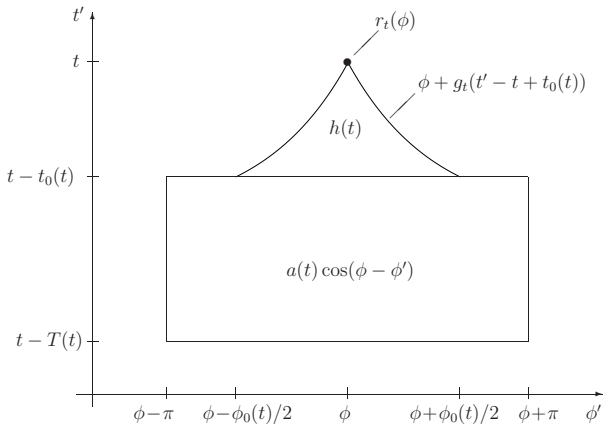

Figure 8: The ambit set $A_t(\sigma)$ for the model defined by (32).

basis has been used and the function h_t was assumed to be of the form

$$h_t(s) = \frac{\phi_0(t)}{2} - \frac{\phi_0(t)}{2t_0(t)}s, \quad s \in [0, t_0(t)].$$

The estimated parameters are given in Table 3 and a simulation under the model is shown in Figure 9.

t	$T(t)$	$t_0(t)$	$\alpha(t)$	$\beta(t)$	$\phi_0(t)$
21	21	19	0.04	−0.033	0.19
25	25	17	0.02	−0.033	0.19
55	18	4	0.01	−0.067	0.23

Table 3: The estimated parameters for the model (32), using a Gaussian Lévy basis.

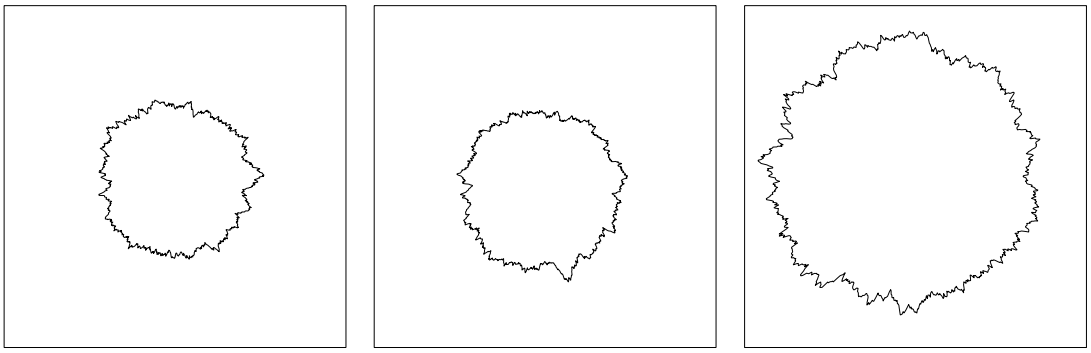

Figure 9: Simulation of the model (32) for time points $t = 21, 25, 51$, using a Gaussian Lévy basis.

Here we have studied the use of Gamma and Inverse Gaussian bases. Simulations under the latter basis are shown in Figure 10. The Inverse Gaussian Lévy basis is chosen such that $\mathbb{E}(R_t(\phi))$ and $\mathbb{V}(R_t(\phi))$ are the same as in the case where a Gaussian basis is used. This means that if $Z(A) \sim \text{IG}(\eta\mu(A), \gamma)$, where μ is the Lebesgue measure, we get that $\eta = \gamma^3$. The upper row shows simulations where $\eta = 316$ and the lower row shows a simulation where $\eta = 5$. For $\eta = 316$ the Inverse Gaussian basis provides fits of a similar quality as the normal basis but for $\eta = 5$, more outburst are observed as is the case for the data. The difference is due to the fact that the Inverse Gaussian distribution has heavier right tails for the latter choice of parameters.

It should be noted that all the profiles simulated under the model (32) using the Lévy basis mentioned in this section show somewhat more fluctuations on a local scale than the observed profiles. At present, it is not known whether this feature is caused by non-perfect model selection and estimation of parameters or artefacts due to the discretisation in the simulation procedure.

7 Appendix

In this appendix we will assume that the measure μ is on the form

$$\mu(d\theta, ds) = g(s)d\theta ds.$$

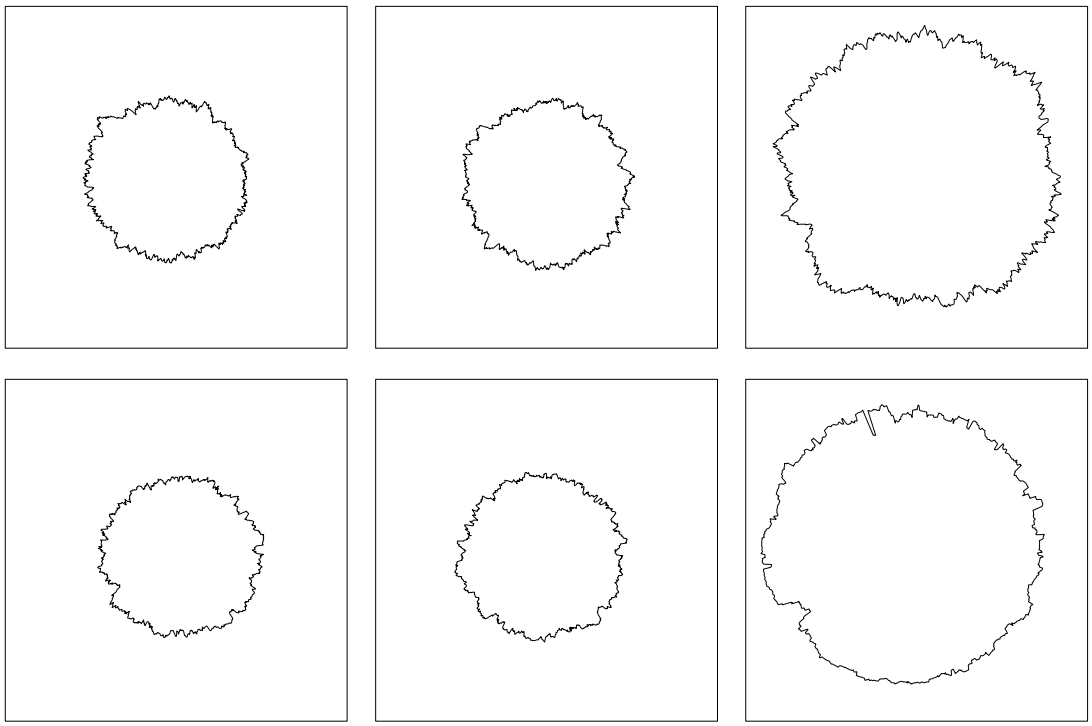

Figure 10: Simulations of the model (32) for time points $t = 21, 25, 51$, using two different types of Inverse Gaussian Lévy basis.

We will study intersections of ambit sets

$$A_t(\phi) = B_t \cap C_\phi,$$

where

$$\begin{aligned} B_t &= \{(\theta, s) : \max(0, t - \Delta_1(t)) \leq s \leq t\}, \\ C_\phi &= \{(\theta, s) :\mid \phi - \theta \mid \leq \Delta_2(s)\}, \end{aligned}$$

so the size and shape of $A_t(\phi)$ does not depend on ϕ. This implies that the measure of the intersection $\mu(A_t(\phi) \cap A_{t'}(\phi'))$ only depends on the angles via the cyclic difference between t and t'. We therefore focus on studying

$$\mu(A_t(0) \cap A_t(\phi)) \quad \text{and} \quad \mu(A_t(0) \cap A_{t+u}(0)),$$

where $u \geq 0$, concentrating on the spatial and temporal covariances/correlations, respectively.

Let $t, u \geq 0$ and assume that $\Delta_1(t+u) - \Delta_1(t) \leq u$, then if $u \leq \Delta_1(t+u)$,

$$\mu(A_t(0) \cap A_{t+u}(0)) = \begin{cases} 2\int_{t^*}^{t} \Delta_2(s) g(s) ds & \text{if } u \leq \Delta_1(t+u), \\ 0 & \text{else,} \end{cases}$$

where $t^* = \max(0, t + u - \Delta_1(t+u))$. In this case one can get various covariance/correlations structure, depending on the choice of Δ_1, Δ_2 and g. A few examples are given in Table 4.

Parameters	$2\Delta_2(s)g(s)$	$\mu(A_t(0) \cap A_{t+u}(0)$
$c > 0$	c (constant)	$c(\Delta_1(t+u) - u)$
$a, b > 0$	ae^{-bs}	$\frac{ae^{-bt}}{b}(e^{-b(u-\Delta_1(t+u))} - 1)$
$a > 0$, $\alpha > 1$	as^α	$(\alpha-1)^{-1}(t^{\alpha+1} - (t+u-\Delta_1(t+u))^{\alpha+1})$

Table 4: The table shows the explicit expression for the integral $\mu(A_t(0) \cap A_{t+u}(0))$ for different choices of $g(s)\Delta_2(s)$.

Let us now study the covariance relating to angular replacements. We get that

$$\mu(A_t(0) \cap A_t(\phi)) = \int_{t^*}^{t} \mathbf{1}_{[0,2\Delta_2(s)]}(|\phi|)\,(2\Delta_2(s) - \min(|\phi|, 2\pi - 2\Delta_2(s)))\,g(s)ds, \quad (33)$$

where $t^* = \max(0, t - \Delta_1(t))$. Here, the integral depends on the separate choices of Δ_2 and g. Note that in the simple case where $\Delta_2(s) \equiv \Delta_2$, then

$$\mu(A_t(0) \cap A_t(\phi)) = 0, \quad \text{for } |\phi| \geq 2\Delta_2,$$

which e.g. implies that for a linear Lévy growth model, the radius-vector function at a fixed time t and different angles ϕ and ϕ' are uncorrelated if $|\phi - \phi'| \geq 2\Delta_2$. Let us instead give an example where $\Delta_1(t) = t$, $\Delta_2(s) = \frac{\Delta_2}{s}$ and $g(s) = s$. For $t \geq \frac{2\Delta_2}{\pi}$, we get

$$\mu(A_t(0) \cap A_t(\phi)) = \begin{cases} \frac{1}{2}\frac{(2\Delta_2)^2}{2\pi - |\phi|} + \left(2\Delta_2 - \frac{|\phi|t}{2}\right)t, & \text{if } |\phi| \leq \frac{2\Delta_2}{t} \\ (2\Delta_2)^2 \frac{\pi}{|\phi|(2\pi - |\phi|)}, & \text{if } \frac{2\Delta_2}{t} < |\phi| \leq \pi. \end{cases}$$

Note that for a linear Lévy growth model $\mathbb{E}(R_t(\phi)) \propto 2\Delta_2 t$, so the covariance $\mathrm{Cov}(R_t(0), R_t(\phi))$ depends for fixed t on $|\phi|$ via $|\phi|t$ for small $|\phi|t$, which is proportional to the distance between to points in directions 0 and ϕ on the boundary of a disc with radius $\mathbb{E}(R_t(\phi))$.

References

Alt, W. (1999). Statistics and dynamics of cellular shape changes. In Chaplain, M. A. J., Singh, G. D., and McLachlan, J. C., editors, *On Growth and Form: Spatio-temporal Pattern Formation in Biology*, pages 287–307. Wiley, Chichester.

Barndorff-Nielsen, O. E., Eggers, H. C., and Schmiegel, J. (2006). Lévy based tempo-spatial modelling; with applications to multiscaling and multifractality. Technical report, MAPHYSTO Research Report 2003-33. To appear in South African Journal of Science.

Barndorff-Nielsen, O. E. and Schmiegel, J. (2003). Lévy based spatio-temporal modelling, with applications to turbulence. *Russian Math. Surveys*, 59(1):65–95.

Barndorff-Nielsen, O. E., Schmiegel, J., Eggers, H. C., and Greiner, M. (2003). A class of spatio-temporal and causal stochastic processes, with application to multiscaling and multifractality. Technical report, MaPhySto Research Report no. 33, University of Aarhus.

Barndorff-Nielsen, O. E. and Thorbjørnsen, S. (2003). A connection between classical and free infinite divisability. Technical report, Research Report 2003-7, University of Aarhus, Denmark.

Brix, A. and Chadoeuf, J. (2002). Spatio-temporal modelling of weeds by shot-noise G Cox processes. *Biom. J.*, 44:83–99.

Brú, A., Pastor, J. M., Fernaud, I., Brú, I., Melle, S., and Berenguer, C. (1998). Super-rough dynamics on tumour growth. *Physical Review Letters*, 81:4008–4011.

Calder, I. R. (1986). A stochastic model of rainfall interception. *J. of Hydrology*, 89:65–71.

Cantalapiedra, I. R., Lacasta, A. M., Auguet, C. E., Peñaranda, A., and Ramirez-Piscina, L. (2001). Pattern formation modelling of bacterial colonies. In *Branching in Nature.*, pages 359–364. EDP Sciences, Springer.

Delsanto, P. P., Romano, A., Scalerandi, M., and Pescarmona, G. P. (2000). Analysis of a "phase transition" from tumor growth to latency. *Phys. Rev. E*, 62:2547–2554.

Feideropoulou, G. and Pesquet-Popescu, B. (2004). Stochastic modelling of the spatio-temporal wavelet coefficients and applications to quality enhancement and error concealment. *EURASIP JASP*, 12:1931–1942.

Fewster, R. M. (2003). A spatiotemporal stochastic process model for species spread. *Biometrics*, 59:640–649.

Gratzer, G., Canham, C., Dieckmann, U., Fischer, A., Iwasa, Y., Law, R., Lexer, M. J., Sandman, H., Spies, T., Splechtna, B., and Szwagrzyk, L. (2004). Spatio-temporal development of forests – current trends in field methods and models. *Oikos*, 107:3–15.

Hobolth, A., Pedersen, J., and Jensen, E. B. V. (2003). A continuous parametric shape model. *Ann. Inst. Statist. Math.*, 55:227–242.

Jónsdóttir, K. Ý. and Jensen, E. B. V. (2005). Gaussian radial growth. *Image Analysis & Stereology*, 24:117–16.

Kallenberg, O. (1989). *Random Measures*. Akademie Verlag, Berlin, 4 edition.

Kwapien, S. and Woyczynski, W. A. (1992). *Random Series and Stochastic Integrals: Single and Multiple*. Birkhäuser, Basel.

Lovejoy, S., Schertzer, D., and Watson, B. (1992). Radiative transfer and multifractal clouds: theory and applications. *I.R.S.*, 92:108–111.

Pang, N. N. and Tzeng, W. J. (2004). Anomalous scaling of superrough growing surfaces: From correlation functions to residual local interfacial widths and scaling exponents. *Phys. Rev. E*, 70(036115).

Peirolo, R. and Scalerandi, M. (2004). Markovian model of growth and histologic progression in prostate cancer. *Phys. Rev. E*, 70(011902).

Pérez-Muñuzuri, V., Lorenzo, M. N., Montero, P., Fraedrich, K., Kirk, E., and Lunkeit, F. (2003). Response of a global atmospheric circulation model to spatio-temporal stochastic forcing: ensemble statistics. *Nonlinear Processes in Geophysics*, 10:453–461.

Rajput, B. S. and Rosinski, J. (1989). Spectral representations of divisible processes. *Probability Theory and Related fields*, 89:451–487.

Sato, K. (1999). *Lévy Processes and Infinitely Divisable Distributions.* Cambridge University Press, Cambridge.

Schmiegel, J. (2006). Self-scaling tumor growth. Technical report, Research Report 2005-7. Thiele Centre, University of Aarhus. To appear in Physica A.

Schmiegel, J., Cleve, J., Eggers, H., Pearson, B. R., and Greiner, M. (2004). Stochastic energy-cascade model for 1+1 dimensional fully developed turbulence. *Phys. Lett. A*, pages 247–253.

Sornette, D. and Ouillon, G. (2005). Multifractal scaling of thermally activated rupture processes. *Phys. Rev. Lett.*, 94(038501).

Paper D

Jónsdóttir, K.Ý., Hoffman, L., Hobolth, A. and Jensen E.B.V. (2006).
On error prediction in circular systematic sampling.
To appear in *Journal of Microscopy*.

On error prediction in circular systematic sampling

Kristjana Ýr Jónsdóttir*,Lars Michael Hoffmann**,
Asger Hobolth*** and Eva B. Vedel Jensen*
* University of Aarhus
** University of Karlsruhe
***North Carolina State University

Abstract

An extended covariogram model is discussed for estimating the precision of circular systematic sampling. The extension is motivated by recent developments in shape analysis of featureless planar objects. Preliminary simulation results indicate that it is important to consider the extended covariogram model.

Keywords: Covariogram, error prediction, shape, stereology, stochastic processes, systematic sampling, variance estimation.

1 Introduction

Recently, the precision of systematic sampling on the circle has been discussed in Gual-Arnau & Cruz-Orive (2000) and Cruz-Orive & Gual-Arnau (2002). In particular, variance estimation formulae based on a global polynomial model for the covariogram have been developed. In Hobolth & Jensen (2002), this approach is discussed both in a design-based and a model-based setting, and an alternative model-based method of estimating the parameter of the covariogram is described.

In this note, we summarise these developments and argue that it may be natural to consider an extension of the polynomial covariogram model, see also the discussion in Hobolth & Jensen (2002). We explain the geometric interpretation of the parameters of the proposed extended model and report preliminary simulation results.

2 A global polynomial covariogram model

In this note, we will focus on the model-based approach to error prediction in circular systematic sampling. In a model-based setting, the aim is to predict an integral of the form

$$Q = \int_0^1 F(2\pi t)dt,$$

where

$$F = \{F(2\pi t) : 0 \leq t < 1\}$$

is a stationary periodic non-negative stochastic process of bounded variation, square integrable and piecewise continuous. Since F is stationary, the mean $\mathbb{E}F(2\pi t)$ does not depend on t and equals μ, say, and the covariance

$$\mathrm{Cov}(F(2\pi h), F(2\pi(h+t))), \tag{1}$$

$0 \leq h, t < 1$, does not depend on h and will be denoted $\sigma(t)$. In (1), we use a periodic extension of F. The covariance function satisfies $\sigma(t) = \sigma(1-t)$ and therefore, its Fourier expansion takes the form

$$\sigma(t) = \lambda_0 + 2\sum_{k=1}^{\infty} \lambda_k \cos(2\pi k t),$$

$0 \leq t < 1$. The predictor of Q to be considered is of the form

$$\hat{Q}(F, \phi, n) = \frac{1}{n}\sum_{j=0}^{n-1} F\left(2\pi\left(\phi + \frac{j}{n}\right)\right),$$

where $\phi \in [0, 1/n[$. Note that the distribution of $\hat{Q}(F, \phi, n)$ does not depend on ϕ, due to the stationarity of F. The prediction error of using $\hat{Q}(F, \phi, n)$ as a predictor of Q can be expressed in terms of the Fourier coefficients λ_k of the covariance function. We thus have

$$\mathbb{E}(\hat{Q}(F, \phi, n) - Q)^2 = 2\sum_{k=1}^{\infty} \lambda_{kn}. \tag{2}$$

Note that the prediction error only depends on Fourier coefficients of order n and higher.

In Hobolth & Jensen (2002), a parametric model for the covariance function is considered,

$$\begin{aligned} \lambda_0 &= \beta_0 - 2\sum_{k=1}^{\infty} \lambda_k, \\ \lambda_k &= \frac{(2p)!}{k^{2p}}\beta, \quad k = 1, 2, \ldots, \end{aligned} \tag{3}$$

where p is a positive integer and the other model parameters β_0 and β are chosen such that $\lambda_k \geq 0$ for $k = 0, 1, \ldots$. Under (3), the prediction error only depends on β

$$\begin{aligned} \mathbb{E}(\hat{Q}(F, \phi, n) - Q)^2 &= 2\sum_{k=1}^{\infty} \lambda_{kn} \\ &= \frac{1}{n^{2p}}(-1)^{p-1}(2\pi)^{2p} B_{2p}\beta, \end{aligned} \tag{4}$$

where B_{2p} is a Bernoulli number. For more details on Bernoulli numbers and the associated Bernoulli polynomials, see Abramovitz & Stegun (1965).

Hobolth & Jensen (2002) suggest to estimate the parameter β using maximum likelihood estimation. It is shown that if F is assumed to be a Gaussian process,

there exists a unique unbiased estimator $\hat{\beta}$ of β with minimum variance. If we have n systematic observations of F,

$$F\left(2\pi\left(\phi+\frac{j}{n}\right)\right), \quad j=0,1,\ldots,n-1,$$

$\phi \in [0, 1/n[$, then

$$\hat{\beta} = \frac{1}{n-1}\sum_{j=1}^{n-1}\frac{\hat{\lambda}_j}{\tilde{\kappa}_j},$$

where for $j = 1, \ldots, n-1$

$$\begin{aligned}\hat{\lambda}_j &= \frac{1}{n^2}\sum_{l,m=0}^{n-1}\cos(2\pi j(l-m)/n) \\ &\quad \times F\left(2\pi\left(\phi+\frac{l}{n}\right)\right)F\left(2\pi\left(\phi+\frac{m}{n}\right)\right) \qquad (5)\\ \tilde{\kappa}_j &= \sum_{k\in\mathbb{Z}}\frac{(2p)!}{(j+nk)^{2p}}.\end{aligned}$$

Using this maximum likelihood estimate of β we can estimate the prediction error (4) by

$$(-1)^{p-1}(2\pi)^{2p}B_{2p}\frac{1}{n^{2p}}\hat{\beta}. \qquad (6)$$

The parametric model (3) for the covariance function has originally been suggested in a design-based setting by Gual-Arnau & Cruz-Orive (2000, page 635). They provide an alternative estimator of the prediction error (4) based on the empirical covariogram $\hat{g}$ at 0 and $1/n$

$$\frac{1}{n^{2p}}\frac{\hat{g}(0)-\hat{g}(\frac{1}{n})}{1-B_{2p}(\frac{1}{n})/B_{2p}}, \qquad (7)$$

where $B_{2p}(t)$ is a Bernoulli polynomial of order $2p$ and

$$\hat{g}\Big(\frac{k}{n}\Big) = \frac{1}{n}\sum_{j=0}^{n-1}F\Big(2\pi\Big(\phi+\frac{j}{n}\Big)\Big)F\Big(2\pi\Big(\phi+\frac{j+k}{n}\Big)\Big),$$

$k = 0, 1, \ldots, n-1$. Note that

$$\hat{g}(0)-\hat{g}\Big(\frac{1}{n}\Big) = \frac{1}{2n}\sum_{j=0}^{n-1}\left(F\Big(2\pi\Big(\phi+\frac{j}{n}\Big)\Big)-F\Big(2\pi\Big(\phi+\frac{j+1}{n}\Big)\Big)\right)^2. \qquad (8)$$

It can be shown that for $n = 2$ and $n = 3$, (6) and (7) coincide.

The estimator (7) only uses the empirical covariogram $\hat{g}$ near the origin. In Cruz-Orive & Gual-Arnau (2002), they suggest a modified estimator

$$\frac{1}{n^{2p}}\frac{1}{[\frac{n}{2}]}\sum_{k=1}^{[\frac{n}{2}]}\frac{\hat{g}(0)-\hat{g}(\frac{k}{n})}{1-B_{2p}(\frac{k}{n})/B_{2p}}, \qquad (9)$$

using more values of the empirical covariogram. The estimators (6), (7) and (9) are all unbiased under the model (3).

3 An extension of the global covariogram model

The model (3) and its design-based analogue have the nice property that analytic expressions of the estimators are available. It turns out, however, that it is natural from a geometric point of view to consider an extension of this model. In a model-based setting, the extended model is known as the $p-$order model (Hobolth et al. 2002; Hobolth et al., 2003). The covariance function of the extended model is determined by Fourier coefficients of the form

$$\lambda_0 \geq 0, \quad \lambda_k^{-1} = \tilde{\alpha} + \tilde{\beta} k^{2p}, \quad k = 1, 2 \ldots, \tag{10}$$

where $\tilde{\alpha}+\tilde{\beta} > 0$, $\tilde{\beta} > 0$ and $p > \frac{1}{2}$. It can be shown that p determines the smoothness of the stochastic process F. In fact, if we assume that F is a Gaussian process, F is $m-1$ times continuously differentiable where m is the integer satisfying $p \in]m - \frac{1}{2}, m + \frac{1}{2}]$. For fixed p, $\tilde{\alpha}$ and $\tilde{\beta}$ determine the global and local fluctuations of the stochastic process F, respectively. Small values of $\tilde{\alpha}$ provide large fluctuations of the process on a global scale, while large values give smaller fluctuations. Also, the smaller $\tilde{\beta}$, the more fluctuations of F on a local scale.

In particular, if $F = R$, where R is the radial function of a planar object K, star-shaped relative to $z \in K$,

$$R(2\pi t) = \max\{r : z + r(\cos(2\pi t), \sin(2\pi t)) \in K\},$$

$0 \leq t < 1$, then p determines the smoothness of the boundary of the object K and for fixed p, $\tilde{\alpha}$ and $\tilde{\beta}$ determine the global and local shape of the object, respectively. If $\tilde{\alpha}$ is small, the global shape of the object K is expected to deviate from circular shape. A small value of $\tilde{\beta}$ is expected to provide an object boundary with many local fluctuations. Typically, in addition, the parameter λ_1 is set to zero if the point z is approximately the center of mass of the object K. For more details, see Hobolth et al. (2003).

As mentioned above the model described in (3) is a special case of the p-order model. It is obtained by choosing p as a positive integer and

$$\tilde{\alpha} = 0, \tilde{\beta} = ((2p)!\beta)^{-1}. \tag{11}$$

It seems natural to include an additional parameter $\tilde{\alpha}$ to allow for more flexibility.

The estimator (6) of the prediction error provided under the restricted model (11) appears, however, to work well under the general model (10) if n is large and F is a Gaussian process. A heuristic argument goes as follows. In Hobolth & Jensen (2002), it is shown for a Gaussian process with a general covariance function that

$$\sum_{j=1}^{n-1} \frac{\hat{\lambda}_j}{\tilde{\lambda}_j} \sim \chi^2(n-1),$$

where $\hat{\lambda}_j$ is given in (5) and

$$\tilde{\lambda}_j = \sum_{k=-\infty}^{\infty} \lambda_{j+nk}.$$

For large n, we have under (10) that

$$\tilde{\lambda}_j \approx \frac{\tilde{\kappa}_j}{\tilde{\beta}(2p)!}.$$

Accordingly, the estimator (6) is approximately $\gamma_n X$ where

$$\gamma_n = (-1)^{p-1}(2\pi)^{2p} B_{2p} \frac{1}{n^{2p}} \frac{1}{\tilde{\beta}(2p)!}$$

and $X \sim \chi^2(n-1)/(n-1)$. Note that for n large, the prediction error is approximated by γ_n since

$$\begin{aligned}
\mathbb{E}(\hat{Q}(F,\phi,n) - Q)^2 &= 2\sum_{k=1}^{\infty} \frac{1}{\tilde{\alpha} + \tilde{\beta}(nk)^{2p}} \\
&\approx 2\frac{1}{\tilde{\beta}} \frac{1}{n^{2p}} \sum_{k=1}^{\infty} \frac{1}{k^{2p}} \\
&= \gamma_n.
\end{aligned}$$

4 Preliminary simulation results

Throughout this section, the *squared* radial function of the simulated objects relative to the origin is given by

$$F(2\pi t) = 1 + \sqrt{2} \sum_{k=1}^{\infty} (A_k \cos(2\pi k t) + B_k \sin(2\pi k t)), \tag{12}$$

$0 \le t < 1$, where all $A_k \sim B_k \sim N(0, \lambda_k)$ are mutually independent. In fact, if F is a stationary periodic Gaussian process, F is distributed as in (12). Note that since F is the squared radial function,

$$\pi \int_0^1 F(2\pi t) dt$$

is the area of the simulated object.

We concentrate on objects with z approximately equal to the centre of mass so λ_1 is set to zero. The remaining Fourier coefficients follow (10). It is natural to use a reparametrisation of the model (Hobolth et al., 2003),

$$\begin{aligned}
&\lambda_0 \ge 0, \quad \lambda_1 = 0, \\
&\lambda_k^{-1} = \alpha + \beta(k^{2p} - 2^{2p}), \quad k = 2, 3, \ldots,
\end{aligned} \tag{13}$$

such that α determines λ_k for small $k \ge 2$ while β determines λ_k for large k. Throughout the study, we use $p = 2$. As a consequence, the object boundary is continuously differentiable.

Figure 1 shows, for selected values of α and β, simulated objects and a log-log plot of the true prediction error (2) together with the estimated prediction errors (6), (7) and (9) calculated from measurements on the shown objects. As supported by the reasoning in Section 3, the estimate (6) seems to perform well for not too small values of

n. The other estimates are somewhat below the true prediction error. For small values of n neither of the estimators delivers satisfying results. It should be emphasised that in Figure 1 the simulated objects follow the model (13) but the estimators examined refer to the model (3).

In Hobolth et al. (2003), it is suggested to use the low frequency Fourier coefficients to estimate the parameters of the model (13). When F is a Gaussian process we can use the likelihood function

$$L(\lambda_k; c_k) = \prod_{k=2}^{K} \lambda_k^{-1} e^{-\lambda_k^{-1} c_k} \tag{14}$$

to find estimates of α, β and p through standard numerical methods. Here,

$$c_k = \frac{a_k^2 + b_k^2}{2}$$

is the k'th phase amplitude, where a_k and b_k are the observed values of the Fourier coefficients A_k and B_k from (12). We used values of K approximately equal to $n/3$. For details about the choice of K, see Hobolth et al. (2003). In this paper, it is also shown that the estimation of p is not critical. For convenience, we used $p = 2$, but estimated α and β by maximising L as a function of α and β. For this purpose, we used the fminsearch-function in Matlab which uses the simplex search method of Lagarias et al. (1998).

Since the prediction error is given by

$$2 \sum_{k=1}^{\infty} \lambda_{nk} \tag{15}$$

and

$$\lambda_k^{-1} = \alpha + \beta(k^{2p} - 2^{2p})$$

for $k \geq 2$, we can use the estimated values of α and β to obtain an estimate of the prediction error. In the log-log plots of Figure 2, we show the true prediction error (solid curve) as a function of n, together with the estimated prediction errors (6) and (7) and the prediction error obtained by inserting the estimated values of α and β into (15). The estimates are based on measurements on the shown objects. The estimate (7) lies somewhat below the other estimates which are quite close to the true prediction error. One should note, though, that the parameters in the model (13) are difficult to estimate if n is smaller then ten (Hobolth et al., 2003). The reason is that the Fourier coefficients a_k and b_k are determined as discretised Fourier integrals based on n measurements of the radial function.

All these results call for a closer investigation of the model (13) and its use in assessment of the precision of circular systematic sampling.

5 Acknowledgements

We want to thank the referees for constructive comments on the manuscript. This research has been supported by the Danish Natural Science Research Council. Lars Michael Hoffmann has been supported by a Marie Curie Research Fellowship under

contract number HPMT-CT-2001-0364.

References

Abramovitz, M. & Stegun, I.A. (1965) *Handbook of Mathematical Functions.* Dover Publications Inc., New York.

Cruz-Orive, L.M. & Gual-Arnau, X. (2002) Precision of circular systematic sampling. *J. Microsc.* **207**, 225–242.

Gual-Arnau, X. & Cruz-Orive, L.M. (2000) Systematic sampling on the circle and on the sphere. *Adv. Appl. Prob. (SGSA)* **32**, 628–647.

Hobolth, A. & Jensen, E.B.V. (2002) A note on design-based versus model-based variance estimation in stereology. *Adv. Appl. Prob. (SGSA)* **34**, 484-490.

Hobolth, A., Kent, J.T. & Dryden, I.L. (2002) On the relation between edge and vertex modelling in shape analysis. *Scand. J. Statist.* **29**, 355–374.

Hobolth, A., Pedersen, J. & Jensen, E.B.V. (2003) A continuous parametric shape model. *Ann. Inst. Statist. Math.* **55**, 227-242.

Lagarias, J.C., Reeds, J.A., Wright, M.H. & Wright, P.E. (1998) Convergence properties of the Nelder-Mead simplex method in low dimensions. *SIAM J. Opt.* **9**, 112-147.

Legends to figures

Figure 1
Simulations under the model (13) with $(\log\alpha, \log\beta) = (3.5, -0.5)$, $(7.5, -0.5)$ and $(7.5, 3.5)$ in the upper, middle and lower row, respectively. The true prediction error (solid curve) is shown in a log-log plot as a function of n, together with the estimated prediction errors (6), (7) and (9) shown as $\diamond$, $\star$ and $\circ$, respectively. The simulated objects are shown in the lower left corners of the plots.

Figure 2
Simulations under the model (13) with $(\log\alpha, \log\beta) = (3.5, -0.5)$, $(7.5, -0.5)$ and $(7.5, 3.5)$ in the upper, middle and lower row, respectively. In the log-log plots, the true prediction error (solid curve) is shown as a function of n, together with the estimated prediction errors (6) and (7), shown as $\diamond$ and $\circ$, and the estimate obtained by plugging in estimates of α and β into (15), shown as $\star$. The simulated objects are shown in the lower left corners of the plots.

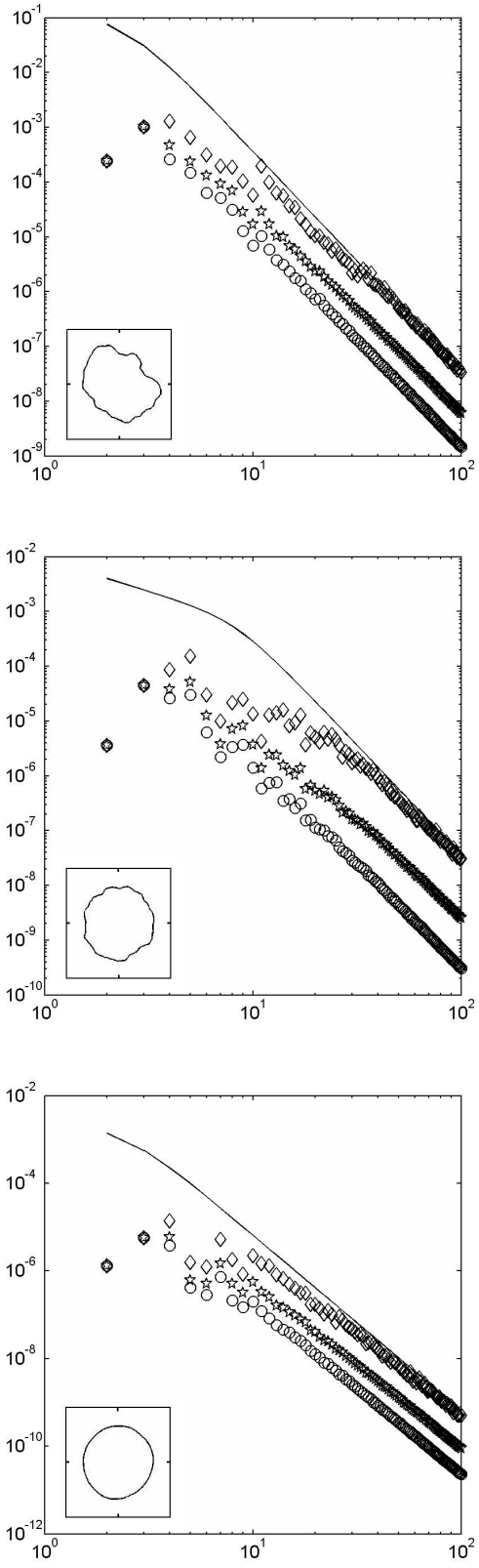
10^-1
10^-2
10^-3
10^-4
10^-5
10^-6
10^-7
10^-8
10^-9
10^0
10^1
10^2
10^-2
10^-3
10^-4
10^-5
10^-6
10^-7
10^-8
10^-9
10^-10
10^0
10^1
10^2
10^-2
10^-4
10^-6
10^-8
10^-10
10^-12
10^0
10^1
10^2

Figure 1

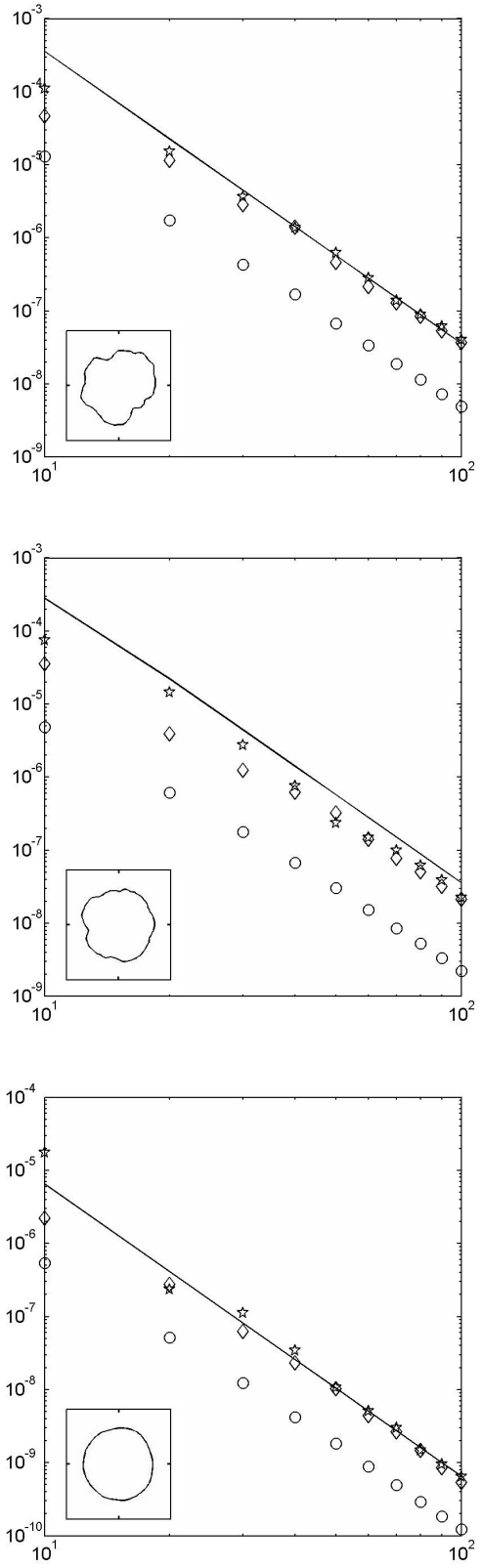
10^-3
10^-4
10^-5
10^-6
10^-7
10^-8
10^-9
10^1
10^2
10^-3
10^-4
10^-5
10^-6
10^-7
10^-8
10^-9
10^1
10^2
10^-4
10^-5
10^-6
10^-7
10^-8
10^-9
10^-10
10^1
10^2

Figure 2

Paper

E

Jónsdóttir, K.Ý. (2006).
Non-stationary spatial survival analysis.
To appear as a Thiele Research report.

Non-stationary spatial survival analysis

Kristjana Ýr Jónsdóttir
University of Aarhus

Abstract

In this report we introduce some basic ideas of how classical tools from survival analysis can be used to study non-stationary spatial data. We will focus on the definition of a local version of the empty space function of a non-stationary random compact set and its hazard rate and an estimation method under the well known Cox proportional hazard model. We will give some concrete examples of applying the estimation method, using both real and simulated data. Finally we will summarise the open questions within this area and discuss some of the further investigations needed to assess how useful the suggested methods are.

1 Introduction

In Baddeley and Gill (1993, 1997) methods from survival analysis are used to estimate characteristics for spatial point processes based on interpoint distances. They study estimators of Kaplan-Meier type based on the analogy with censored survival data. The distance from a fixed point to the nearest point of the process is censored by its distance to the boundary of the observation window. In Baddeley and Gill (1994) and Hansen et al. (1996, 1999) a Kaplan-Meier estimator of the first contact distribution of a random compact set is introduced and analysed under certain regularity condition. These papers only consider estimation of statistics of stationary spatial data. It is of interest to try to use analogues from survival analysis to estimate statistics of non-stationary spatial data, since the standard analysis cannot be applied in this case. The question is whether we can find some non-parametric or semi-parametric methods to analyse non-stationary data sets using methods from classical survival analysis. In this report, we will mainly focus on the local version of the empty space function of a non-stationary random compact set X

$$F_\xi(r) = \mathrm{P}(X \cap b(\xi, r) \neq \emptyset),$$

and the local version of its hazard rate,

$$\lambda_\xi(r) = \frac{f_\xi(r)}{1 - F_\xi(r)},$$

where $b(\xi, R)$ is the sphere in $\mathbb{R}^d$ with radius r centred at $\xi \in \mathbb{R}^d$ and f_ξ is the derivative of F_ξ (if it exists).

We will start by summarising some known methods to estimate the empty space function for stationary data, including methods using tools from survival analysis. In Section 3 we will define a local version of the empty space function of a non-stationary

random compact set and its hazard rate. We will introduce some ideas of how known methodology from survival analysis, i.e. the Cox proportional hazard model and the accelerated lifetime model, can be used for semi-parametric estimation. Examples of application to real and simulated data will be given. Finally we will discuss the open problems within this area and try to highlight the most important further investigations which need to be done.

2 Stationary spatial survival analysis

We assume that we have a realisation of a stationary random closed set X in $\mathbb{R}^d$ observed within a compact and regular window W. Thus the data consists of $X \cap W$ and W. Even though W could also be regarded as a random set, all analysis will be conditionally on W. Based on this data, we want to study some properties of the spatial pattern X by using the empty space function and its hazard function as defined below.

The empty space function F is defined as

$$F(r) = \mathrm{P}(X \cap b(0,r) \neq \emptyset), \quad r \geq 0, \tag{1}$$

where $b(\xi, r)$ denotes the sphere in $\mathbb{R}^d$ with radius r centred at $\xi \in \mathbb{R}^d$. The empty space function is also known as the first contact distribution of X with respect to the test set $b(0,r)$. An alternative definition of the empty space function is given by

$$F(r) = \mathrm{P}(\rho(0,X) \leq r), \quad r \geq 0, \tag{2}$$

where

$$\rho(\xi, X) = \inf\{|\xi - a| : a \in X\}, \tag{3}$$

is the distance from ξ to the the random set $X \subset \mathbb{R}^d$. The survival function of $\rho(0,X)$ will be denoted by $S(r) = 1 - F(r)$. If the empty space function is differentiable for all $r \in \mathbb{R}_0^+$, then we let f be the derivative (or density) of F and we define the hazard rate of X by

$$\lambda(r) = \frac{f(r)}{1 - F(r)} = -\frac{d}{dr}\log(1 - F(r)), \quad r > 0, \tag{4}$$

which implies that

$$F(r) = 1 - \exp(-\int_0^r \lambda(s)ds).$$

For more details cf. Baddeley and Gill (1994) and Hansen et al. (1996, 1999).

It is useful to compare the estimated empty space function and/or hazard rate of some spatial pattern to its theoretical counterpart of a completely random spatial pattern. Below we will give two important examples of completely random spatial patterns.

Example 2.1. If the random set X is a Poisson point process in $\mathbb{R}^2$ with intensity α we have that

$$F(r) = 1 - \exp(-\alpha\pi r^2) \quad \text{and} \quad \lambda(r) = 2\alpha\pi r.$$

Moreover, an indicator of clustering or regularity of the point process can be seen by comparing the estimated hazard rate $\hat{\lambda}$ to the hazard rate of a Poisson process. At least for small values of r, $\hat{\lambda}(r) \leq \lambda(r)$ indicates clustering or aggregation, whereas $\hat{\lambda}(r) \geq \lambda(r)$ is a indication of regularity. □

Example 2.2. If X is a Boolean model in $\mathbb{R}^2$ with convex grains, then

$$F(r) = 1 - \exp(-\alpha(a + b + \pi r^2)) \quad \text{and} \quad \lambda(r) = \alpha(b + 2\pi r),$$

where a and b are the mean area and boundary length of the typical convex grain, respectively. In the special case where the grains are random discs $b(0, R_i)$, where the R_is are positive independent and identically distributed random variables, $R_i \sim R$, then

$$F(r) = 1 - \exp(-\alpha\pi\mathbb{E}(R + r)^2) \quad \text{and} \quad \lambda(r) = 2\alpha\pi(\mathbb{E}(R) + r).$$

□

Different estimators for the empty space function have been suggested in the literature. The most simple one is the reduced-sample estimator which is easily derived using classical minus sampling. This estimator is given by

$$\hat{F}^{\text{rs}}(r) = \frac{|W_{\ominus r} \cap X_{\oplus r}|_k}{|W_{\ominus r}|_k}, \tag{5}$$

where $|\cdot|_k$ denotes the k-dimensional Lebesgue measure,

$$A_{\oplus r} = \{\xi \in \mathbb{R}^d : \rho(\xi, A) \leq r\},$$
$$A_{\ominus r} = \{\xi \in \mathbb{R}^d : \rho(\xi, A^{\text{c}}) > r\},$$

and $^{\text{c}}$ denotes the compliment. This estimate is unbiased, but note that $\hat{F}^{\text{rs}}(r)$ is not necessarily a distribution function. For more details, cf. Stoyan et al. (1995).

A more efficient estimator is the so-called Kaplan-Meier estimator proposed by Baddeley and Gill (1997):

$$\hat{F}(r) = 1 - \frac{|W \setminus X|_k}{|W|_k} \exp(-\int_0^r \hat{\lambda}(s)ds), \tag{6}$$

where $\hat{\lambda}$ is the ratio-unbiased estimator of λ,

$$\hat{\lambda}(r) = \frac{|\partial(X_{\oplus r}) \cap W_{\ominus r}|_{k-1}}{|W_{\ominus r} \setminus X_{\oplus r}|_k}, \tag{7}$$

and $\partial(X)$ denotes the boundary of X. In practise the sampling window W will be discretised on a regular lattice and as the lattice becomes finer, the discrete Kaplan-Meier estimator converges to $\hat{F}$. For more details, cf. Baddeley and Gill (1994) and Hansen et al. (1996, 1999).

3 Non-stationary spatial survival analysis

Now we assume that we have a realisation of a *non-stationary random set* X in $\mathbb{R}^d$ observed within a compact and regular window W. In non-stationary spatial statistics, a counterpart of the empty space function in the stationary case is the local empty space function F_ξ at a position $\xi \in \mathbb{R}^d$, defined as

$$\begin{aligned} F_\xi(r) &= \text{P}(X \cap b(\xi, r) \neq \emptyset) \\ &= \text{P}(\rho(\xi, X) \leq r), \end{aligned}$$

where $r \geq 0$ and the local survival function of $\rho(\xi, X)$ by $S_\xi(r) = 1 - F_\xi(r)$. If the empty space function is differentiable for all $(\xi, r) \in \mathbb{R}^d \times \mathbb{R}_0^+$, then we let f_ξ be the derivative (or density) of F_ξ and we define the local hazard rate of X by

$$\lambda_\xi(r) = \frac{f_\xi(r)}{1 - F_\xi(r)} = -\frac{d}{dr} \log(1 - F_\xi(r)), \quad r > 0, \tag{8}$$

which implies that

$$F_\xi(r) = 1 - \exp(-\int_0^r \lambda_\xi(s)ds) \quad \text{and} \quad S_\xi(r) = \exp(-\int_0^r \lambda_\xi(s)ds). \tag{9}$$

The aim is now to try to find some methods to estimate the local empty space function and its hazard rate by using non-parametric or semi-parametric methods.

A popular method in classical survival analysis is to fit semi-parametric models to the hazard rates. This means that one studies the relationship of survival distributions to some known covariates, e.g. one can try to fit a Cox proportional hazards model

$$\lambda_\xi(r) = e^{\beta \cdot s(\xi)} \lambda(r), \tag{10}$$

or an accelerated life time model

$$\lambda_\xi(r) = e^{\beta \cdot s(\xi)} \lambda(e^{\beta \cdot s(\xi)} r), \tag{11}$$

where λ is some baseline hazard rate, β is k-dimensional vector of parameters and $s : \mathbb{R}^d \to \mathbb{R}^k$ is a vector valued covariate. The baseline does not need to have a special form and can be estimated non-parametrically. These methods can easily be adapted to non-stationary spatial statistics, where the covariates are known or an observed function of ξ. The function $s(\xi)$ could e.g. represent soil type or altitude at position ξ or a function derived from another spatial pattern.

The two models above also have an interesting intuitive appeal. If we have a union $X^\star$ of n independent copies of a stationary random closed set X with empty space function F and hazard rate λ, then the union $X^\star$ has hazard rate $\lambda^\star(r) = n\lambda(r)$, corresponding to the transformation occurring in the Cox proportional hazard model. On the other hand if one considers a scaled version of X, $X^\star = cX$, $c > 0$, $X^\star$ has hazard rate $\lambda^\star(r) = c^{-1}\lambda(c^{-1}r)$. This corresponds to the transformation occurring in the accelerated life time model. Therefore, the models in (10) and (11) have the intuitive appeal of describing non-stationary change of intensity and non-stationary change of scale, respectively.

It is important to study the properties of the local empty space function of some known models for inhomogeneous spatial patterns. The majority of inhomogeneous models for point processes has been constructed by introducing inhomogeneity into a homogeneous template point process. This includes e.g. independent location dependent thinning (cf. Baddeley et al. (2000)) and transformation of the homogeneous process, (cf. Jensen and Nielsen (2000)). Also, one can define an inhomogeneous point process as a locally scaled version of the homogeneous template process, cf. Hahn et al. (2003). Other examples, as first-order inhomogeneous Markov point processes, introduce the inhomogeneity by allowing non-constant first-order terms in the density of the process with respect to the unit rate Poisson process, c.f. Stoyan and Stoyan

(1998). Some Cox point processes are also important in the description of inhomogeneous point patterns, c.f. Møller et al. (1998) and Brix and Møller (2001). However, there does not seem to exist any simple way of studying the properties of the local empty space functions for these models. In Section 4 we will study a more tractable model, then the models mentioned above.

4 Cox proportional hazard model

A special class of inhomogeneous germ-grain models for non-stationary random compact sets in $\mathbb{R}^d$, is a Cox proportional hazard model for the local hazard rate with $s(\xi) = \xi$, see (10).

4.1 The germ-grain model

The definition of the model is as follows. Let

$$X = \cup_{y \in Y} \{y + Z_y\},$$

where Y is an inhomogeneous Poisson process on $\mathbb{R}^d$ with a log-linear intensity function

$$\gamma(y) = \alpha \exp(\beta \cdot y), \quad \alpha > 0, \beta \in \mathbb{R}^d$$

and $\{Z_y\}_{y \in Y}$ is a sequence of independent and identically distributed random compact sets in $\mathbb{R}^d$ that are independent of the Poisson process Y. We will assume that $Z_y \sim Z$ for all $y \in Y$, where Z has the distribution $\mathbb{Q}$. The random compact set X can also be regarded as a marked Poisson point process $\{y, Z_y\}$ with points in $\mathbb{R}^d$ and mark space $\mathcal{K}$, where $\mathcal{K}$ denotes the class of compact sets in $\mathbb{R}^d$. A germ-grain model of this type can e.g. be used to model data with a spatial trend along a specific axis.

Denote

$$n(\mathcal{F}) = \sum_{y \in Y} \mathbf{1}\{y + Z_y \in \mathcal{F}\}, \quad \mathcal{F} \in \mathcal{K}',$$

where $\mathcal{K}' = \mathcal{B}(\mathcal{K} \setminus \{\emptyset\})$. Then the intensity measure of the random compact set X is given by

$$\Lambda(\mathcal{F}) = \mathbb{E}\{n(\mathcal{F})\} = \int_{\mathbb{R}^d} \int_{\mathcal{K}} \mathbf{1}\{y + Z \in \mathcal{F}\} \gamma(y) d\mathbb{Q}(Z) dy$$

where $\mathcal{F} \in \mathcal{K}'$. Now define the hitting distribution T_X of the random compact set by

$$T_X(K) = \mathrm{P}\{X \cap K \neq \emptyset\}, \quad K \in \mathcal{K}.$$

It is clear that

$$\begin{aligned} T_X(K) &= \mathrm{P}\{X \cap K \neq \emptyset\} = 1 - \mathrm{P}\{X \cap K = \emptyset\} \\ &= 1 - \mathrm{P}\{n(\mathcal{F}_K) = 0\} = 1 - \exp(-\Lambda(\mathcal{F}_K)), \end{aligned}$$

where $K \in \mathcal{K}$ and $\mathcal{F}_K = \{F \in \mathcal{K} : F \cap K \neq \emptyset\}$. The local empty space function of the random compact set X at position ξ is given by

$$F_\xi(r) = T_X(b(\xi, r)) = 1 - \exp(-\Lambda(\mathcal{F}_{b(\xi,r)})).$$

We have that

$$\begin{aligned}\Lambda(\mathcal{F}_{b(\xi,r)}) &= \int_{\mathbb{R}^d}\int_{\mathcal{K}} \mathbf{1}\{y+Z\in\mathcal{F}_{b(\xi,r)}\}\gamma(y)d\mathbb{Q}(Z)dy \\ &= \int_{\mathbb{R}^d}\int_{\mathcal{K}} \mathbf{1}\{(y+Z)\cap b(\xi,r)\neq\emptyset\}\gamma(y)d\mathbb{Q}(Z)dy \\ &= \mathbb{E}_{\mathbb{Q}}\Big\{\int_{b(\xi,r)\oplus\check{Z}}\gamma(y)dy\Big\} = \mathbb{E}_{\mathbb{Q}}\Big\{\int_{b(0,r)\oplus\check{Z}}\gamma(y+\xi)dy\Big\} \\ &= \exp(\beta\cdot\xi)\mathbb{E}_{\mathbb{Q}}\Big\{\int_{b(0,r)\oplus\check{Z}}\gamma(y)dy\Big\} = \exp(\beta\cdot\xi)\Lambda(\mathcal{F}_{b(0,r)}),\end{aligned}$$

where $\check{Z}=\{-z : z\in Z\}$ and thus

$$\begin{aligned}F_\xi(r) &= 1-\exp\big(\exp(\beta\cdot\xi)\log(1-F_0(r))\big) = 1-(1-F_0(r))^{\exp(\beta\cdot\xi)},\\ S_\xi(r) &= (S_0(r))^{\exp(\beta\cdot\xi)}.\end{aligned}$$

It follows that the local hazard rate of the random compact set X at ξ fulfils

$$\lambda_\xi(r)=\exp(\beta\cdot\xi)\lambda_0(r),$$

and the model is therefore a special type of the Cox proportional hazard model, see (10).

4.2 The Poisson point process

A special case of the germ-grain model described above is the Poisson point process with log-linear intensity function $\gamma(\xi)=\alpha\exp(\beta\cdot\xi)$, i.e. $Z_y=\emptyset$. The following relations for the local empty space function, local hazard rate and the local survival function of X were found above,

$$F_\xi(r) = 1-(1-F_0(r))^{\exp(\beta\cdot\xi)}, \tag{12}$$

$$S_\xi(r) = S_0(r)^{\exp(\beta\cdot\xi)}, \tag{13}$$

$$\lambda_\xi(r) = \exp(\beta\cdot\xi)\lambda_0(r). \tag{14}$$

Using the specific form of the intensity function one gets that

$$S_0(r) = \exp\left(-\frac{2\pi r\alpha}{|\beta|}I_1(r|\beta|)\right), \tag{15}$$

$$\lambda_0(r) = 2\pi\alpha r I_0(r|\beta|), \tag{16}$$

where I_ν is the modified Bessel function of the first kind of order ν. The calculations can be found in the Appendix.

Since the Cox proportional hazard model only includes the parameter β, we need an estimation method for the parameter α. This can be done by solving the equation

$$\mathbb{E}(n(X\cap W)) = \alpha\int_W \exp(\hat{\beta}\cdot\eta)d\eta,$$

for α, where $n(x)$ denotes the cardinality of x and $\hat{\beta}$ is an estimate of β. This implies that we can estimate α by

$$\hat{\alpha} = n_W\Big(\int_W\exp(\hat{\beta}\cdot\eta)d\eta\Big)^{-1}, \tag{17}$$

where n_W is the observed number of points in the window W.

The fitted model can be used to check for complete randomness of a point process, by comparing the estimated baseline hazard rate $\hat{\lambda}_0$ to the hazard rate λ_0 of an inhomogeneous Poisson process with intensity $\gamma(\xi) = \alpha \exp(\beta \cdot \xi)$, replacing α and β with its estimates. The deviations of the estimated hazard rate to the hazard rate of the Poisson process can also give an indication of clustering or regularity as in the stationary case. $\hat{\lambda}_0(r) \leq \lambda_0(r)$ indicates clustering or aggregation and $\hat{\lambda}_0(r) \geq \lambda_0(r)$ indicates regularity, at least for small r. In addition, the estimated survival function can be compared to the survival function of the inhomogeneous Poisson point process.

4.3 Estimation method for the Cox proportional hazard model

In this section we will explain how the parameter β can be estimated in the Cox proportional hazard model.

Our data consists of the local empty space distances

$$\rho(\xi, X \cap W) = \inf\{|\xi - a| : a \in X \cap W\},$$

and the local distances to the observation window

$$\rho(\xi, \partial W) = \inf\{|\xi - a| : a \in \partial W\}.$$

The true distance $\rho(\xi, X)$ is censored by the distance to the boundary $\rho(\xi, \partial W)$, since

$$\rho(\xi, X) \wedge \rho(\xi, \partial W) = \rho(\xi, X \cap W) \wedge \rho(\xi, \partial W),$$

where $a \wedge b = \min\{a, b\}$. Like in survival analysis we therefore define the "observed failure times"

$$t(\xi) = \rho(\xi, X \cap W) \wedge \rho(\xi, \partial W),$$

and a censoring indicator

$$d(\xi) = \mathbf{1}[\rho(\xi, X) \leq \rho(\xi, \partial W)] = \mathbf{1}[\rho(\xi, X \cap W) \leq \rho(\xi, \partial W)].$$

We suggest calculating $(t(\xi), d(\xi))$ for some points ξ in a regular lattice L on W, having observations $\{(t(\xi), d(\xi))\}_{\xi \in L}$ and then fitting a Cox proportional hazard model

$$\lambda_\xi(r) = \exp(\beta \cdot \xi)\lambda_0(r), \tag{18}$$

with parameter $\beta \in \mathbb{R}^d$, using the standard methods from survival analysis to estimate β, i.e. the partial likelihood function

$$L(\beta) = \prod_{\xi \in L} \left(\frac{\exp(\beta \cdot \xi)}{\sum_{\eta \in R(\xi)} \exp(\beta \cdot \eta)} \right)^{d(\xi)},$$

where $R(\xi) = \{\eta \in L : t(\eta) \geq t(\xi)\}$. Then non-parametric methods are used to estimate the baseline hazard rate λ_0. For more details see cf. Andersen and Gill (1982).

One should note that using this estimation method, the observations on the lattice L are treated as independent which is clearly not the case for spatial patterns. It is also clear that we can actually observe continuous data, since the $(t(\xi), d(\xi))$ could be observed for all $\xi \in W$. We postpone a more detailed discussion of these issues to Section 6.

4.4 Examples

In this section we will apply the estimation method discussed in Section 4.3 to a simulated data set and real data set describing the location of adult Longleaf Pine trees.

Example 4.1. (**Simulated data**) We have simulated a Poisson point pattern on the unit square window with intensity

$$\gamma(x, y) = 300 \exp(-2x).$$

Figure 1 shows the simulated point pattern. When we fit a Cox proportional hazard

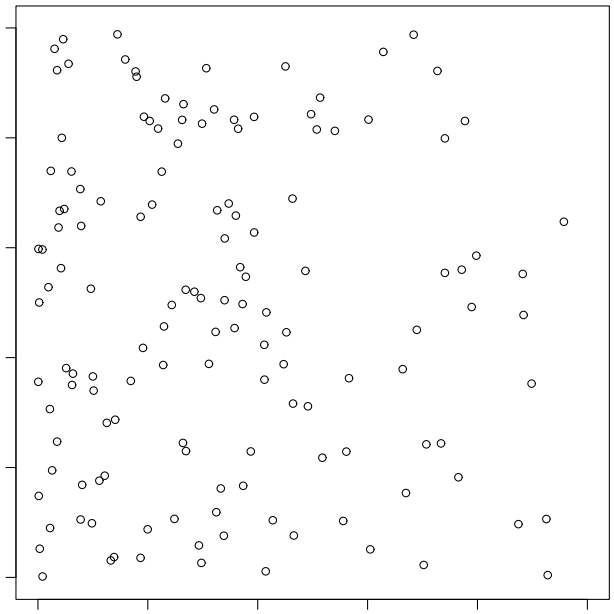

Figure 1: A simulated inhomogeneous Poisson point pattern on the unit square window. The intensity is given by $\rho(x, y) = 300 \exp(-2x)$.

model using the observed failure times and censoring indicators of the simulated data and, by using the `coxph` function in `R`, we get estimates $\hat{\beta} = (-1.858, -0.692)$ and using equation (17) we get $\hat{\alpha} = 424.07$. Now using the `survfit` function in `R` we get an estimate of the survival function at the point $\xi_0 = (0.5, 0.5)$, $\hat{S}_{\xi_0}(r)$ and using the function `D1ss` we get an estimate of the local hazard rate $\hat{\lambda}_{\xi_0}$. These estimates can now be compared with the survival function and the local hazard at ξ_0 of an inhomogeneous Poisson process with intensity $\gamma(\xi) = \hat{\alpha} \exp(\hat{\beta} \cdot \xi)$. Figure 2 shows the estimated local hazard rate $\hat{\lambda}_{\xi_0}(r)$ and the local hazard rate of the inhomogeneous Poisson process with intensity $\hat{\alpha} \exp(\hat{\beta} \cdot \xi)$ for $r < 0.14$. Equation (14) and (16) are used to calculate the local hazard rate of the inhomogeneous Poisson process.

In Figure 3, a log-plot of the estimated survival function $\hat{S}_{\xi_0}(r)$ is shown against the survival function of the inhomogeneous Poisson process with intensity $\hat{\alpha} \exp(\hat{\beta} \cdot \xi)$. Equations (13) and (15) are used to calculate the survival function of the inhomogeneous Poisson process.

The plotted line in Figure 3 coincides with the line $x = y$. In Figure 4, a plot of the estimated baseline survival function at ξ_0 and the survival function at ξ_0 of an inhomogeneous Poisson process with intensity $\hat{\alpha} \exp(\hat{\beta} \cdot \xi)$ are shown.

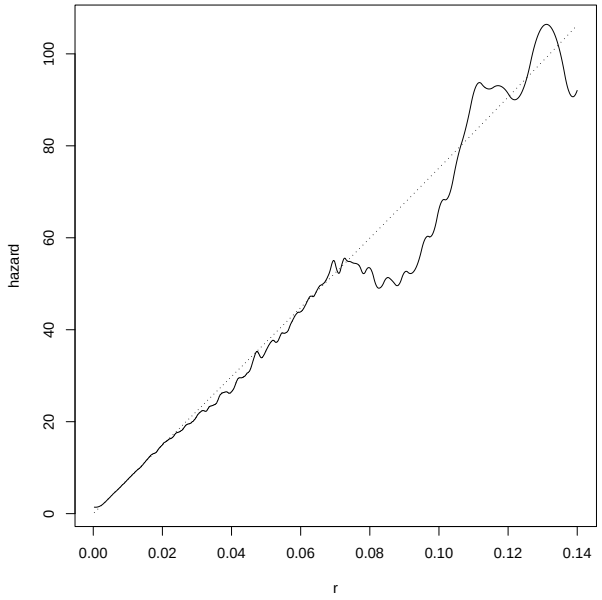

Figure 2: The estimated local hazard rate $\hat{\lambda}_{\xi_0}$ for the simulated data (full line) and the local hazard rate of an inhomogeneous Poisson process with intensity $\hat{\alpha}\exp(\hat{\beta}\cdot\xi)$ (dotted line). The plot shows only the values for $r < 0.14$.

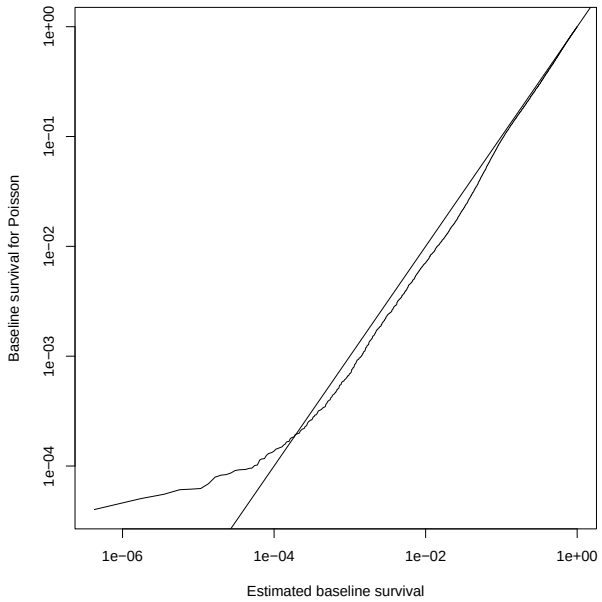

Figure 3: A log-plot of the estimated baseline survival function for the simulated data at $\xi_0 = (0.5, 0.5)$ vs. the survival function at ξ_0 of an inhomogeneous Poisson process with intensity $\hat{\alpha}\exp(\hat{\beta}\cdot\xi)$

All these figures indicate that the inhomogeneous Poisson process is a good fit to the simulated data, as expected.

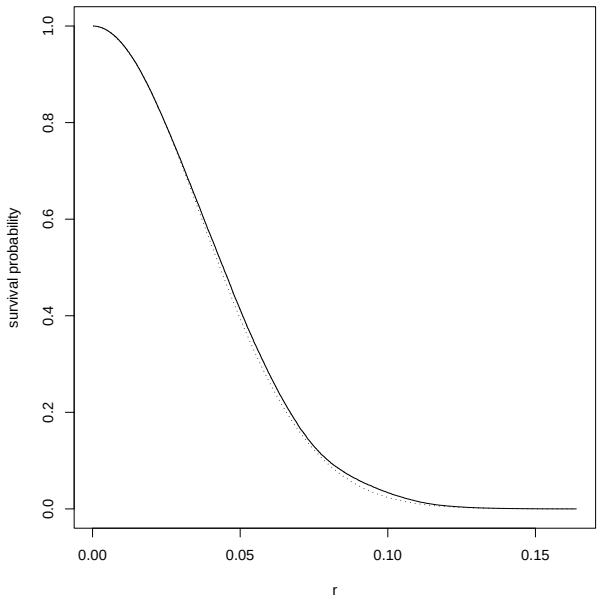

Figure 4: A plot of the estimated baseline survival function for the simulated data at $\xi_0 = (0.5, 0.5)$ (full line) and the survival function at ξ_0 of an inhomogeneous Poisson process with intensity $\hat{\alpha} \exp(\hat{\beta} \cdot \xi)$ (dotted line).

Example 4.2. (**Adult Longleaf Pine tree data**) The data in Figure 5 show the locations of adult Longleaf Pine trees (trees of diameter greater or equal than 30 cm), in a 200 $\times$ 200 metre region. The data is a subset of a larger data-set which has been analysed in e.g. Cressie (1993). Note that this data set shows a clear spatial trend along the x-axis, suggesting a log-linear intensity.

Let us fit the Cox proportional hazard model

$$\lambda_\xi(r) = \exp(\beta \cdot \xi)\lambda_0(r),$$

where $\lambda_\xi(r)$ is the local hazard function of the distribution of $\rho(\xi, X)$ and X is the observed point pattern. This gives us the following $\hat{\beta} = (-7.2974 \cdot 10^{-3}, 1.4481 \cdot 10^{-5})$. We want to see if there is some evidence of deviation from an inhomogeneous Poisson model with intensity $\gamma(\xi) = \alpha \exp(\beta \cdot \xi)$. We get an estimate $\hat{\alpha} = 0.013007$ using equation (17). Using the same estimation procedure as in the last example we compare the estimated hazard rate and the estimated survival function at $\xi_0 = (100, 100)$ with their theoretical values, using the above estimates of α and β. The plots are shown in Figures 6-8. The plots indicate some clustering of the trees.

Note that the estimated local hazard rate can not be interpreted for large values of r due to the finite size of the sampling window.

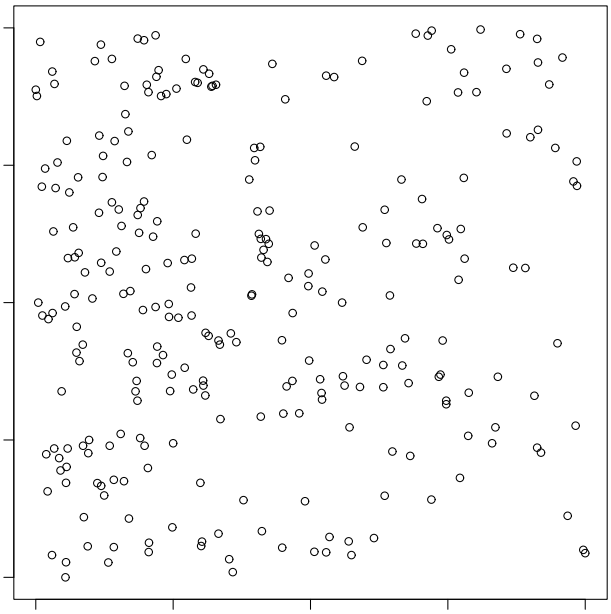

Figure 5: The locations of adult Longleaf Pine trees.

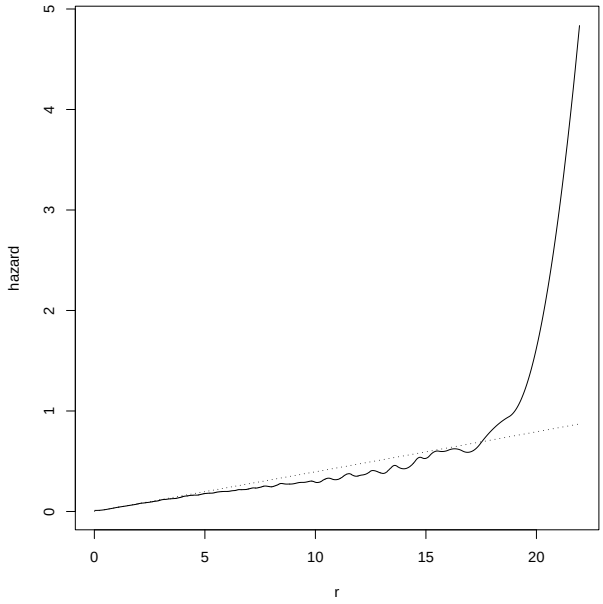

Figure 6: A plot of the estimated local hazard rate for the adult Longleaf Pine tree data at $\xi_0 = (100, 100)$ (full line) and the local hazard rate at ξ_0 of an inhomogeneous Poisson process with intensity $\hat{\alpha} \exp(\hat{\beta} \cdot \xi)$ (dotted line).

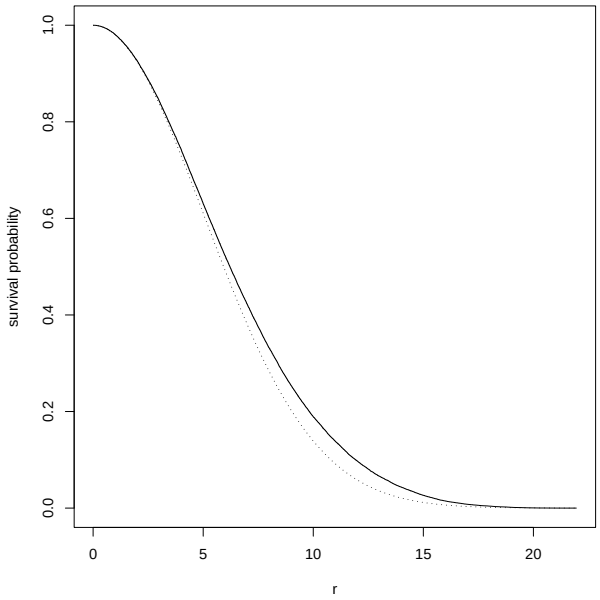

Figure 7: A plot of the estimated baseline survival function adult Longleaf Pine tree data at $\xi_0 = (100, 100)$ (full line) and the survival function at ξ_0 of an inhomogeneous Poisson process with intensity $\hat{\alpha} \exp(\hat{\beta} \cdot \xi)$ (dotted line).

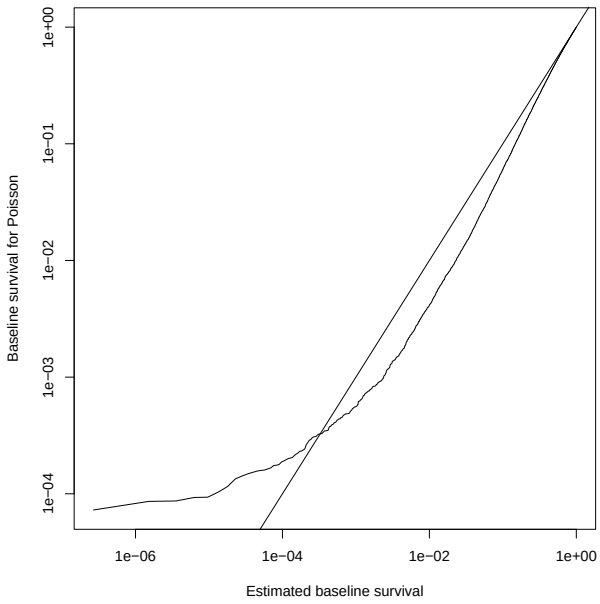

Figure 8: A log-plot of the estimated baseline survival function adult Longleaf Pine tree data at $\xi_0 = (100, 100)$ vs. the survival function at ξ_0 of an inhomogeneous Poisson process with intensity $\hat{\alpha} \exp(\hat{\beta} \cdot \xi)$

5 Accelerated lifetime model

We will now look at the spatial analogue of the accelerated lifetime model for the local hazard rate. Until now, we have not been able to find a random compact set such that the local hazard rate fulfils an accelerated lifetime model. Intuitively, a prominent candidate would be a germ-grain model, where the germs are a locally scaled Poisson process with scaling function $s(\xi)$ and the grains are independent but a scaled version of each other with scaling function s. However, this type of germ-grain model does not fulfil an accelerated lifetime model as seen below.

Let

$$X = \cup_{y \in Y} \{y + Z_y\},$$

where Y is a locally scaled Poisson process on $\mathbb{R}^d$ with scaling function

$$s(y) = \alpha \exp(\beta \cdot y),$$

i.e. with intensity function $\gamma(y) = s(y)^{-d}$, $\{Z_y\}_{y \in Y}$ is a sequence of independent random compact sets in $\mathbb{R}^d$ which are independent of Y and $Z_y \sim s(y)Z$, where Z is a random compact set with distribution $\mathbb{Q}$. The counting measure is of the form

$$n(\mathcal{F}) = \sum_{y \in Y} \mathbf{1}\{y + s(y)Z \in \mathcal{F}\}, \quad \mathcal{F} \in \mathcal{K}',$$

and the intensity measure Λ of the random compact set X is given by

$$\Lambda(\mathcal{F}) = \mathbb{E}\{n(\mathcal{F})\} = \int_{\mathbb{R}^d} \int_{\mathcal{K}} \mathbf{1}\{y + s(y)Z \in \mathcal{F}\} \gamma(y) d\mathbb{Q}(Z) dy,$$

where $\mathcal{F} \in \mathcal{K}'$. As in Section 4, the hitting distribution T_X can be calculated by

$$T_X(K) = 1 - \exp(-\Lambda(\mathcal{F}_K)), \quad K \in \mathcal{K},$$

and the local empty space function of X at position ξ is

$$F_\xi(r) = 1 - \exp(-\lambda(\mathcal{F}_{b(\xi,r)})).$$

We have that

$$\Lambda(\mathcal{F}_{b(\xi,r)}) = \int_{\mathbb{R}^d} \int_{\mathcal{K}} \mathbf{1}\{(y + s(y)Z) \cap b(\xi, r) \neq \emptyset\} s(y)^{-d} d\mathbb{Q}(Z) dy,$$

and if we make the substitution $t = \frac{y-\xi}{e^{\beta \cdot \xi}}$, so $dy = (e^{\beta \cdot \xi})^d dt$ and $y = \xi + te^{\beta \cdot \xi}$, we get

$$\Lambda(\mathcal{F}_{b(\xi,r)}) = \int_{\mathbb{R}^d} \int_{\mathcal{K}} \mathbf{1}\{(\xi + te^{\beta \cdot \xi} + s(\xi + te^{\beta \cdot \xi})Z) \cap b(\xi, r) \neq \emptyset\} s(\xi + te^{\beta \cdot \xi})^{-d} (e^{\beta \cdot \xi})^d d\mathbb{Q}(Z) dt.$$

Since

$$s(\xi + te^{\beta \cdot \xi}) = \frac{s(\xi) s(te^{\beta \cdot \xi})}{\alpha},$$

we get that

$$\begin{aligned}
\Lambda(\mathcal{F}_{b(\xi,r)}) &= \int_{\mathbb{R}^d} \int_{\mathcal{K}} \mathbf{1}\left\{\left(\xi + te^{\beta \cdot \xi} + \frac{s(\xi) s(te^{\beta \cdot \xi})}{\alpha} Z\right) \cap b(\xi, r) \neq \emptyset\right\} s(te^{\beta \cdot \xi})^{-d} d\mathbb{Q}(Z) dt \\
&= \int_{\mathbb{R}^d} \int_{\mathcal{K}} \mathbf{1}\{(t + s(te^{\beta \cdot \xi})Z) \cap b(0, e^{-\beta \cdot \xi} r) \neq \emptyset\} s(te^{\beta \cdot \xi})^{-d} d\mathbb{Q}(Z) dt \\
&= \tilde{\Lambda}(\mathcal{F}_{b(0, e^{-\beta \cdot \xi} r)}),
\end{aligned}$$

where $\tilde{\Lambda}$ is the intensity measure of a random compact set $\tilde{X}$ of the local scaling type defined above, but with scaling function $\tilde{s}_\xi(t) = s(te^{\beta\cdot\xi})$. Thus

$$F_\xi(r) = \tilde{F}_{0,\xi}(\exp(-\beta\cdot\xi)r),$$
$$\lambda_\xi(r) = \exp(-\beta\cdot\xi)\tilde{\lambda}_{0,\xi}(\exp(-\beta\cdot\xi)r),$$

where $\tilde{F}$ and $\tilde{\lambda}$ are the local empty space function and local hazard rate at position ξ of the random compact set $\tilde{X}$, respectively. Since the hazard rate $\tilde{\lambda}_{0,\xi}$ depends on ξ, we do not have an accelerated lifetime model.

6 Discussion

In this section we will try to summarise the open questions within this area and discuss the possible problems with the methods used.

One of the problems arising in this report is the question of the existence of λ_ξ. Existence is ensured if F_ξ is differentiable for all $\xi \in W$. It is needed to try to find some regularity conditions on the random compact set X, such that $F_\xi(r)$ is differentiable for all $\xi \in W$ and $r > 0$.

Another possibly problematic issue is the question of existence of a random compact set X with a local hazard rate fulfilling a given Cox proportional hazard model or an accelerated lifetime model. This problem could possibly be solved by using a similar strategy as proposed by Zimmerman (1991).

In Section 4.3 we proposed a method of estimating β based on the partial likelihood in the Cox proportional hazard model (18) and a non-parametric method to estimate λ_0. The observations are functions of distances $\rho(\xi, X)$ and $\rho(\xi, \partial W)$ from points ξ in a lattice L. One should note that these observations are heavily dependent since

$$|\rho(\xi, X) - \rho(\eta, X)| \leq |\eta - \xi|. \tag{19}$$

Fitting the model (18), using the suggested methods, means ignoring this spatial dependence.

Another problem concerning the estimation methods is the fact that the observations $\rho(\xi, X)$ and $\rho(\xi, \partial W)$ can be observed at every point ξ of the observation window W. Therefore a very interesting problem is to find a continuous analogue of the partial likelihood estimation method and investigate its properties. In practise, one would however probably always use the discrete version of the likelihood. This involves a number of open questions concerning the asymptotic properties of the estimators. One could e.g. study asymptotic results concerning the size of the window W and size of the lattice used.

As mentioned in Section 4.2, the Cox proportional hazard model only includes the parameter β. This means that using the suggested estimation methods we need an estimate for α. If the observed random set is such that the grains do not intersect, one can find reasonable estimates of the parameter α, using similar considerations as in Section 4.2,

$$\hat{\alpha} = n_W \Big(\int_W \exp(\hat{\beta}\cdot\eta) d\eta \Big)^{-1}, \tag{20}$$

where n_W is the number of observed grains in the observation window W. One can also use the empirical distribution of the shapes of the grains as an estimate of the

distribution $\mathbb{Q}$ and simulate the theoretical local hazard rates and survival functions using this estimate and the estimates of the parameters determining the intensity function. This involves calculating

$$\mathbb{E}_{\mathbb{Q}}\Big\{\int_{b(0,r)\oplus\check{Z}}\gamma(y)dy\Big\},$$

where the parameters in the intensity are the estimated α and β. If the grains overlap, the estimation of α will be more complicated.

Many distance and size variables in stochastic geometry can be considered as generalisations of one-dimensional waiting times. This suggests that statistics and functions in spatial statistics can be estimated and/or analysed by using methods from survival analysis. One could try to use the ideas suggested here for other first contact distance functions then the empty space function, using different test sets. This could perhaps be used to investigate anisotropy of non-stationary random compact sets. It is also of interest to look at local versions of other functions based on interpoint distances, e.g. the G and J function and try to find analogues from survival analysis to estimate these functions.

Acknowledgements

This work was done during an academic visit of the author at the University of Western Australia under the supervision of Professor Adrian Baddeley. The research results presented here have been obtained in close collaboration with Adrian and represent a continuation of earlier research ideas formulated by Adrian Baddeley, Martin B. Hansen and Richard Gill.

Appendix: Calculation of the hazard rate and the survival function for a non-stationary Poisson point process at ξ

Let X be a Poisson point process with intensity function $\gamma(y) = \alpha\exp(\beta\cdot\xi)$. It is easy to see that the local survival function is given by

$$S_\xi(r) = \exp\Big(-\int_{b(\xi,r)}\gamma(\eta)d\eta\Big),$$

implying that the local empty space function is given by

$$F_\xi(r) = 1-\exp\Big(-\int_{b(\xi,r)}\gamma(\eta)d\eta\Big),$$

and the local hazard rate is given by

$$\lambda_\xi(r) = \int_{\partial b(\xi,r)}\alpha\exp(\beta\cdot\eta)d\eta = \alpha\exp(\beta\cdot\xi)\int_{\partial b(0,r)}\exp(\beta\cdot\eta)d\eta.$$

Letting

$$\psi = \arcsin\left(\frac{\beta_1}{|\beta|}\right) = \arccos\left(\frac{\beta_2}{|\beta|}\right),$$

then

$$\begin{aligned}\int_{\partial b(0,r)} \exp(\beta \cdot \eta) d\eta &= r \int_0^{2\pi} \exp(r\beta_1 \cos\theta + r\beta_2 \sin\theta) d\theta \\ &= r \int_0^{2\pi} \exp(r|\beta|(\sin\psi \cos\theta + \cos\psi \sin\theta)) d\theta \\ &= r \int_0^{2\pi} \exp(r|\beta| \sin(\psi + \theta)) d\theta \\ &= 2\pi r I_0(r|\beta|),\end{aligned}$$

where I_ν is the modified Bessel function of the first kind of order ν. Note that

$$\begin{aligned}\int_{b(0,r)} \exp(\beta \cdot \eta) d\eta &= \int_0^r \int_{\partial b(0,s)} \exp(\beta \cdot \eta) d\eta ds \\ &= \int_0^r 2\pi s I_0(s|\beta|) ds \\ &= \frac{2\pi}{|\beta|^2} \int_0^{r|\beta|} w I_0(w) dw = \frac{2\pi r}{|\beta|} I_1(r|\beta|).\end{aligned}$$

Using equation (9), we get that

$$\begin{aligned}S_\xi(r) &= \exp\Big(-\alpha \int_{b(\xi,r)} \exp(\beta \cdot \eta) d\eta\Big) \\ &= \exp\Big(-\alpha \exp(\beta \cdot \xi) \int_{b(0,r)} \exp(\beta \cdot \eta) d\eta\Big) \\ &= \exp(-\alpha \exp(\beta \cdot \xi)) \exp\left(\frac{2\pi r}{|\beta|} I_1(r|\beta|)\right),\end{aligned}$$

and

$$F_\xi(r) = 1 - \exp((-\alpha \exp(\beta \cdot \xi)) \exp\left(\frac{2\pi r}{|\beta|} I_1(r|\beta|)\right).$$

References

Andersen, P. K. and Gill, R. D. (1982). Coxs regression model for counting processes: a large sample study. *Ann. Statist.*, 10:1100–1120.

Baddeley, A. J. and Gill, R. D. (1993). Kaplan–Meier estimators of interpoint distance distributions for spatial processes. Technical report, Research Report, BS-R9315, Centrum voor Wiskunde en Informatics, Amsterdam.

Baddeley, A. J. and Gill, R. D. (1994). The empty space hazard of a spatial pattern. Technical report, Research report 1994/3, Department of Mathematics, The University of Western Australia.

Baddeley, A. J. and Gill, R. D. (1997). Kaplan–Meier estimators of interpoint distance distributions for spatial processes. *Ann. Statist.*, 25:263–292.

Baddeley, A. J., Møller, J., and Waagepetersen, R. P. (2000). Non- and semiparametric estimation of interaction in inhomogeneous point patterns. *Statistica Neerlandica*, 54:329–350.

Brix, A. and Møller, J. (2001). Space-time multitype log Gaussian Cox processes with a view to modelling weeds. *Scand. J. Statist.*, 28:471–488.

Cressie, N. (1993). *Statistics for Spatial Data*. John Wiley & Sons, New York.

Hahn, U., Jensen, E. B. V., van Lieshout, M. N. M., and Nielsen, L. S. (2003). Inhomogeneous point processes by location dependent scaling. *Adv. Appl. Prob. (SGSA)*, 35(2):319–336.

Hansen, M. B., Baddeley, A. J., and Gill, R. D. (1996). Kaplan–Meier type estimators for linear contact distributions. *Scand. J. Statist.*, 23:129–155.

Hansen, M. B., Baddeley, A. J., and Gill, R. D. (1999). First contact distributions for spatial patterns: regularity and estimation. *Adv. Appl. Prob. (SGSA)*, 31:15–33.

Jensen, E. B. V. and Nielsen, L. S. (2000). Inhomogeneous Markov point processes by transformation. *Bernoulli*, 6:761–782.

Møller, J., Syversveen, A. R., and Waagepetersen, R. P. (1998). Log Gaussian Cox processes. *Scand. J. Statist.*, 25:451–482.

Stoyan, D., Kendall, S. W., and Mecke, J. (1995). *Stochastic Geometry and its Applications*. John Wiley & Sons, Chichester.

Stoyan, D. and Stoyan, H. (1998). Non homogeneous Gibbs process models for forestry – a case study. *Biometrical Journal*, 40:521–531.

Zimmerman, D. (1991). Censored distance-based intensity estimation of spatial point processes. *Biometrika*, 78:287–294.